An Abstract of the Thesis of

Philip L. Wurst for the degree of Master of Science in Civil Engineering presented on December 19, 1983 .

Title: CENTRIFUGAL MODELING TO INVESTIGATE ICE FORCES AND ICE FLOE FAILURE MECHANISMS ON A VERTICAL PILE

Abstract approved: Redacted for Privacy

Ted S. Vinson

The ice forces and ice floe failure mechanisms associated with an ice sheet surrounding a vertical cylindrical pile were evaluated using the technique of centrifugal modeling. A test system was developed to model ice forces in gravity environments from 1 to 50 g's on a small geotechnical centrifuge. The components of the test system included: (1) an environmental model container in which ice sheets could be created and subsequently failed in flight on the centrifuge, and (2) the instrumentation required to observe, control, measure, and record the freezing process and the failure phenomena. An experimental program was conducted in which the following parameters were considered: (1) g levels of 1, 20 and 50, (2) model pile diameters of 1/2 and 3/4 in. (1.27 and 1.91 cm.), (3) ice thicknesses from 0.080 to .380 in. (.203 and .965 cm.), (4) pile penetration velocities from 0.05 to 2.00 in. per minute (.127 and 5.080 cm. per minute), and (5) ice temperatures near -0.5 °C. Samples of the ice created and failed were saved for crystallographic and compressive strength studies.

The experimental results associated with the ice failure were evaluated using dimensional analysis. The dimensionless numbers considered included the normalized force, the Froude number squared, the aspect ratio, and the g level. It was determined that the normalized force is directly proportional to the logarithm of the Froude number squared. As the penetration velocity increases or the ice thickness decreases the normalized force increases. A linear relationship was also found to exist between the normalized force and the logarithm of the g level. As the g level increased the normalized force increased. The normalized force was also observed to be a function of the aspect ratio; as the aspect ratio increased the normalized force decreased, although no quantitative relationship could be established.

The ice failure mechanism at the onset of failure was purely compressional; as the pile continued to penetrate the ice sheet, the mechanism transitioned to a flexural failure. It was observed that maximum forces on the pile were measured at the onset of penetration. The force on the pile decreased with continued penetration. The ice sheet thickness was found to be proportional to the square root of the product of time and temperature below freezing. The results of the present study were compared to the results of other studies and reasonable agreement was found to exist.

CENTRIFUGAL MODELING TO INVESTIGATE ICE FORCES AND ICE FLOE FAILURE MECHANISMS ON A VERTICAL PILE

by

Philip L. Wurst

A THESIS

submitted to

Oregon State University

in partial fulfillment of

the requirements for the

degree of

Master of Science

Completed December 19, 1983

Commencement June 1984

APPROVED:

Redacted for Privacy

Professor of Civil Engineering in Charge of Major

Redacted for Privacy

Head of Department of Civil Engineering

Redacted for Privacy

Dean of Graduate School

Date thesis presented: December 19, 1983

Typed by Jane L. Jarvi for Philip L. Wurst

ACKNOWLEDGEMENTS

I would like to thank Catherine, my wife and friend, for her support, patience, and love. I would like to thank Dr. Ted Vinson for his support and letting me have the opportunity to try some of my own ideas. I would like to thank Andy Brickman for his electrical genius and showing me which wires belonged where.

I would like to thank Chuck Swenson and Loren Sundberg for their fine craftmanship and advice while building the experimental apparatus. I would also like to thank everyone at the Boeing Company, Dr. Robert Schmidt, Harris Watson, Jerry Fink, and Dick Parker for their cooperation and help throughout the testing program. I also want to thank Mike Schrieber, Herb Clough, Cliff Mukai, and Orvin Richards for their help and Jane Jarvi for the overtime work involved in typing this thesis.

The research work described herein was supported by the National Science Foundation under Grant No. CEE-8116162 for the project entitled "Centrifugal Modeling to Determine Ice Forces and Failure Mechanisms for Offshore Structures".

TABLE OF CONTENTS

TABLE OF CONTENTS (continued)

LIST OF FIGURES

LIST OF FIGURES (continued)

LIST OF FIGURES (continued)

LIST OF TABLES

CENTRIFUGAL MODELING TO INVESTIGATE ICE FORCES AND ICE FLOE FAILURE MECHANISMS ON A VERTICAL PILE

1.0 INTRODUCTION

1.1 Background

To reduce North American dependence on imported fossil fuels, it may be necessary to develop the resources of arctic offshore regions. At the present time considerable attention is being focused on problems associated with exploration and production of petroleum reserves which lie beneath ice covered waters for the majority of the year. Any permanent structure considered for service in this hostile yet fragile environment must be capable of resisting the forces generated by a surrounding ice floe with a low probability of failure.

A portion of the Alaskan and Canadian offshore areas has been leased to oil companies and exploration in shallow water is presently being conducted from artificial islands. Monopod, cone, and semi-submersible platforms have been proposed for use in areas of deeper water. The successful peformance of these structures depends upon the ability of the offshore structure and underlying geologic foundation to resist lateral ice loads encountered during service. An assessment of the resistance of the offshore structure involves consideration of the interaction between the ice floe, structure, and geologic foundation.

Many investigators have attempted to quantify the forces that a moving ice sheet will exert on a structure. The techniques presently

employed to determine the magnitude of ice forces include: (1) analytical modeling, (2) small scale laboratory modeling utilizing both real and artificially weakened ice, (3) in situ testing with naturally occurring ice sheets, and (4) observation and measurement of instrumented structures. Each of these methods has inherent disadvantages.

The success of any analytical model depends on the reliability of the input data, an accurate constituitive model for the materials, and a correct assumption of the failure mechanism. The extrapolation of small-scale laboratory modeling results to the full-scale situation requires that the appropriate scaling relationships are used and the model tests correctly represent the field condition. In reality all ice properties (strength, elasticity, density) cannot be scaled down in unison. Further, the scaling relationships between ice strength and physical parameters such as loading rate are not completely known (Maattanen, 1983). In situ testing is generally conducted at a scale less than that anticipated for the service conditions of the structure and consequently the problem of extrapolating to a larger event still exists. The observation and measurement of instrumented field structures is an expensive alternative and the researcher is dependent on natural occurrences to provide the desired conditions. Also, it is difficult to measure the basic parameters such as ice strength and elasticity, floe velocity, and ice thickness while a test is being conducted. Further, in the field, it is difficult to conduct a controlled experiment or to study the effect of various parameters which might influence the results. Field data is extremely important, however, as it provides all researchers dealing with analytical models or models at less than full-scale the opportunity to validate their

results.

To date, researchers evaluating the magnitude of ice loadings on structures have not addressed the entire problem, namely, that of ice floe, offshore structure, and geologic foundation interaction. To accurately model the geologic foundation response, or the offshore structure if it is comprised of soil, the stress-strain-strength dependency of the foundation material on the overall stress state must be addressed. To accomplish this in a physical model study a direct equivalence between the state of stress of a given soil element at corresponding points in the full-scale structure and the model must be achieved. This will not be the case in conventional small-scale modeling if the same materials are used in the model as in the full-scale structure unless a model the same size as the full-scale structure is constructed. Alternatively, the technique of centrifugal modeling may be employed to create the same stress states at corresponding points in a small scale model and full-scale field structure. Morris (1979) succinctly stated the fundamental principle of centrifugal modeling as follows:

> "Centrifugal modeling relies on the fundamental equivalence of gravitational and inertial fields to set up a one-to-one correspondence between similar points in a full scale prototype and in a model in a centrifuge. If the linear modeling scale is defined as $n > 1$, then the general stress level under a depth of z of soil of density ρ, is $z\rho g$. At a corresponding point in a centrifuge model, the linear dimension z is decreased to z/n, and the centrifugal (or quasi-gravitational) acceleration is increased to ng. The stress level at this point in the model will be the same as in the prototype. Similarly, the state of strain will be identical, if both the model and prototype are constructed of the same material."

1.2 Problem Statement

While the ice floe and structure interaction problem has been addressed, the ice, structure, and geologic foundation interaction has not yet been considered in the analysis of arctic offshore structures. Centrifugal modeling has been proposed as a technique to study this problem (Vinson, 1983). Centrifugal modeling would allow the stress-strain-strength dependencies of the structure or foundation materials on the overall stress state to be accomodated, owing to the fundamental equivalence between gravitational and inertial fields.

Before the solution to the problem of ice floe, offshore structure, and geologic foundation interaction can be addressed, it must be demonstrated that centrifugal modeling is a valid technique to investigate lateral ice forces on a structure. As a first step to accomplish this objective the forces on a simple structure should be examined. The results of an investigation involving a simple structure can be compared with previously published results to confirm the validity of the centrifugal modeling technique to address more complicated interaction problems.

1.3 Purpose and Scope

The purpose of this study is to employ the centrifugal modeling technique to investigate ice forces and ice floe failure mechanisms on a vertical pile. More specifically the force against a vertical cylindrical pile associated with the movement and failure of a surrounding freshwater ice floe is considered.

The scope of this thesis is limited to the ice floe and structure interaction problem. In Chapter 2 a review of the technique and philosophy of centrifugal modeling is presented. In Chapter 3 the general problems associated with structures proposed for service in the arctic offshore environment are considered. In Chapter 4 the design of an experimental apparatus to create and fail ice sheets against a pile and to monitor the failure event is presented. The apparatus design reflects the requirements for use in the 1 g laboratory environment and in the high inertial environment associated with a centrifuge. Chapter 5 presents the experimental data and results pertaining to the ice sheet formation and to the ice failure events. A discussion and analysis of the experimental results is given in Chapter 6. A dimensional analysis approach was used to interpret the results. In Chapter 6 a comparison of the results obtained in this study to results obtained by others is also presented. Chapter 7 summarizes this study; conclusions are drawn and recommendations for further research are made.

2.0 THE CENTRIFUGAL MODELING TECHNIQUE

2.1 General

In the following sections a history of the development and application of the centrifugal modeling technique is presented together with a discussion of the principles of centrifugal modeling. This material should facilitate an appreciation for the application of the technique to the problems of arctic offshore structures.

2.2 Historical Background

Cheney (1982) has stated the following:

> "The earliest suggestion of the use of a centrifuge to properly simulate the self weight effects in models of engineered structures was by a Frenchman (Phillip) in 18XX. His suggestion was related to the self weight stresses in structural beams and this being of minor importance in construction, the technique was not carried forward."

Bucky (1931) was the first to use the centrifugal modeling technique in the United States. He applied the method to study the failure of mining structures and tested model beams while increasing their self weight in an inertial field. He concluded:

> "If in the model the pull of gravity on each part can be increased in the same proportion as the linear scale is decreased, then the unit stress at similar points in the model and prototype will be the same, and the displacement or deflection of any point in the model will represent to scale the displacement of the corresponding point in the prototype."

Bucky later showed that similarity exists between the model and prototype in both the elastic range of response and beyond using photoelastic photography to observe the behavior of materials in an inertial field. Bucky's apparatus is shown in Figure 2.1.

After Bucky, the centrifugal modeling technique was not pursued in the United States until recently. However, the Soviets have a long history of experience with the method. Pokrovsky and Fedorov, in 1936, summarized the investigations of four Soviet laboratories using centrifuges. The problems considered included: "(a) the stability of slopes, (b) pressure distributions beneath foundations, (c) pressure distributions around buried pipes, and (d) settlement of foundations" (Al-Hussaini, 1976). This was the first application of centrifugal modeling to problems in geotechnical engineering. The Soviets between the years of 1932 and 1980 constructed over 50 centrifuges for civilian and military testing (Cheney, 1982).

In the late 1960's and early 1970's Schofield and his co-workers began centrifuge studies in England. At the same time the countries of Denmark, Sweden, Netherlands, France, and Japan also developed similar facilities. Scientists and engineers in the United States were amongst the last to join the community of centrifugal modelers. A small machine was built at the University of California, Davis, in 1972; Scott at the California Institute of Technology, Pasadena, began work as early as 1975; a larger machine was built at U.C.-Davis in 1976, and Schmidt studied cratering phenomena in 1976, at the Boeing Company, Seattle, Washington. Upon completion of the U.S. National Geotechnical Centrifuge Facility at the NASA-Ames Research Center,

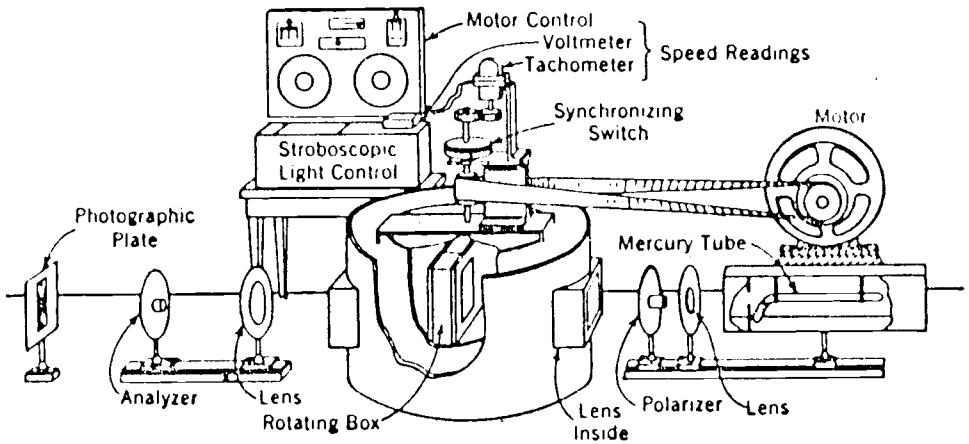

Figure 2.1 Combined centrifugal and photoelastic equipment used by Bucky (after Al-Hussaini, 1976).

Mountain View, California, the U.S. will become a major participant in the field of centrifugal modeling of geotechnical problems. This centrifuge is a modification of a centrifuge which was originally used to spin an Apollo space capsule. The capacity of a centrifuge is generally expressed in units of g-tons which represents the product of the allowable inertial acceleration at the maximum payload capacity. The National Geotechnical Centrifuge will have an initial capacity of 900 g-tons and will later be modified to accept a 2000 g-tons capacity making it one of the largest centrifuges in the world. The National Geotechnical Centrifuge is pictured in Figure 2.2.

2.3 Principles of Centrifugal Modeling

The Boeing 66 g-ton centrifuge, shown in Figure 2.3, was used in this study. The centrifuge represents an example of a modern geotechnical centrifuge. The centrifuge has the following primary components:

1. Power plant, rotor, and arm assembly.
2. Swinging buckets to accommodate models with water or cohesionless materials.
3. Slip rings to pass electrical signals and hydraulic lines for control and instrumentation of the model.
4. An enclosure to minimize air drag.
5. A containment structure to isolate the centrifuge from personnel in the event of a failure.

The Boeing centrifuge is equipped with a variable speed, 15 hp, 3 phase electric motor and has a belt drive to power the rotor. The

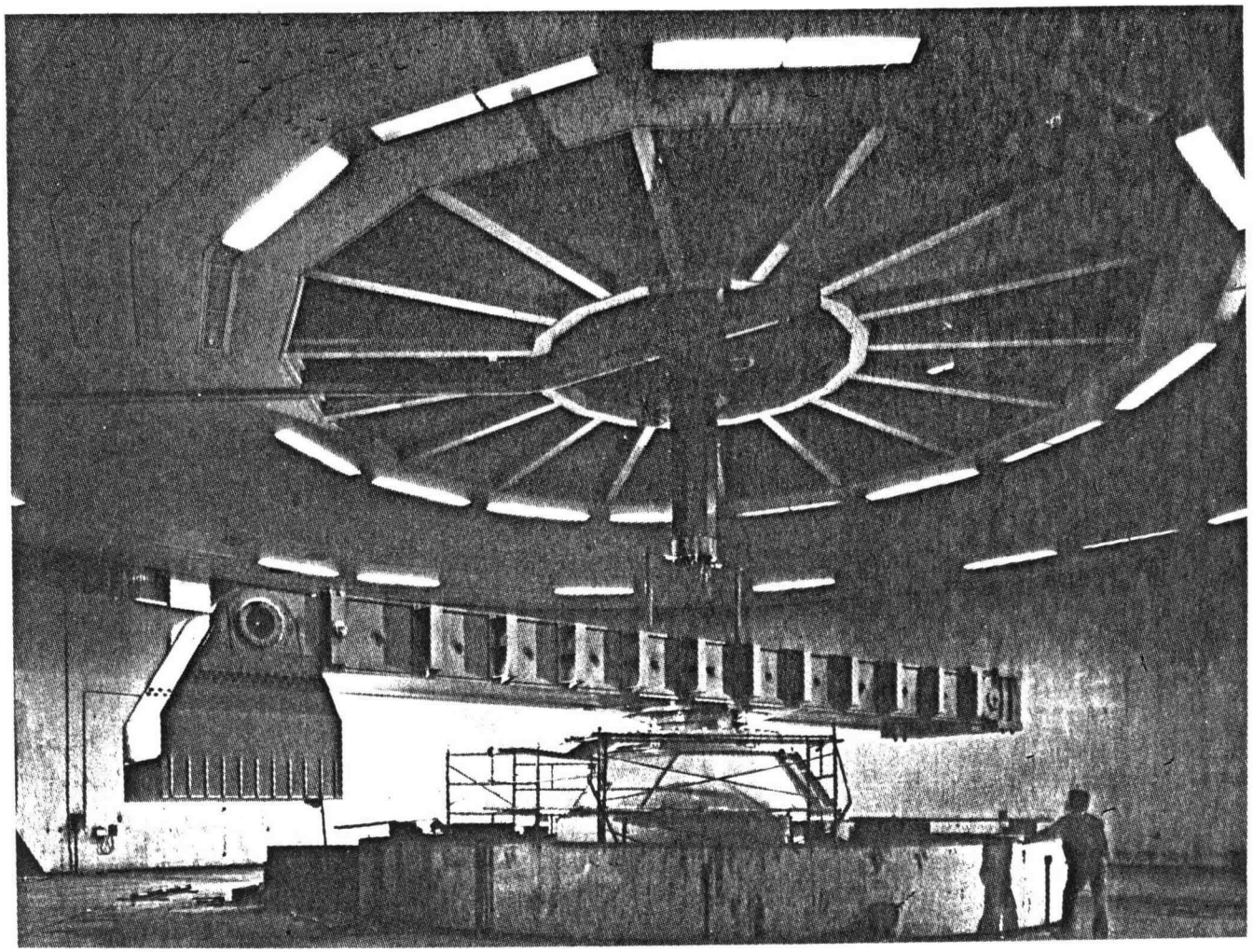

Figure 2.2 National Geotechnical Centrifuge under construction at the NASA-Ames Research Center, Mountain View, California.

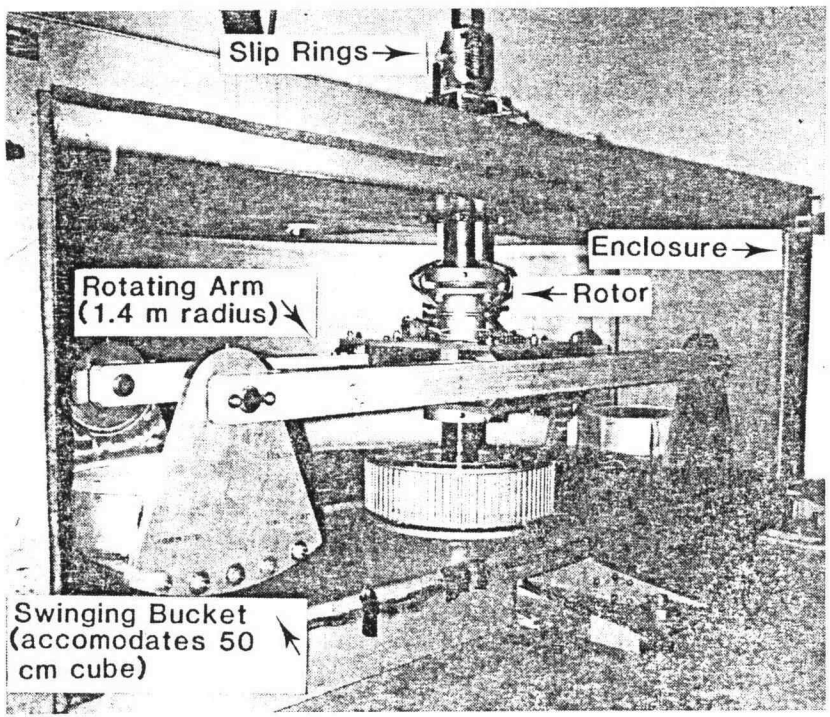

Figure 2.3 The Boeing 66 g-ton centrifuge

radius from the centerline of the hub to the base plate of each bucket is 55 in. (140 cm). The operator uses a tachometer and manual control to establish and maintain the desired rpm during testing. The swinging buckets can accommodate a payload package with maximum dimensions of 19½ x 19½ in. (49.5 x 49.5 cm) in plan view by 11 in. (28 cm) in depth. Located at the centrifuge hub are 26 brush type electrical slip rings, 24 rated at 1 amp maximum current and 2 rated at 5 amps. A hydraulic slip ring is available for either gas or liquid use and is rated at 100 psi (690 kPa) maximum gas pressure, or 25 psi (172 kPa) maximum liquid pressure.

The general test procedure associated with a centrifuge model study involves weighing the model container and contents before attaching it to the bucket. Counterbalance weight is added to the opposite bucket to maintain a gyroscopically balanced configuration. The centrifuge operator inspects the experimental apparatus to ascertain if everything is properly secured for the test. The enclosure used to minimize air drag is closed and all personnel exit the containment structure. The operator accelerates the centrifuge to the revolutions per minute (rpm) corresponding to the desired centrifugal acceleration of the test. This is known as the "spin up".

A test on a physical model in the model container is conducted with the operator maintaining the "g level". This condition is known as being "in flight" on the centrifuge. At the conclusion of the test the centrifuge is "spun down" and the operator makes a safety check before allowing the investigators to enter the containment structure and examine their model.

Centrifugal acceleration is expressed in units of "g's" which are defined as:

$$\frac{rw^2}{g}$$

in which r is the radius from the centerline of the centrifuge hub to the point within the package of concern, w is the angular velocity in radians per second, and g is the acceleration of gravity. An example can best illustrate the g concept. If an acceleration of 100 g's is desired at a point in the centrifugal model located at a radial distance of 50 in. (127 cm) from the hub centerline then the required test rpm, w, would be calculated as follows:

$$\text{"g level"} = \frac{\text{centrifugal acceleration}}{\text{acceleration of gravity}}$$

in which, centrifugal acceleration = rw^2

acceleration of gravity = 32.2 ft/sec^2 = 386.4 in./sec^2 (980 cm/sec^2)

$$\text{"g level"} = \frac{rw^2}{386.4 \text{ in./sec}^2}$$

$$w = \left(\frac{386.4 \text{ in./sec}^2 \times \text{'g level'}}{r} \right)^{1/2}$$

for a desired 100 g's at a 50 in. (127 cm) radius,

$$w = \left(\frac{386.4 \text{ in. sec}^2 \times 100}{50 \text{ in.}} \right)^{1/2}$$

$$w = 27.8 \text{ radians/sec}$$

or

$$w = 27.8 \text{ radians/sec} \times \frac{1 \text{ revolution}}{2\pi \text{ radians}} \times \frac{60 \text{ sec}}{\text{minute}}$$

$$w = 265 \text{ rpm}$$

The inertial field created by a centrifuge may be developed by considering the centrifuge in plan view:

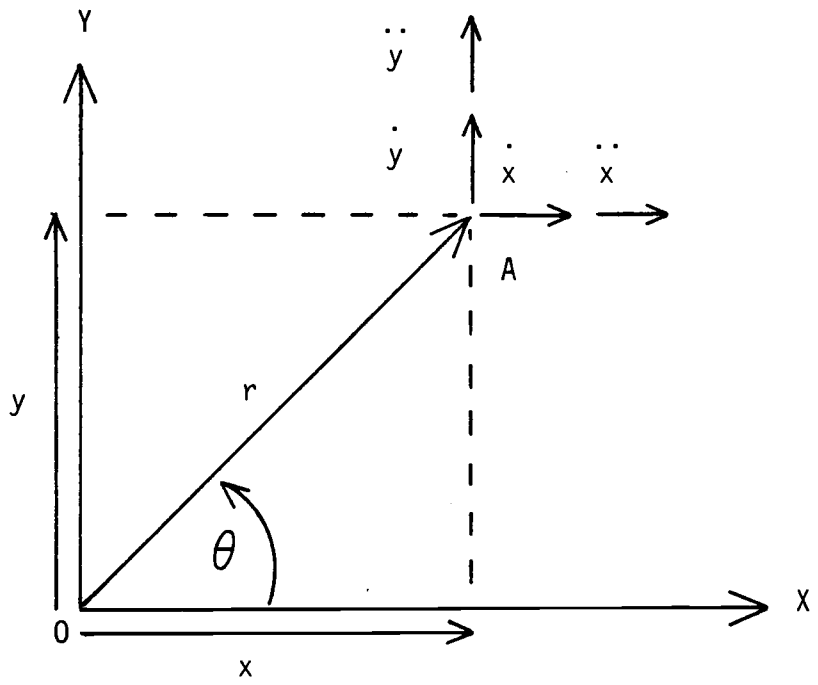

Point O and A denote, respectively, the axis of rotation and a point of interest; r denotes the radius from the center of rotation to the point of interest; Θ denotes the angle of rotation. The pairs (x,y), $(\dot{x},\dot{y})$, $(\ddot{x},\ddot{y})$ denote, respectively, the Cartesian coordinate displacement, velocity, and acceleration of the point in interest.

In Cartesian coordinates the position of point A is:

$$x = r\cos\Theta \tag{2.1}$$

$$y = r\sin\Theta \tag{2.2}$$

The velocity of point A may be expressed as the first derivative of position with respect to time:

$$\dot{x} = r\cos\Theta - r\dot{\Theta}\sin\Theta \tag{2.3}$$

$$\dot{y} = r\sin\Theta + r\dot{\Theta}\cos\Theta \tag{2.4}$$

The acceleration of point A may be expressed as the second derivative of position with respect to time:

$$\ddot{x} = \ddot{r}\cos\theta - 2\dot{r}\dot{\theta}\sin\theta - r\ddot{\theta}\sin\theta - r\dot{\theta}^2\cos\theta \qquad (2.5)$$

$$\ddot{y} = \ddot{r}\sin\theta + 2\dot{r}\dot{\theta}\cos\theta + r\ddot{\theta}\cos\theta - r\dot{\theta}^2\sin\theta \qquad (2.6)$$

These Cartesian expressions may be transformed into radial and tangential velocities and accelerations

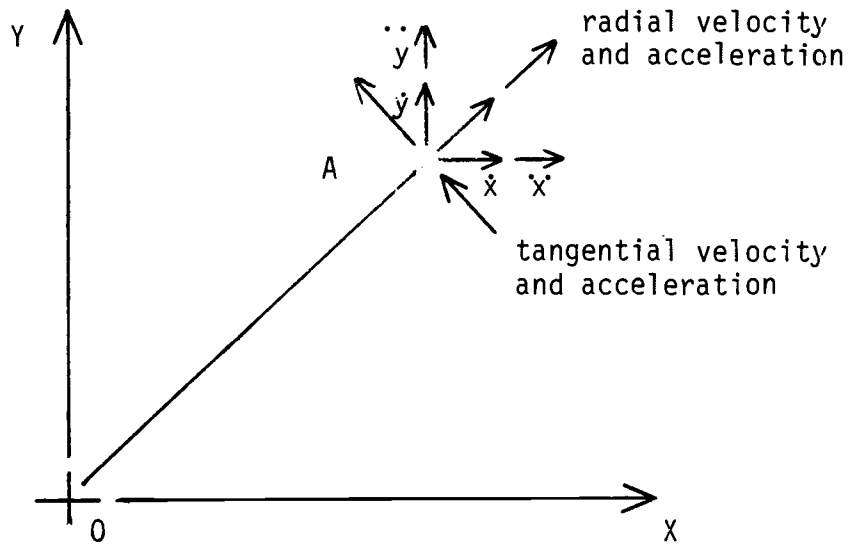

The radial and tangential velocities can be represented respectively as:

$$\dot{r} = \dot{x}\cos\theta + \dot{y}\sin\theta \qquad (2.7)$$

$$r\dot{\theta} = \dot{y}\cos\theta - \dot{x}\sin\theta \qquad (2.8)$$

The radial and tangential accelerations can be expressed respectively as:

$$\ddot{r} - r\dot{\theta}^2 = \ddot{x}\cos\theta + \ddot{y}\sin\theta \qquad (2.9)$$

$$2\dot{r}\dot{\theta} + r\ddot{\theta} = \ddot{y}\cos\theta - \ddot{x}\sin\theta \qquad (2.10)$$

A closer examination of equations 2.7 through 2.10 yields some simplifications and a better understanding of the inertial phenomena. When a point in space is replaced with a model of real dimensions it must be realized that the inertial acceleration on different points in the model is variable. The equipotentials of the inertial field conform to the shape of a cylinder with an axis coincident to the axis of rotation of the centrifuge. For example, a free water surface in a centrifugal model assumes a curvature with a radius equivalent to the radial distance from the water surface to the axis of rotation. This effect of curvature on a physical model is reduced with increasing radius of the centrifuge. It must also be noted that the inertial acceleration increases linearly with the radial distance from the axis of rotation. The implications of this can be neglected if the depth of the physical model is small with respect to the radius of the machine. It is usual procedure to conduct experiments at a constant rotational velocity and under these conditions the $\ddot{\theta}$ term (re. eqn. 2.10) is zero. Only when a model container is "spun up" or "spun down" will the $\ddot{\theta}$ term come into consideration. A centrifuge operator typically accelerates the centrifuge to the desired rpm slowly and also gently brakes the machine to a stop after the test has been concluded in order to minimize the effects of the $\ddot{\theta}$ term. The $\ddot{r}$ term can be neglected unless large movements in the model relative to the

centrifuge radius are anticipated during the conduct of the experiment. The Coriolis acceleration, $2\dot{r}\dot{\theta}$, is dependent on the term r when the rotational velocity $\dot{\theta}$ is a constant, as is typically the case since most experiments are performed at a constant g level. The term r represents the movement of individual particles with respect to the total mass of the material comprising the model. When this movement is slow, as it is in most soil mechanics applications, the Coriolis effect is of little consequence. For the majority of practical applications only the centrifugal acceleration, $r\dot{\theta}^2$, enters into the analysis of increased self weight in an inertial field.

The principal advantage of centrifugal modeling over other small scale physical modeling techniques is that it allows an assessment of the physical behavior of large structures whose response is stress state or gravity dependent using the same materials comprising the full scale structure. Centrifugal modeling can be used to evaluate a problem before field experiments are conducted or prototype behavior is predicted with an analytical model. The results obtained in centrifugal modeling experiments provide an opportunity to validate both the constitutive equations for material behavior and the theoretical basis for an analytical model. Sutherland (1982) has illustrated these advantages by means of a flow chart as shown in Figure 2.4.

Centrifugal modeling is especially useful when considering three-dimensional problems, even with complex geometries, since analytical modeling in this case can often be very expensive and time consuming, if not impossilbe. Commonly, when a three-dimensional problem is approached by analytical techniques, the problem must be simplified to

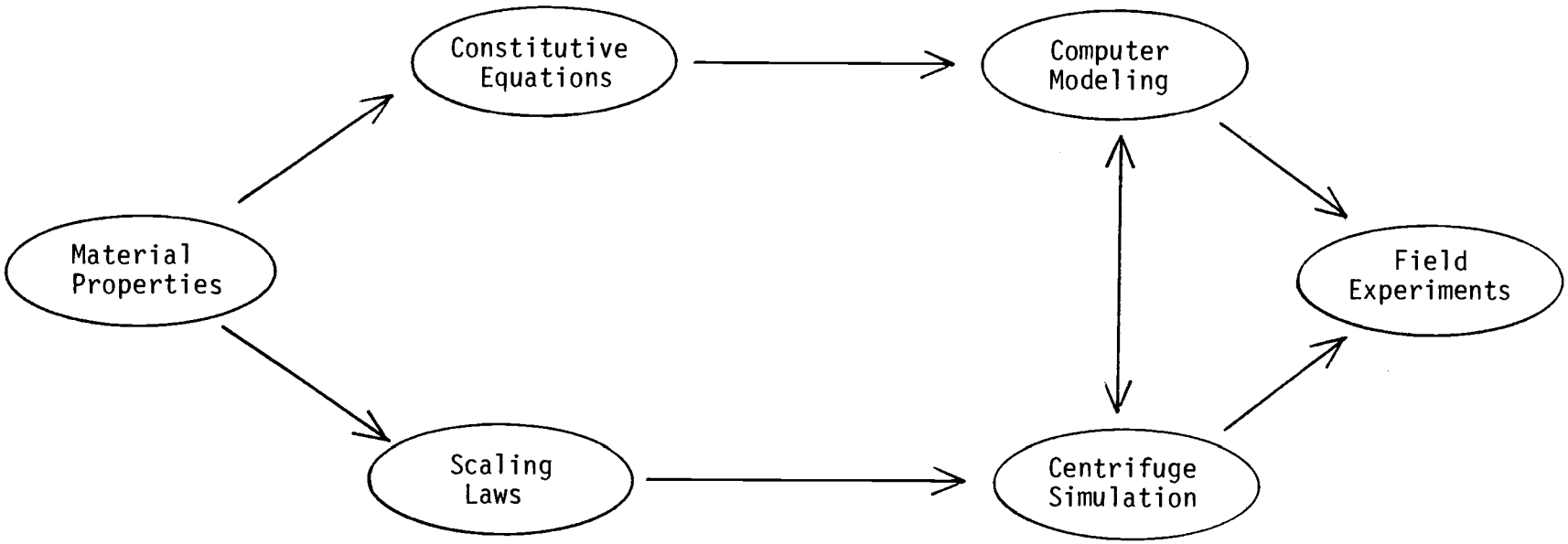

Figure 2.4 Flow chart representing the general philosophy of centrifuge model testing (after Sutherland, 1982)

two dimensions. Following this effort the results are extended to the three-dimensional case through approximations.

Centrifugal modeling also has the advantage that model behavior can be observed to failure. Analytical modeling is used to make predictions of prototype behavior and these predictions can only be verified by making observations of a physical model of the full scale structure. A knowledge of prototype behavior is difficult to obtain, especially when considering failures. Embankment dams illustrate this problem since they rarely fail. The analytical modeler can never be quite certain how conservative a design is or how accurately the factor of safety against failure has been predicted (Ko, 1982).

Scaling laws are important to centrifugal modeling. Al-Hussaini (1976) mentions two important laws of similarity, as follows:

1. "If soils with identical friction, cohesion, and density are formed into two geometrically similar bodies, one a prototype of full scale and one a model of 1/n scale, and if the 1/n scale model is accelerated so that the self weight increased by n times, the stresses at corresponding points are then similar if they are similar on the boundaries."

2. "Once the excess pore water pressure distribution has been made to correspond in model and prototype, all subsequent primary flow processes of pore water are correctly modeled after time t_m in the model that is less than time t_p in factor n, i.e., $t_m/t_p = 1/n^2$."

Scott (1975) presented a summary of scaling relationships for centrifugal model studies which is reproduced in Table 2.1.

Table 2.1 Scaling relations pertaining to centrifugal modeling (after Scott, 1975).

Quantity	Full Scale (Prototype)	Centrifuge Model at n g's
Linear Dimension	1	1/n
Area	1	$1/n^2$
Volume	1	$1/n^3$
Time: Dynamic Events	1	1/n
Hydrostatic Events	1	$1/n^2$
Viscous Flow	1	1
Velocity (distance/time)	1	1
Acceleration (distance/time^2)	1	n
Mass	1	$1/n^3$
Force	1	$1/n^2$
Energy	1	$1/n^3$
Stress (force/area)	1	1
Strain (displacement/unit length)	1	1
Density	1	1
Frequency	1	n

To ensure the consistency of centrifuge experiments over a range of inertial accelerations a 'modeling of models' investigation may be conducted. Modeling of models is a way to verify similitude between the model and full scale. This involves, for example, model tests at 1/20th scale and 20 g's, model tests at 1/50th scale and 50 g's, and model tests at 1/100th scale and 100 g's. If a reasonable correlation is found to exist between the test results at various scale then extrapolation to the full scale situation may be justified (Cheney, 1982).

Before embarking on an extensive investigation into any problem modeled on a centrifuge it is essential to establish the relationships between the variables that may enter into the problem and their significance. This can be accomplished in two ways, (1) by analyzing the differential equations that govern the phenomena, if the physics of the problem are well established, or (2) using dimensional analysis to determine a tentative list of groups which may be significant and then methodically investigate their individual contributions to the phenomena observed (Cheney, 1982).

Al-Hussaini (1976) has presented a summary of the limitations of centrifugal modeling for geotechnical applications as follows:

(1) The centrifugal acceleration in the model is directed radially outwards from the centrifuge hub and varies linearly with the radius from the center of rotation. In the case of the 1g full-scale structure, gravity exists essentially as parallel and vertical and does not vary with depth for practical purposes. This may cause some distortions in the model especially if the model depth is large with respect to the centrifuge radius or if

the plan view subtends a large arc with respect to the centrifuge circumference.

(2) Not only must the stress at each point in the model match the stress at corresponding points in the prototype but also the model and prototype must share similar overconsolidation pressures and stress and strain cycles. It may not be possible to reproduce complex ground conditions for centrifugal testing.

(3) Upon accelerating and deaccelerating from the test rpm the model undergoes a stress history that the prototype has not be subjected to.

(4) While primary consolidation in the model occurs at a rate according to $t_m/t_p = 1/n^2$ creep or secondary consolidation rates may not obey this same relation.

(5) When the macroscopic structure of a soil influences behavior it may not be possible to reproduce the proper size effects. An example would be the modeling of a fissured clay when the same matrix of macrocracks could not be reproduced in the model as exist in the prototype. Size effects in most normally or slightly overconsolidated clays, in sands, and silty soils may be ignored. Rockfills may be modeled by pulverizing, sieving, and mixing the materials to obtain a scaled down grain size and a similar gradation.

(6) Problems with boundary conditions and side friction are inherent to conventional soil testing and centrifugal modeling as well.

The limitations associated with centrifugal acceleration varying with the radius may be minimized with a large diameter machine and a model height less than 10% of the centrifuge radius. For this case the acceleration error will be less than ±5%. The stress history in a prototype may be approximated by the application or removal of surcharges in the centrifugal model. If a suitable sample can be obtained from a fairly uniform soil deposit, all of which has been subjected to the same stress history, then this may be used as the model material. Model cone penetrometer tests may be used in flight on a centrifuge to measure the actual soil properties. The effects of creep rate and secondary compression may be estimated from existing soil mechanics theories. It may not be possible to accurately model all grain size effects, but if the effect of grain size on model behavior is known independent of the centrifuge study then it may be possible to take these effects into account before predicting prototype behavior. With careful design and construction of a centrifugal model on a large centrifuge the boundary conditions of the prototype may be closely approximated.

2.4 Summary

Centrifugal modeling is a relatively new technique to study engineering problems that is beginning to gather momentum as a research tool in the United States. It compliments the established techniques of analytical modeling and field testing and has the advantage that three-dimensional problems with complex geometries can be considered. Further, models can be tested to failure and failure

mechanisms can be established. Centrifugal modeling relies on the equivalence of gravitational and inertial fields to establish the proper self-weight effects of model materials.

A centrifugal modeling program must include an investigation of the importance of the variables that influence the problem. This may be accomplished considering the differential equations that govern the phenomena or utilizing dimensional analysis and methodically testing the significant PI groups (re. section 6.3).

The centrifugal modeling technique has some limitations but the investigator can with some imagination and creativity avoid potential problems or, alternatively, account for differences observed between model and prototype behavior.

3.0 ICE FORCES ON STRUCTURES

3.1 General

A qualitative discussion of the arctic offshore environment and the types of structures proposed for service in that environment is given to serve as an introduction to the problem of determining ice forces and ice floe failure mechanisms. A review of the previous approaches used to quantify the freshwater ice forces on a vertical pile is presented followed by a discussion of the important parameters which influence the problem. Considerations of scale are given to simplify the extrapolation of small scale data to the full scale situation and a summary of the theoretical and experimental results available for comparison with and validation of centrifugal model studies follows.

3.2 Problems of the Offshore Arctic

The offshore arctic environment is hostile. The coastal strip of the Beaufort Sea remains ice free for only about 3 months out of the year. Shinde and Wards (1982) describe the typical extent of sea ice in the arctic.

> "New ice formation in the Southern Beaufort Sea begins in late September or early October. It initially forms near the shoreline and extends slowly seawards. The rate and direction of growth is dependant on meteorological conditions. As the winter progresses the ice sheet between the shoreline out to the 20 meter depth contour becomes landfast. The landfast ice is so termed because it's motion is reduced by it's boundary with land. This ice can reach a thickness of 2.2 meters by the end of the winter. The area known as the shear zone lies between the landfast ice and the polar pack. This zone is characterized by extensive ice movements and deformations."

Sea ice is a nonhomogeneous and anisotropic material. Sea ice crystals begin to form when the air temperature drops below the freezing point of seawater. The crystal orientation is somewhat random when the freezing process is initiated and the crystals exhibit a small grain size. This transitions to the favored orientation of a vertical c-axis and a larger crystal size as freezing continues. Brine pockets are trapped within the crystal matrix and brine volume is an important parameter determining the sea ice strength (Weeks, 1976). A typical section through an ice sheet is shown in Figure 3.1.

Topographical features of the arctic ice sheet include pressure ridges and zones of ice which have survived the summer melt. Pressure ridges are formed when ice floes move against each other and fail in compression. Zones of multiyear ice are stronger than the surrounding first year ice because in the summer fresh melt water flushes out some of the brine pockets.

Gravel islands have been successfully employed in areas of shallow water for exploration purposes. The plan and profile view of a typical gravel island is shown in Figure 3.2. Monopod and cone type structures have been proposed for use in areas of deeper water, and an example of this type of design is shown in Figure 3.3. Semisubmersible rigs have also been proposed due to their worldwide success in more temperate waters (Noble and Singh, 1982).

The failure modes of a moving ice sheet surrounding an offshore structures may be categorized as: (1) crushing failure, (2) bending failure, (3) buckling failure, or (4) a combination of crushing, bending, or buckling. Maattanen (1983) has presented a summary of the present understanding of the various failure modes.

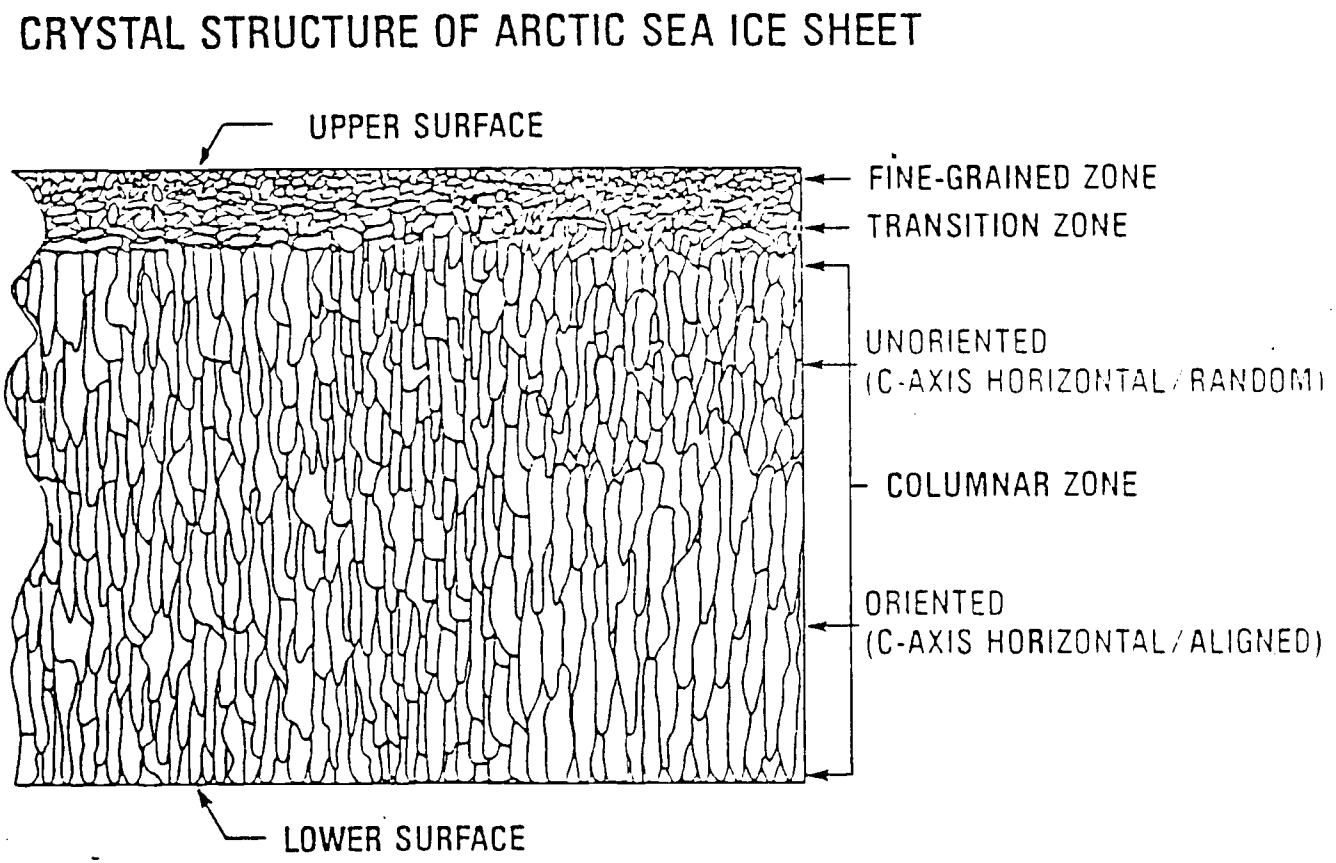

Figure 3.1 Crystal structure of an arctic sea ice sheet (after Wang, 1979).

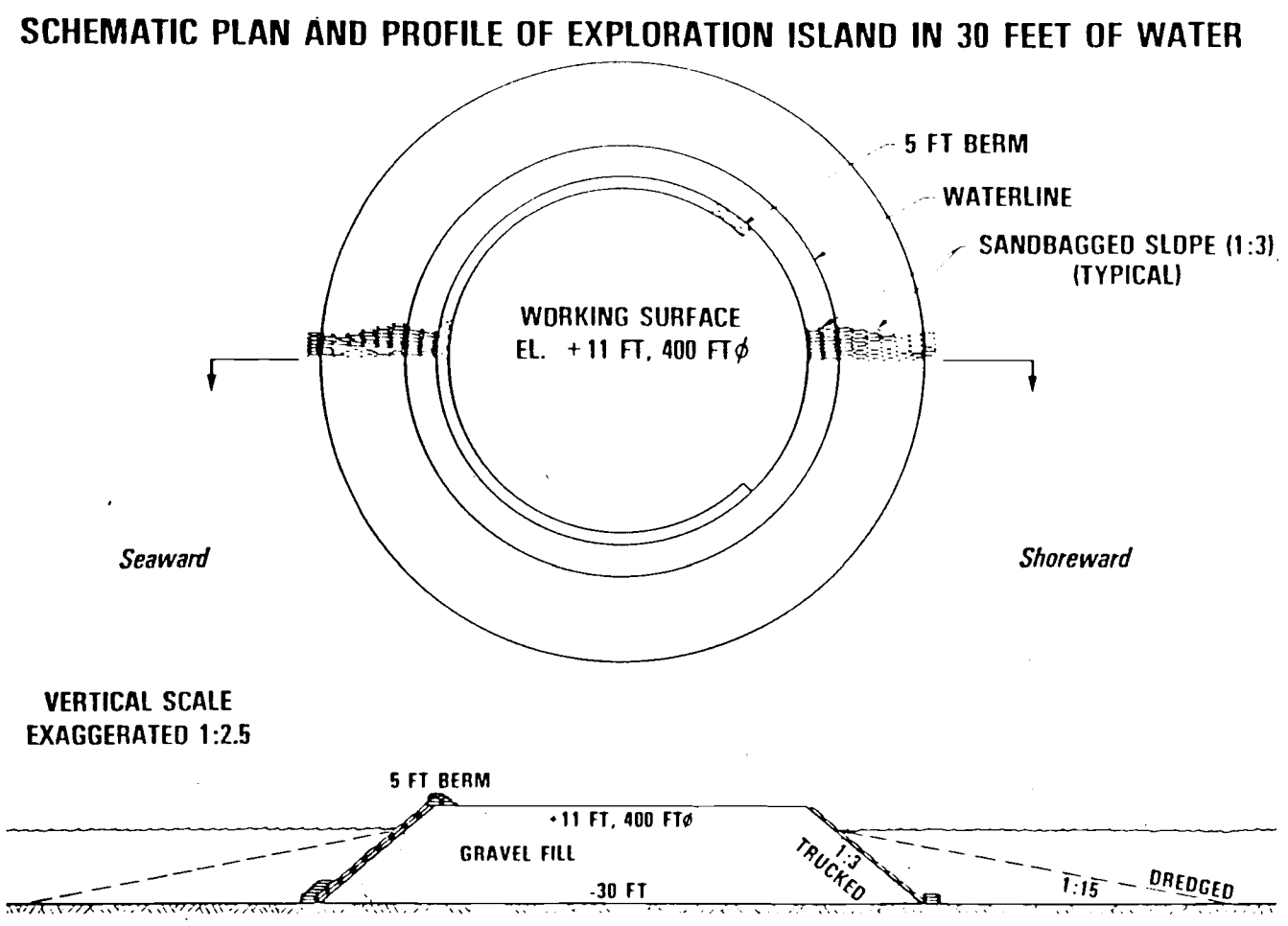

Figure 3.2 Schematic plan and profile of exploration gravel island in 30 feet of water (after Jahns, 1979)

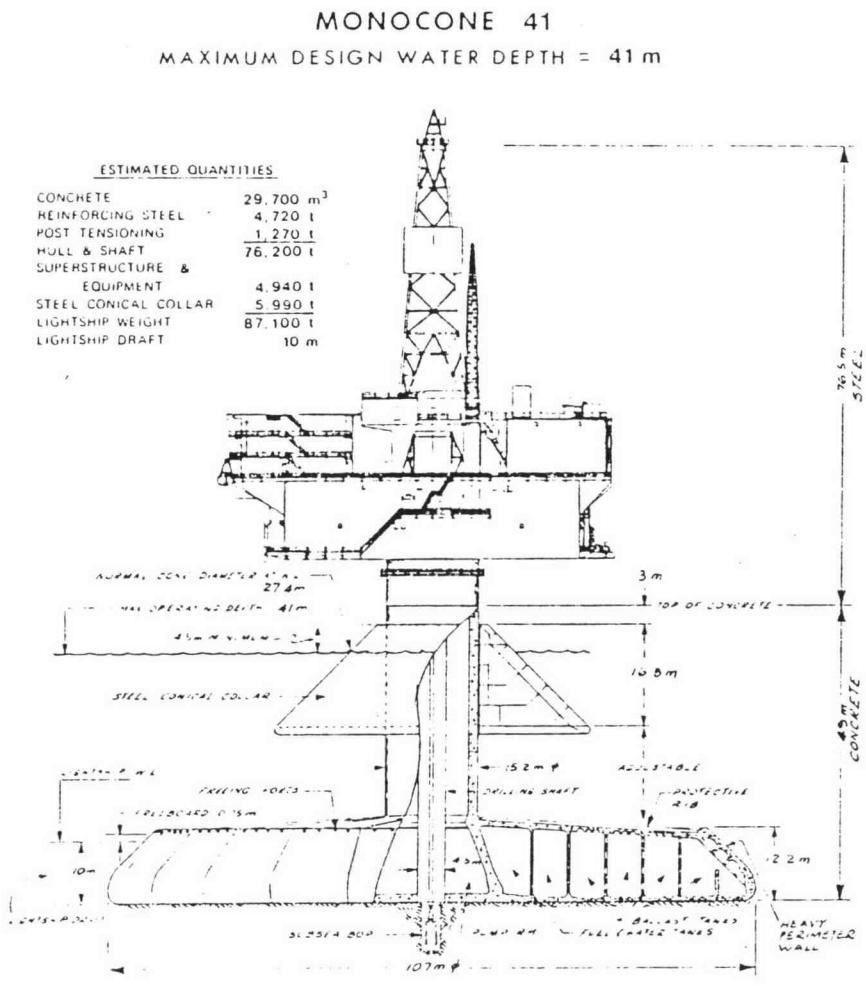

Figure 3.3 Monocone drilling rig proposed for service in arctic offshore waters (after Jazrawi and Khauna, 1977)

Crushing is exhibited when ice moves against a vertical or near vertical surface. This situation is illustrated in Figure 3.4. The crushing force is directly proportional to the product of the compressive strength of ice and the contact area, that is:

$$F = k\sigma_c dt \tag{3.1}$$

where: F = crushing force

σ_c = ice compressive strength

d = diameter of structure

t = ice thickness

k = a coefficient that depends on the structure shape, contact efficiency, the ratio of ice thickness to structure diameter, and the ice velocity.

The ice compressive strength is defined as the strength measured when ice fails against an infinitely wide structure. This condition is impossible to achieve since a uni-directional stress state would exist in the ice and, therefore, the ice would fail in buckling. Uniaxial compressive strength tests have been adopted to characterize the compressive strength of ice after correction factors have been applied to account for the difference in scale between the specimen and the infinite width condition.

It is important to note that when ice fails around a structure a three-dimensional state of stress is established in the ice sheet. Further complications to the problem include local shearing of wedges at the top and bottom of the contact face, crack propagation, forces associated with pushing the ice rubble to either side of the

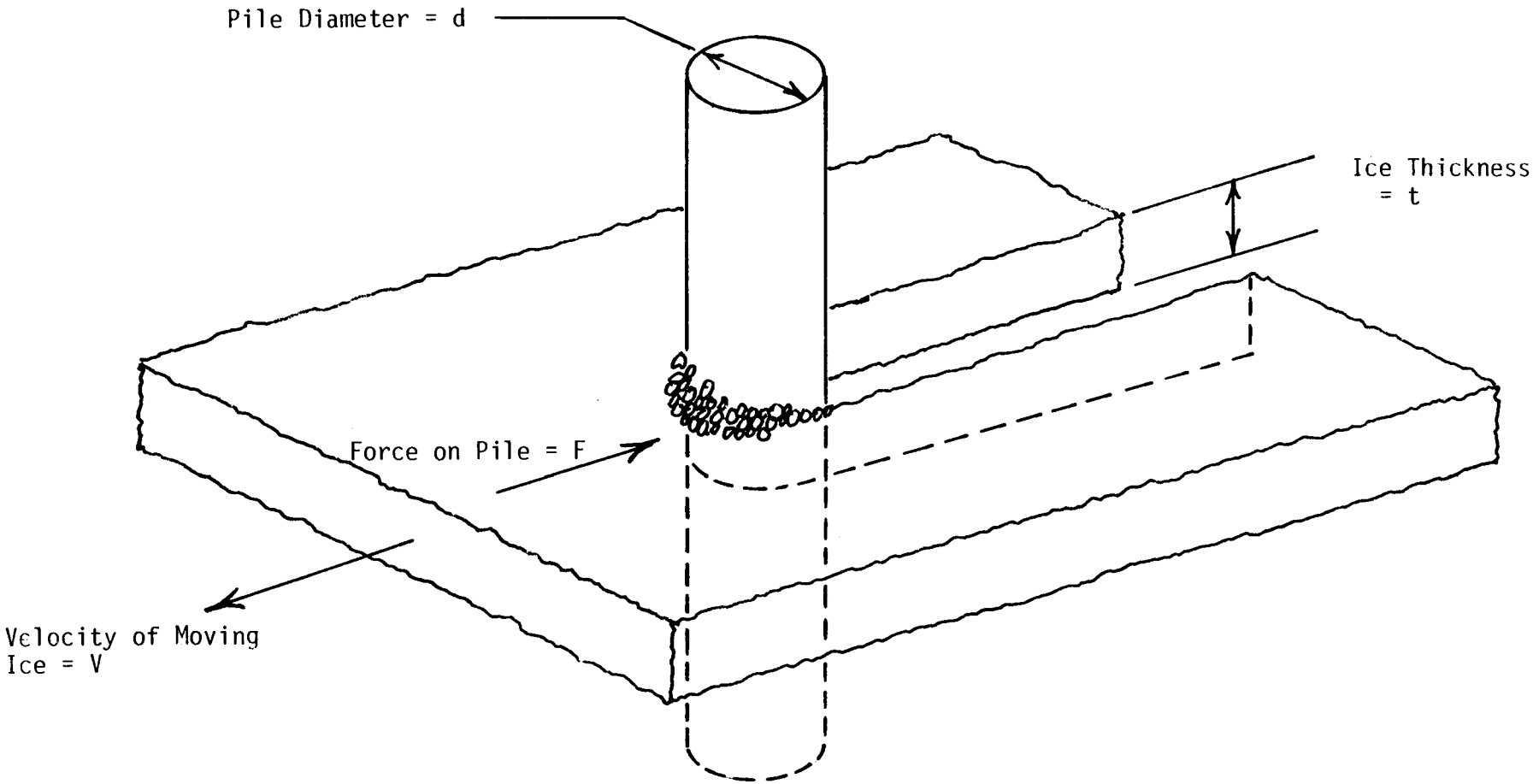

Figure 3.4 Ice crushing failure against a vertical cylindrical pile (after Maattanen, 1983).

structure, and non-homogenieties in the ice as continuous crushing occurs. The compressive strength of ice is dependent on the loading rate and the ice temperature. When ice fails in front of a wide structure the failure is initiated in different zones at different times and results in a reduction of the maximum ice force.

A bending failure occurs when ice fails around a conical structure. This situation is depicted in Figure 3.5. Examples of other geometries which produce a bending failure include bridge piers with a sloping leading edge, inclined piles with a sloping leading edge, and artificial islands with a sloping beach. There are some advantages to adopting a sloping contact face since the bending strength of ice is usually less than half of the compressive strength.

When an ice sheet moves against an inclined face, horizontal and vertical components of force result. The ice will ride up the inclined face if the vertical component of the causing force is greater than the sum of the gravity and resolved frictional forces. A conical structure will initiate radial cracks in the ice sheet and circumferential cracks will occur as the cantilevered ice section fails in bending. When an ice sheet is against a wide planar structure, such as an artificial island, the same pattern of radial cracks is not observed. Frictional forces and forces required to push the ice rubble up the slope complicate the analysis. In the case of artificial islands extensive rubble fields in front of the structure are created and the failure zone can be relocated from the ice-structure interface to the contact zone between the rubble and the unbroken ice.

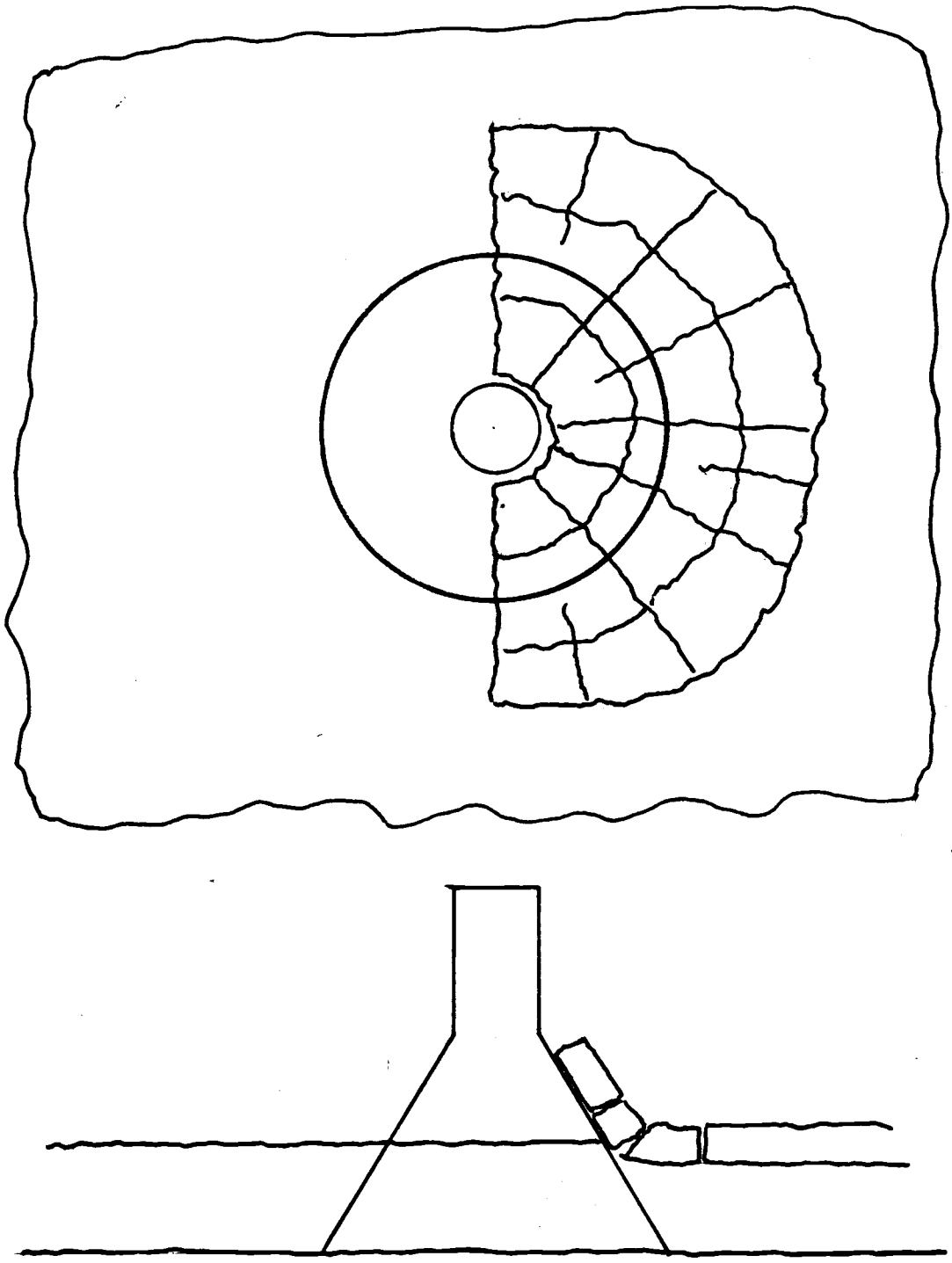

Figure 3.5 Plan and profile view of ice bending failure against a conical structure (after Maattanen, 1983).

Considerations of dynamic effects complicate the characterization of both the compressive and bending modes of failure. Large vibrations have been observed when ice fails around certain types of structures. The force an ice sheet exerts on a structure is dynamic whenever the fluctuations of the force occur in time periods less than the natural periods of vibration of the lowest structural modes. The dynamic response of the structure can be expressed in matrix formulation as:

$$[K]\{\delta\} + [D]\{\dot{\delta}\} + [M]\{\ddot{\delta}\} = F(t) \qquad (3.2)$$

in which,

[K], [D], and [M] are the stiffness, damping, and mass matrices of the structure respectively,

$\{\delta\}$, $\{\dot{\delta}\}$, $\{\ddot{\delta}\}$ are the displacement, velocity, and acceleration of the structural degrees of freedom and

F(t) is the forcing function

The uncertainty in characterizing the dynamic response is associated with establishing F(t) , since methods for obtaining the other quantities are well established from other structural dynamics applications, such as the design of earthquake resistant structures.

3.3 Previous Approaches Used to Determine Ice Forces

The available literature for comparison of freshwater ice failure forces on vertical cylindrical structures is somewhat limited since greater attention has been given to the saline ice problem. (See Haynes et al. (1983), Kato and Sodhi (1983), Lewis (1982), Maattanen (1983), Nakajima, Koma, and Inoue (1981), Nevel, Perham, and Hogue

(1977), Noble and Singh (1982), and Saeki and Ozaki (1983), for a further discussion of the saline ice problem.)

Most investigators have started with the assumption that the maximum pressure that ice can exert on a vertical structure is limited by the compressive strength of the ice. Several methods have been employed to determine the compressive strength of representative ice specimens. To date, however, no standardized method has been adopted.

Previous investigations to determine the forces exerted by freshwater ice on vertical structures may be categorized as: (1) small scale laboratory coldroom tests, (2) medium scale tests on freshwater lakes, and (3) large scale tests on instrumented piles.

Kry (1981) described a small scale coldroom laboratory test program. This included:

> "...installing machined ice sheets 1 m wide and 0.5 m high in a constraint system which prevented buckling and simulated the elastic properties of a semi-infinite ice sheet, the constraint system was mounted on the lower platen of a testing machine and semi-cylindrical indentor fastened to the upper platen was forced into the ice sheet at a constant rate."

Kry (1981) and Taylor (1981) used a similar, if not identical, apparatus for their freshwater field tests on Eagle Lake, near Calgary, Alberta, Canada. The test apparatus is shown in Figure 3.6. Taylor considered both round and flat indentors, while Kry was concerned with only round indentors. Both testing programs involved sawing test "ponds" in the lake ice and allowing the ponds to refreeze. A portable gantry equipped with "jack-up legs" was towed into position to suspend hydraulic rams used to fail the refrozen ice with either flat or semi-circular indentors. The original lake ice was used to supply the reaction face for the hydraulic rams. Various

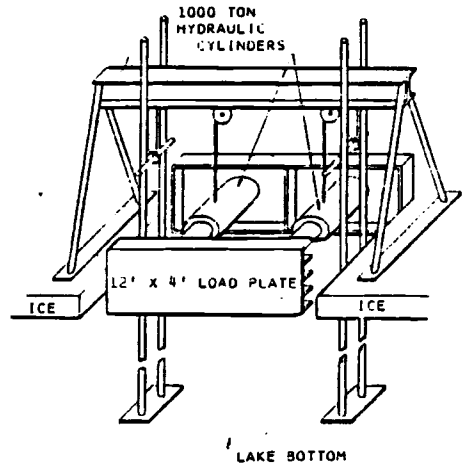

Figure 3.6 Schematic of hydraulic lake ice tester (after Kry, 1981).

widths and diameters of indentors, ice thicknesses and penetration velocities were considered. The experimental results obtained in the Kry study and in the Taylor study which pertain to a circular pile are shown in Table 3.1. Included are measurements of ice thickness, pile diameter, penetration velocity, ice temperature, and the maximum pressure that the ice exerted on the pile.

Schwarz (1970) conducted large scale tests on an instrumented pile during the winters of "1967/68 and 1968/69 at the pile of a bridge, which crosses the tidal estuary of the Eider River during the construction of a tidal barrier." The ice forces which were measured are the result of the following situation:

> "Along the entire German coast of the North Sea and also just outside the estuary of the Eider lie large flat areas (Wadden ground), where the fields can grow very quickly. These ice fields float up only at higher tides and then drift with the tidal currents against the bridge, where the ice fields are cut up by the piles."

The 60 cm diameter instrumented pile consisted of a shield containing 50 pressure cells, in 5 rows and 10 columns, halfway encompassing the pile and located on the seaward face. Although the forces measured on the instrumented pile were associated with saline ice some of the conclusions reached in the study are applicable to the freshwater ice problem and will be discussed later.

Schwarz provides only an empirical equation describing his observations and not the data which substantiates this relationship. The relationship he proposes is as follows:

$$P = [A\ B(\sigma_o + C\alpha(t_L - t_w) + D(n-E)]\ h\text{-}b \qquad (3.3)$$

in which:

P = ice pressure exerted on the pile

A = coefficient of contact = 0.5

Table 3.1 Results of the Kry and Taylor study for circular piles.

Researcher	Ice Thickness, t		Pile Diameter,d		Penetration Velocity,v		Ice Temperature,T	Maximum Ice Pressure, P_{max}	
	(in)	(cm)	(in)	(cm)	(in/min)	(cm/min)	(°C)	(psi)	(MPa)
(1)	(2)		(3)		(4)		(5)	(6)	
Kry	1.01	2.57	5	12.7	0.49	1.24	-2.0	580	4.00
Kry	1.00	2.54	10	25.4	0.48	1.22	-2.0	420	2.90
Kry	1.00	2.54	5	12.7	0.48	1.22	-10.0	435	3.00
Kry	1.01	2.57	5	12.7	0.30	0.76	-10.0	870	6.00
Kry	0.98	2.49	10	25.4	0.29	0.74	-10.0	565	3.90
Kry	0.40	1.27	5	12.7	0.30	0.76	-10.0	493	3.40
Kry	0.50	1.27	5	12.7	0.30	0.76	-10.0	754	5.20
Kry	0.50	1.27	5	12.7	0.15	0.38	-10.0	667	4.50
Kry	11.9	30.2	48	122	0.50	1.27	-2.0	435	3.00
Kry	11.7	29.7	48	122	1.40	3.56	-2.0	348	2.40
Kry	10.5	25.9	48	122	4.45	11.3	-2.0	408	3.50
Kry	9.29	23.6	48	122	11.2	28.5	-2.0	363	2.50
Taylor	32.0	81.3	12	30.5	4.80	12.2	-2.0	515	3.55
Taylor	31.0	78.7	24	51.0	5.40	15.3	-2.0	510	3.52

B = coefficient of form = 0.66

σ_o = cubic compressive strength of ice at 0°C and at a strain rate of 3×10^{-3}/sec

C = coefficient at temperature = 0.35

α = rate of change of strength with respect to temperature

$(t_L - t_w)$ = temperature difference across the ice sheet

D = coefficient relating to the ratio of ice thickness to pile width = 12.5

n = ratio of ice thickness to pile width

h = ice thickness

b = pile width

Lipsett and Gerard (1980) measured ice forces against instrumented bridge piers on Canadian rivers during the spring breakup. Their instrumented pier at Pembridge was vertical and cylindrical. The situation in which their ice forces were generated is different than those considered in this study. The ice forces which they measured are a result of smaller ice floes impacting the pier while they are carried by the river current, whereas the ice forces measured in this study are the result of the movement of a surrounding semi-infinite ice sheet failing against a pile. Their results are provided, however, in the hope that they may provide further insight into the general problem of ice forces on a circular pile. Their results which include a measurement of floe velocity are given in Table 3.2

Table 3.2 Events at Pembridge

Event	Pile Diameter, d		Ice Thickness, t		Floe Velocity, v		Maximum Ice Force, F_{max}	
	(in)	(cm)	(in)	(cm)	(m/sec)	(cm/sec)	(lbs)	(kN)
(1)	(2)		(3)		(4)		(5)	
P74.04.17.22.07.28	33.86	86.0	17.72	45.0	40.97	104	78,700	350
.22.10.16	33.86	86.0	17.72	45.0	51.97	132	182,000	810
.22.13.07	33.86	86.0	17.72	45.0	49.21	125	128,000	569
.22.14.31	33.86	86.0	17.72	45.0	62.99	160	115,000	512
.22.40.05	33.86	86.0	17.72	45.0	70.87	180	117,000	520
.22.41.50	33.86	86.0	17.72	45.0	75.80	190	124,000	522

3.4 Important Parameters

A review of the available literature indicates that the important parameters influencing the force that an ice sheet exerts on a vertical cylindrical pile include:

(1) pile diameter

(2) ice thickness

(3) penetration velocity

(4) ice temperature

(5) grain size and orientation

(6) ice strength

The product of the ice thickness and pile diameter is referred to as the projected area. An examination of Equation 3.1 reveals that ice force is directly proportional to the product of ice compressive strength and projected area. The ratio of pile diameter to ice sheet thickness is known as the aspect ratio and influences the constant of proportionality between ice force and the product of projected area and compressive strength. Kry (1981) refers to the ratio of ice force to projected area as effective ice pressure.

The penetration velocity with which the pile is driven into the ice sheet determines the strain rate associated with the ice failure. Kry (1981) reports that there is no generally agreed upon relationship between penetration velocity and strain rate. Relationships have been suggested including non-dimensionalizing velocity with either ice thickness or pile diameter. Kry (1981) presents his results in terms of strain rate defined as the ratio of penetration velocity to ice

sheet thickness. Since Kry's results represent the most considerable body of data with which to compare the results of this investigation, the definition of strain rate as the ratio of penetration velocity to ice thickness has been adopted herein.

Ice temperature is known to influence the strength of both fresh and saline ice. Schwarz (1970) reports that as ice temperature decreases from 0°C to -20°C the strength of ice increases at a nearly linear rate. The increase in strength with decreasing temperature is greater for freshwater ice than for saline ice.

Grain size and crystal orientation are also known to influence the measured ice force. The direction of the C-axis in ice is used to specify the crystal orientation. Taylor (1981) indicates that the results from his field testing indicate that ice with a horizontal C-axis is much stronger than ice with a vertical C-axis. Results from his laboratory determinations of compressive strength indicate the opposite. This leads Taylor to believe that it is reasonable to suppose that the number of grain boundaries in a specimen or at the contact face strongly affects the measured strength. Weeks (1969) found that as the cross-sectional area of a specimen is increased and, hence, represents a greater number of crystals, unconfined compressive strength decreases.

Schwarz (1970) in conjunction with his instrumented bridge pile work determined the variation of compressive strength with respect to temperature, strain rate, and direction of applied pressure from compression tests on cube specimens of fresh and saline ice . The results of his investigation for the case of freshwater ice are reproduced in Figure 3.7. The force an ice sheet exerts on a vertical

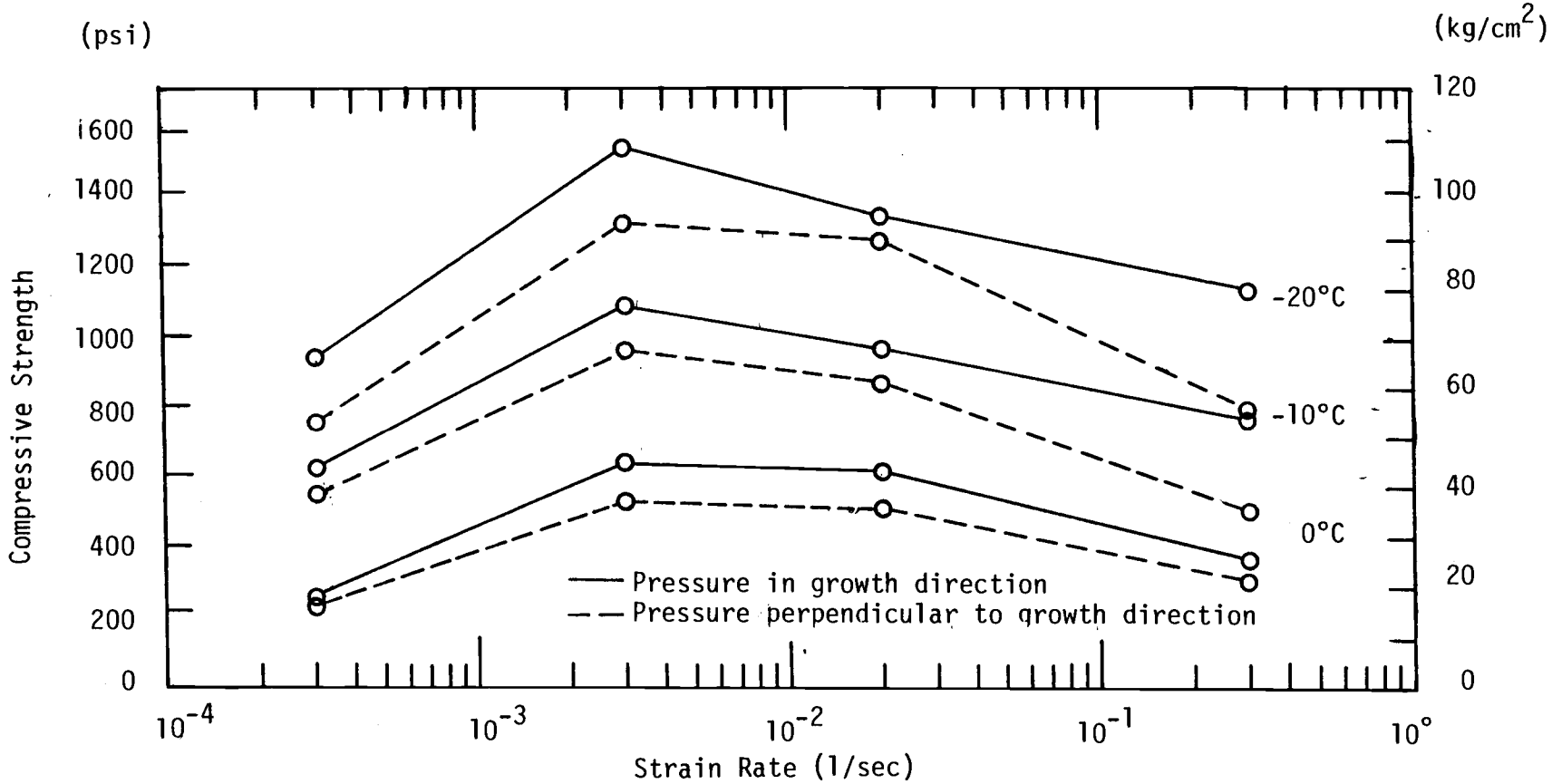

Figure 3.7 Compressive strength of ice versus strain rate as a function of temperature and direction of applied pressures (after Schwart, 1970).

pile depends on the compressive strength perpendicular to the direction of growth.

The force that an ice sheet exerts on a vertical cylindrical pile is believed by many researchers to be a function of the aspect ratio. Iyer (1983) shows one such relationship between normalized indentation pressure (the ratio of effective ice pressure to ice compressive strength) and aspect ratio in Figure 3.8. Lipsett and Gerard (1980) show a similar relationship after Neill (1976) in Figure 3.9.

It is obviously necessary to extrapolate the results from small scale tests and modeling to the full-scale field condition. Iyer (1983) discusses scale effects for freshwater ice and round indentors. Review of the currently available data reveals that brittle ice exhibits size effects similar to those observed with rock and coal. Although the reasons are not completely understood an increase in size results in a decrease in strength. Iyer presents a relationship for the decrease in the effective pressure as $a^{-0.6}$, where a is defined as the square root of the projected area. This relationship is in close agreement with strength decreasing as $a^{-0.5}$ in other materials. The data which substantiates this relationship for ice is shown in Figure 3.10.

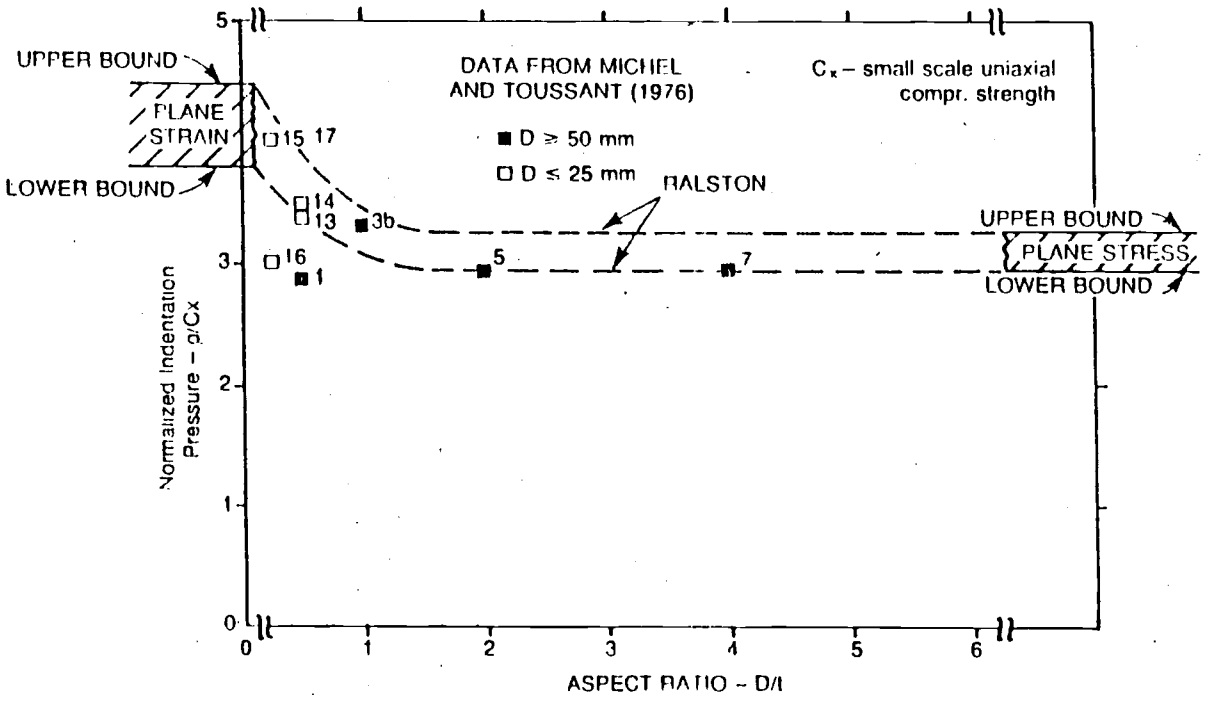

Figure 3.8 Normalized indentation pressure versus aspect ratio (modified after Iyer, 1983).

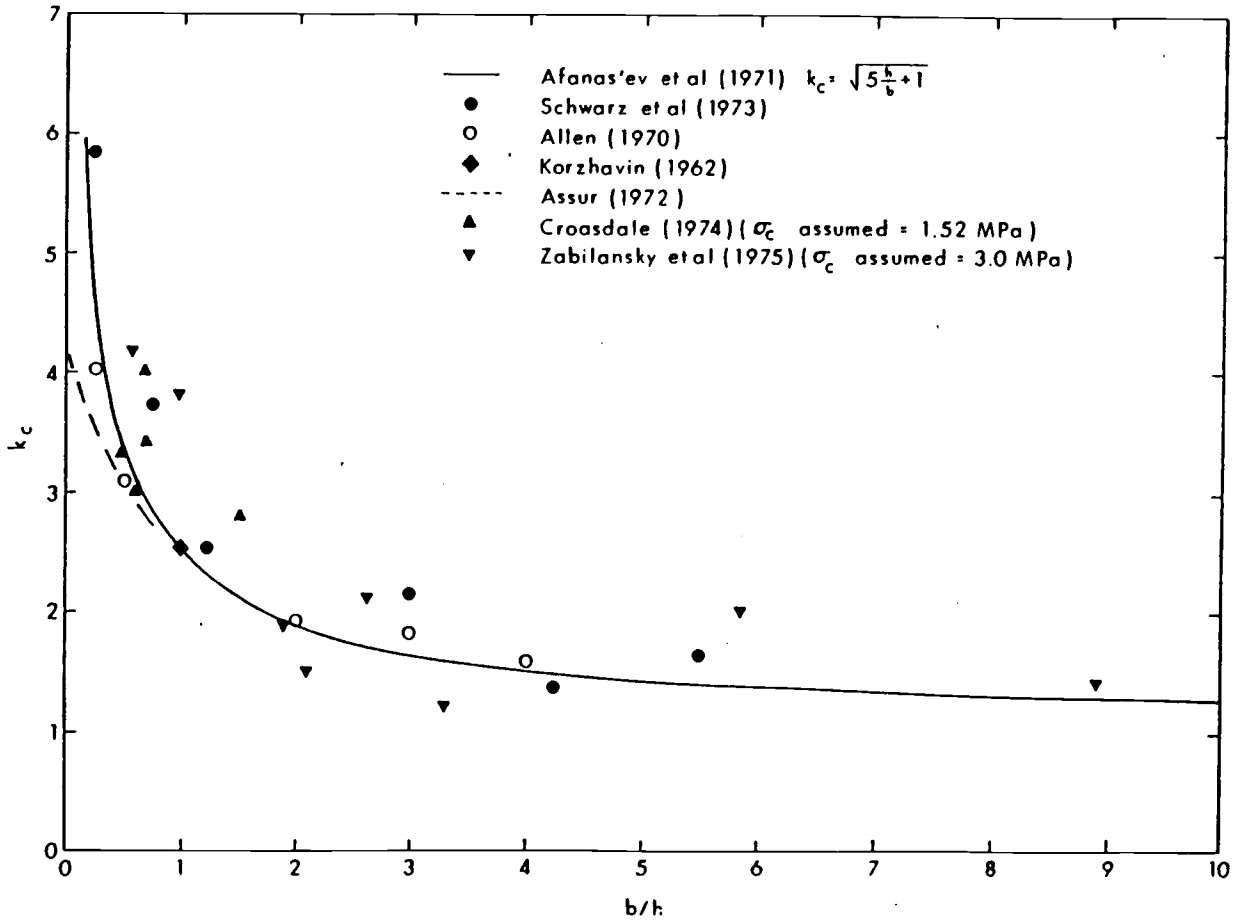

Figure 3.9 Normalized ice pressure versus aspect ratio (after Neill, 1976).

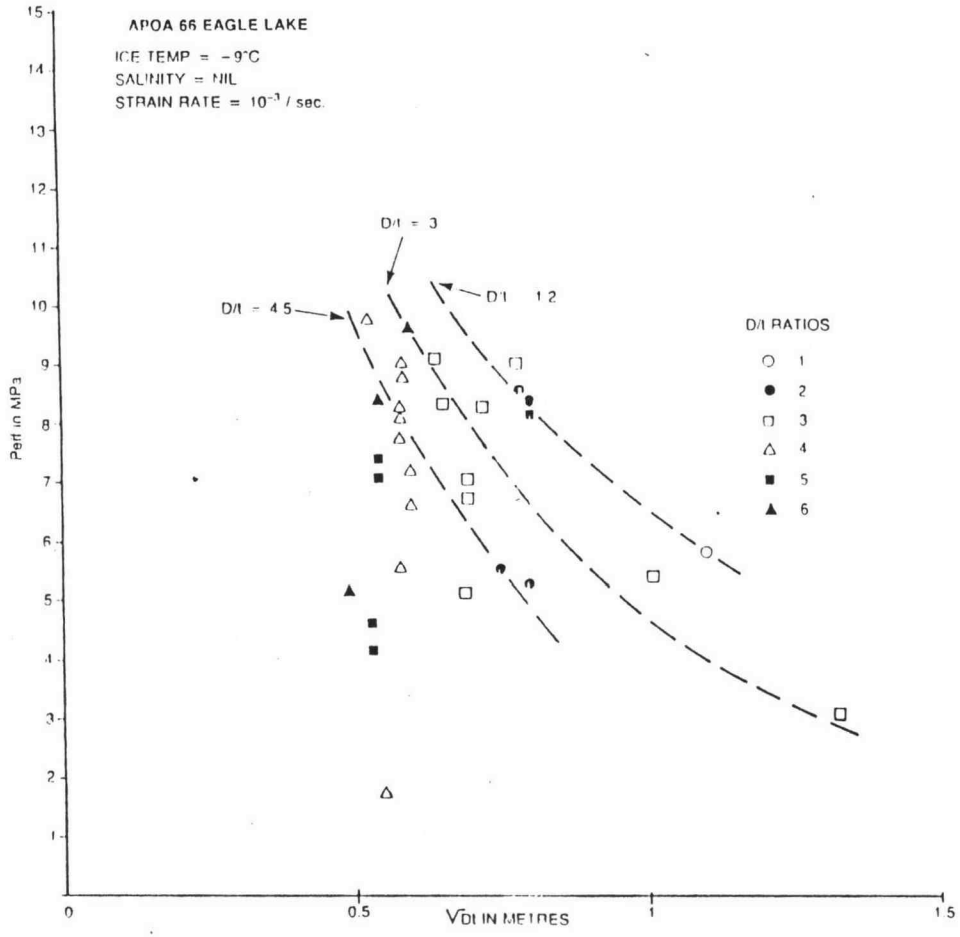

Figure 3.10 Effective ice pressure versus contact dimension (after Iyer, 1983).

4.0 EXPERIMENTAL APPARATUS

4.1 General

A test system was developed to physically model the ice forces on a single vertical pile in gravity and inertial environments from 1 to 50 g's. The components of the system included: (1) an environmental model container in which ice sheets could be created and subsequently failed in flight on the Boeing 66 g-ton centrifuge, and (2) the instrumentation required to observe, control, measure, and record the freezing process and the failure phenomena. The development of the test system and experimental techniques served three purposes as follows: (1) to demonstrate that ice mechanics problems could be addressed with the centrifugal modeling technique, (2) to investigate the gravity dependence of the ice force and ice floe failure mechanisms on a single vertical pile, and (3) to serve as a "proving ground" for ideas that may be incorporated later in the development of a larger environmental model container for use at the National Geotechnical Centrifuge Facility.

4.2 Design Requirements

To investigate ice forces and ice floe failure mechanisms on a single vertical pile, it was necessary to construct an environmental model container in which a uniform ice sheet could be created and failed, under a controlled rate of deformation condition, while in flight on the Boeing 66 g-ton centrifuge. During the test it was necessary to measure the ice force, deformation rate, air, water, and

ice temperatures. The ability to photograph the ice sheet failure in flight was also desirable. The Boeing centrifuge was equipped with a pair of remotely controlled cameras at the centrifuge hub for photogrametric observation of experiments. The overall dimensions of the environmental model container were limited to 19½ x 19½ x 11 in. (49.5 x 49.5 x 27.9 cm) to be compatable with the swinging container buckets of the Boeing centrifuge. All electrical and hydraulic connections for control and instrumentation were required to pass through the 26 electrical slip rings and one hydraulic slip ring located at the centrifuge hub. All components of the environmental model container had to be able to withstand the high inertial forces they would experience in service and needed to be both corrosion and water resistant.

4.3 Design Development

The two principal problems to be solved in designing the environmental model container were (1) to create an ice sheet and (2) fail the sheet with a pile driven at a controlled rate of deformation, while in flight on the Boeing 66 g-ton centrifuge. A liquid nitrogen system was employed to form an ice sheet in flight. The system relied on heat transfer occurring in the lines between the liquid nitrogen tank and model container to warm the liquid to vapor. This nitrogen vapor supplied the cold atmosphere above the water necessary to form an ice sheet. The use of liquid nitrogen offered several advantages that a conventional refrigeration system did not. These advantages included: (1) the working fluid was inert, (2) the fluid could provide

a large cold side temperature, (3) the system required no return line, (4) the refrigerant flow could be easily controlled with a solenoid valve, and (5) no special refrigeration equipment was required.

Failing the ice sheet in flight presented a significant problem. The ice failure could be initiated by either forcing the ice against the pile or by forcing the pile against the ice. Since it is believed that the ice forces depend on the relative velocity between the ice and the pile, and not the frame of reference from which the event is observed, a system to force the pile against the ice was designed because it offered the greatest mechanical simplicity. An electric motor was used to power a lead screw assembly which drove the pile through the ice. The motor speed was controlled with a tachometer feedback loop.

4.4 Environmental Model Container

The environmental model container that was used in this study is pictured in Figure 4.1. The essential components include: (1) the container, (2) drive motor and lead screw assembly, (3) instrumented model pile and linear variable differential transformer (LVDT), (4) nitrogen nozzle system, (5) circular boundary condition ring, (6) thermistors, (7) retrievable cover and latch system, and (8) stereo-photo calibration blocks.

The container was constructed from ½ in. (1.27 cm) thick 6061-T6 aluminum plate. All mating surfaces were sealed with silicon caulk and connected with ¼ in. x 20 x 3/4 in. stainless steel allen cap screws. The container was designed considering the hydrostatic load

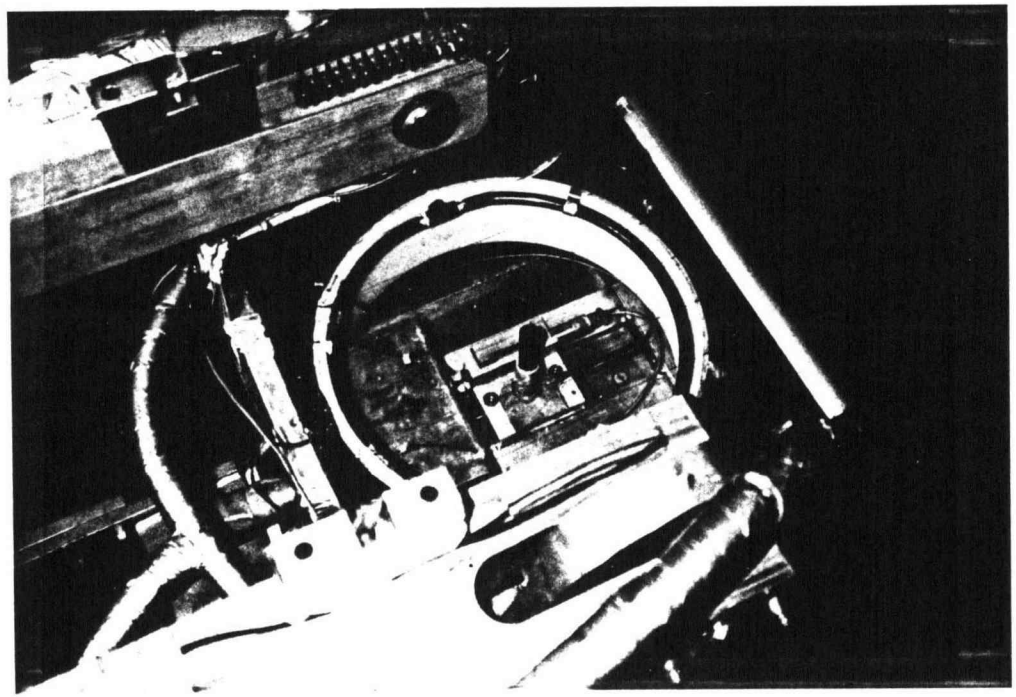

Figure 4.1 Environmental model container on board the Boeing 66 g-ton centrifuge.

associated with a 9 in. (23 cm) water depth in a 100 g inertial field. The container was lined with ¼ in. (0.635 cm) thick acrylic plastic sheet and surrounded on the outside with 1 in. (2.54 cm) thick polystyrene for insulation.

The electric drive motor was a 1/3 hp, variable speed, DC motor with a 100 to 1 gear ratio and a tachometer feedback loop control. It was manufactured by ElectroCraft Corporation of Hopkins, Minnesota, under model #552-004-113. The lead screw assembly was equipped with a single, 20 threads per inch, lead screw and a special modified base with babbit pads and bronze bearings. It was manufactured and modified by Velmex, Inc. of Bloomfield, New York under Unislide model #3-6000. When coupled, the motor and lead screw were capable of developing a rated maximum force of 300 lbs and could resist a 320 in.-lbs. moment at the slide base while moving the pile at speeds of .005 to 2.5 in. per minute (.013 to 6.35 cm per minute). The drive shaft passes through the container wall by means of a bearing and seal. A coupler which tolerates misalignment joins the motor and lead screw.

The instrumented pile assembly consisted of 1 in. (2.54 cm) diameter 6061-T6 aluminum rod stock fixed to a base plate with a threaded hole at the top to accept different diameter micarta model piles. The cantilever pile was instrumented at the base with strain gages sealed with a waterproofing compound. Micarta was used for the various diameters of model piles because it is a better thermal insulator than aluminum and consequently minimized the formation of a thicker section of ice at the ice and pile interface caused by heat conduction. An LVDT was fixed to the base of the pile and the wall of

the container to locate the position of the pile and monitored the deformation rate during an experiment.

The nitrogen nozzle system consisted of ½ in. (1.27 cm) O.D. copper refrigeration tubing with 1/16 in. (0.16 cm) holes spaced at 1 in. (2.54 cm) intervals around the interior of the ring to project the nitrogen vapor flow radially inward across the water surface. The vapor flow entered the ring at two "T" connections located on opposite sides of the model container. Another "T" connection outside the container, was connected to the single umbilical line from the hydraulic slip ring at the centrifuge hub.

A circular boundary condition ring at the water surface provided a boundary condition which was believed to be superior to a square boundary (from an analytical viewpoint). The circular ring was constructed of cold rolled, ¼ in. (0.64 cm) thick, 6061-T6 aluminum plate lined with a ¼ in. (0.64 cm), heat formed, plastic liner. The plastic liner was employed to reduce heat transfer in the ring and reduce the likelihood of an increased thickness of ice at the ring boundary.

Two thermistors were located in the atmosphere above the water, two in the water, and two floating just under the surface of the water, to monitor atmosphere, water, and ice temperatures, respectively. The thermistors in the atmosphere were part of a feedback loop used to control the nitrogen flow to provide a nearly constant cold side temperature.

A retrievable cover and nichrome burn wire latch was designed to keep the cold nitrogen vapor atmosphere against the water surface

during the freezing processes. The cover could be opened to allow stereo photography of an experiment by remote controlled cameras located at the centrifuge hub. The retrievable cover was constructed of a 10 mil mylar sheet and was supported beneath with tensioned piano wire guides to prevent the mylar sheet from collapsing into the box in flight. The mechanism used to retrieve the cover operated on the same principle as a roller window shade (without the ratchet used to hold a window shade down). A nichrome burn wire was fused with an electrical current to open the cover.

Stereo calibration blocks were located in the upper corners of the container above the water surface to provide known control points for future photogrammetric interpretation of ice failure events.

4.5 Test Instrumentation and Control

During an experiment it was necessary to measure or control: (1) pile velocity and position, (2) ice force, (3) air, water, and ice temperatures, and (4) nitrogen flow.

The pile velocity was governed with the tachometer feedback loop motor controller. This automatic system regulated the drive motor during varying ice loads to provide a constant deformation rate. The tachometer readout allowed the desired pile velocity to be established before conducting a test owing to the linear relationship between pile velocity and motor rpm. An LVDT fixed to the pile base and container wall enabled the pile position to be monitored during a test and was also used to confirm the relationship between pile velocity and motor rpm.

The model pile base was instrumented with a strain gage bridge to measure flexure at the base of the cantilever. Knowing the point of application of the ice load, the magnitude of the ice force could be easily established to a reasonable degree of accuracy.

The measurement of air, ice, and water temperatures was accomplished using thermistors and known relationships between measured thermistor resistance and temperature. The liquid nitrogen flow was controlled manually with a solenoid valve in the nitrogen line by an operator monitoring the temperature of the atmosphere above the water.

An X-Y plotter, multimeter, the motor controller, and an HP9845 data acquisition system with an HP 85B computer were used to gather the needed data during the conduct of a test. Figure 4.2 shows the instrumentation used to control and monitor the experiments.

4.6 Experimental Procedures

Figure 4.3 illustrates the experimental procedures developed to model the ice force and ice floe failure mechanism experiments on board the centrifuge. The procedures were identical for the "1 g" experiments conducted in the laboratory if the steps involving the centrifuge are omitted. Precooling the model container and the water to approximately 0°C before a test reduces the amount of nitrogen required for freezing by eliminating the need to remove the heat capacity of the water and container before starting a test. Pile diameters of 1/2 and 3/4 in. (1.27 and 1.91 cm) were considered in this study with pile velocities between .005 and 2.5 in. per minute (.013 and 6.35 cm per min). Program listings, flow charts and documentation of the computer programs developed for use in this study

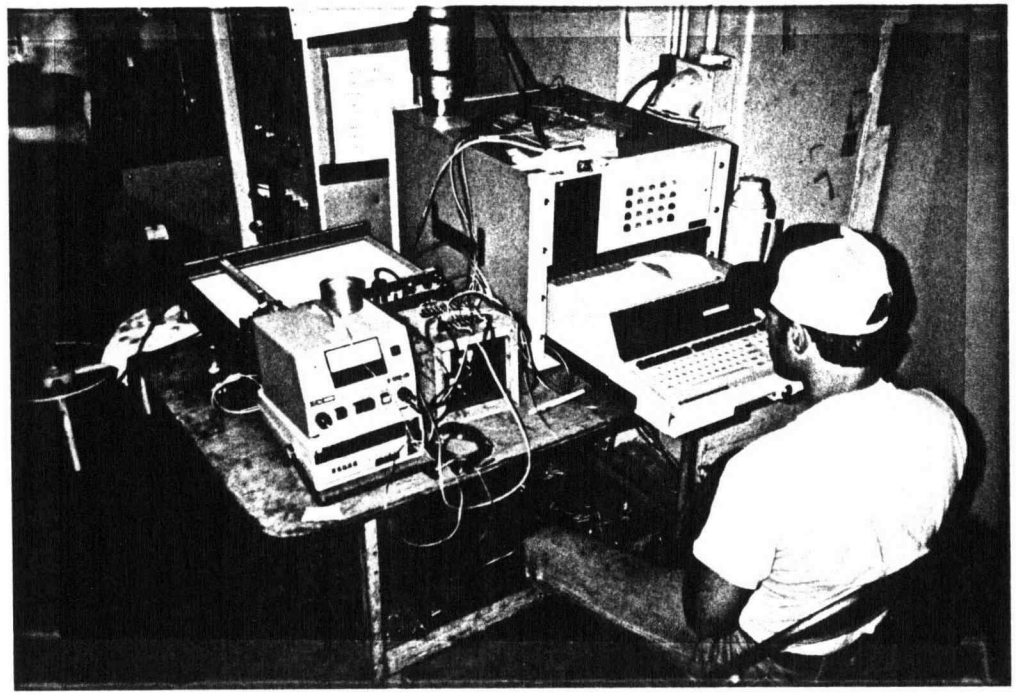

Figure 4.2 Instrumentation used to control and monitor the experiments.

Figure 4.3 Outline of experimental procedures followed during testing

1. Set up experimental apparatus (see section 4.7)
2. Test all electrical and mechanical systems
3. Precool distilled H_2O to approximately 0°C
4. Precool liquid nitrogen lines and model container
5. Add precooled distilled water to model container
6. Select pile diameter, penetration velocity, and position
7. Close model container cover and exit centrifuge containment structure
8. "Spin up" centrifuge to desired "g" level
9. Start computer program to measure and record temperatures
10. Control liquid nitrogen to freeze ice sheet
11. Stop freezing according to established time/temperature/ice thickness relationship
12. Open container cover if stereo photography is required
13. Initiate computer program to measure ice force, pile penetration, and temperatures
14. Start motor and fail ice sheet
15. Record ice force versus penetration with X-Y plotter and data acquisition system.
16. Stop motor at end of travel
17. "Spin down" centrifuge
18. Enter containment structure and observe ice sheet failure and measure ice sheet thickness at several locations
19. Record ice thickness data

are included in Appendix A. The relationship established between ice thickness, freezing temperature and time is discussed later. Two records of ice force versus pile travel were recorded. These include a continuous plot of force versus travel on the X-Y recorder, and a digitized record on the data acquisition system. Ice temperature was measured with two thermistors frozen into the ice sheet and recorded with the data acquisition system. Ice sheet thickness was measured after photographs of the ice failure were taken by sawing the ice into sections and measuring the ice thicknesses with plastic calipers while noting the relative location of the measurements within the overall sheet. Figure 4.4 illustrates the method used to measure ice thicknesses.

4.7 Apparatus Set Up

A considerable amount of time and effort was involved each time the experimental apparatus was set up at the Boeing facility. Boeing personnel provided the liquid nitrogen tank and the plumbing required to have a liquid nitrogen supply available at the centrifuge hub. The tasks which remained included:

(1) mounting the environmental model container to the swinging bucket and the counterbalance weight to the other bucket,

(2) locating the data acquisition system, computer, motor controller, and X-Y plotter outside the containment structure,

(3) locating the "Action Pack" signal conditioners at the centrifuge hub to amplify the electrical signals from

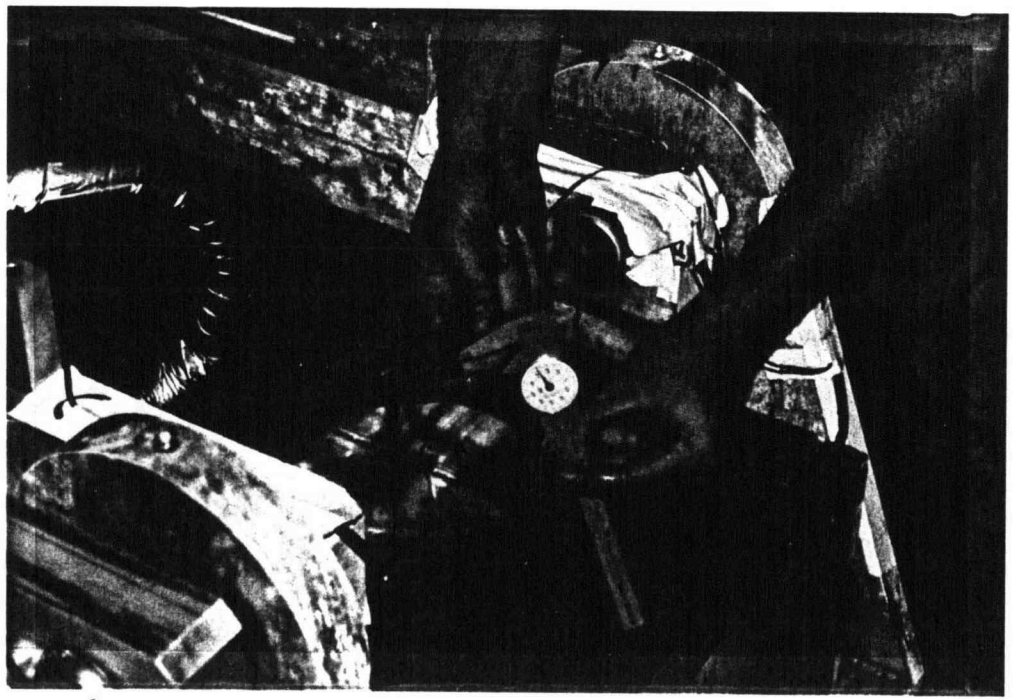

Figure 4.4 Measurement of ice sheet thicknesses with plastic calipers.

the strain gages and LVDT before passing through the slip rings,

(4) making electrical connections between the instruments located outside the containment structure and the centrifuge slip rings,

(5) making electrical connections between the slip rings and signal conditioners and the environmental model container,

(6) locating the umbilical nitrogen line between the centrifuge hub and the model container,

(7) securing all electrical cables and the nitrogen line to the arms of the centrifuge with tape,

(8) lifting the centrifuge bucket with the environmental model container attached into the horizontal "in flight" configuration to make certain that adequate clearance was provided to insure the lines would not rub inside the centrifuge enclosure while the model container was "in flight",

(9) testing the instrumentation and control systems to make certain that they functioned properly.

To facilitate the equipment set-up all electrical cables were made to the proper length and fitted with banana plugs and screw type connectors. The umbilical nitrogen line was also prefabricated with Swagelock fittings for easy connection.

5.0 EXPERIMENTAL RESULTS

5.1 General

The development of the experimental apparatus and procedures is discussed to document the methodology used to approach the problem of creating and subsequently failing an ice sheet in flight in a centrifuge. From this discussion an appreciation for the ideas that are successful in designing such an apparatus, for service on a centrifuge, can be gained and the design of a larger apparatus for use on a larger centrifuge can be facilitated. A comparison between the actual performance of the experimental apparatus to the design objectives is a measure of the success of the design.

The presentation of the experimental data is given in two sections, namely, the freezing process and formation of an ice sheet, and the ice sheet failure. The experimental data is associated with testing under conditions of 1 g and under conditions of 20 and 50 g's so that the gravity dependence of the ice force and ice floe failure mechanism problem may be investigated. The 1 g data serves as the control condition for the 20 and 50 g data. All 1 g experiments were performed at the Oregon State University Civil Engineering laboratory, while all centrifuge experiments were conducted at the Boeing Company Centrifuge Facility, Kent, Washington.

5.2 Experimental Apparatus Development and Performance

The development of the experimental apparatus followed the philosophy that the separate components should be tested independently on the centrifuge before integration into the final design configuration. It was necessary to demonstrate that the proposed nitrogen system was capable of forming an ice sheet in flight and that an electric motor could be used to drive a structure into the ice sheet. Furthermore, it was necessary to demonstrate that an LVDT and strain gages could function in a high inertial field so that they could be used to monitor the failure event.

The problem of forming an ice sheet on a water surface in flight on a centrifuge has apparently not been addressed by the centrifugal modeling community. To form an ice sheet it is necessary to remove heat from the water with a cold side atmosphere until the water temperature is depressed to the freezing point and ice is formed. The heat transfer problem involves conduction, convection, and radiation. To quantify the problem and incorporate all heat transfer processes would be a difficult task. It was determined that the water temperature, cold side atmosphere, and time were the most important variables in the problem. The problem was approached by intuition and trial and error rather than analytically. As a working hypothesis, it was recognized that if a cold side temperature sufficiently below the freezing point of water could be supplied for a sufficiently long period of time then ice would be formed on the water surface. Preliminary experiments of pouring liquid nitrogen directly on a water surface produced rather violent freezing and a cracked and non-uniform ice

sheet. This indicated the need to allow sufficient heat transfer from the liquid nitrogen supply lines to preclude any liquid from reaching the environmental chamber. Preliminary calculations indicated that if the water was precooled to near freezing from room temperature before attempting to use nitrogen for freezing, a significant savings of both nitrogen and time could be realized.

To test the hypothesis the tank of the environmental model container was fabricated, with the intent that the other components could be added later, and fitted with a nitrogen line and a 0.25 in. (.6 cm) thick aluminum lid that bolted to the top. A single nozzle was located above the water surface on one side of the tank to distribute the nitrogen vapor. A thermistor was located so that the temperature above the water could be monitored. Nitrogen flow was controlled by observing the cold side temperature and periodically actuating a solenoid valve on the liquid nitrogen supply line to maintain a nearly constant temperature atmosphere over the water.

After demonstrating that an ice sheet could be formed in a 1 g environment, the system was tested in flight on the Boeing centrifuge. Two ice sheets were successfully formed on October 28, 1982. The first ice sheet had an average thickness of 0.10 in. and was the result of applying a -13.3°C cold side temperature for 15 minutes. The second ice sheet had an average thickness of 0.14 in. and was the result of applying a -13.3°C cold side temperature for 25 minutes. The product of temperature below freezing and time is defined as the freezing index. The first and second ice sheets had freezing indexes of 200°C minutes and 330°C minutes, respectively. The ice sheets were non-uniform due to the use of a single nozzle to distribute the liquid

nitrogen. These non-uniformities are evidenced by the contour lines on the ice thickness maps shown in Figures 5.1 and 5.2. A nitrogen distribution system which utilized two nozzles was tested and found to offer no improvement over the one nozzle system. The results of the tests with two nozzles are shown in Figures 5.3 and 5.4. The freezing indexes for these tests were 490°C minutes and 780°C minutes, respectively. The ice sheets formed in these two tests were unsatisfactory since some areas of the water surface were not frozen.

The final configuration of the nitrogen distribution system is shown in Figure 5.5. This system is compatible with the circular boundary condition ring. The ice sheets formed by this system are more uniform than the sheets formed with either the single or double nozzle systems. The non-uniformities that exist in the ice sheets formed by this system appear to be the result of heat conduction at the boundary wall and at the model pile. The micarta pile and the plastic lined aluminum boundary ring are better thermal conductors than the surface of the ice sheet and since greater heat transfer from the water to the cold atmosphere exists at the pile and ring a thicker section of ice exists adjacent to those boundaries.

The problem of failing the ice sheet with the model pile involved selecting a drive mechanism capable of operating in a high inertial field. Several alternatives were considered including electric, hydraulic, and pneumatic motors mounted either at the model container or at the centrifuge hub. Hydraulic or pneumatic rams were also considered as well as more exotic schemes such as falling weights through a system of cables and pulleys. A system incorporating an electric motor was considered to be easiest to implement and control.

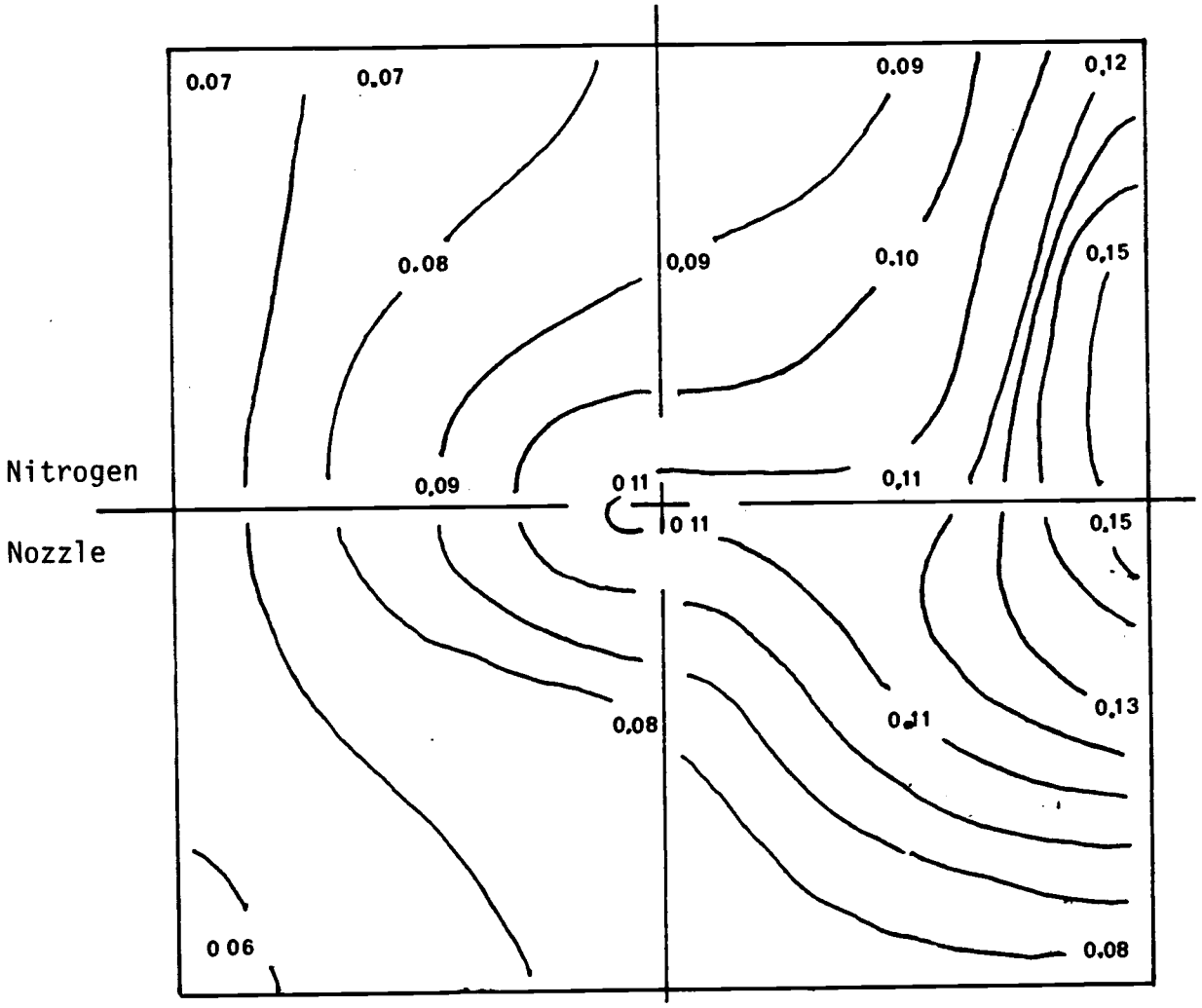

Note: Ice thickness in inches.

Figure 5.1 Ice thickness map with contour lines showing nonuniformities of first ice sheet.

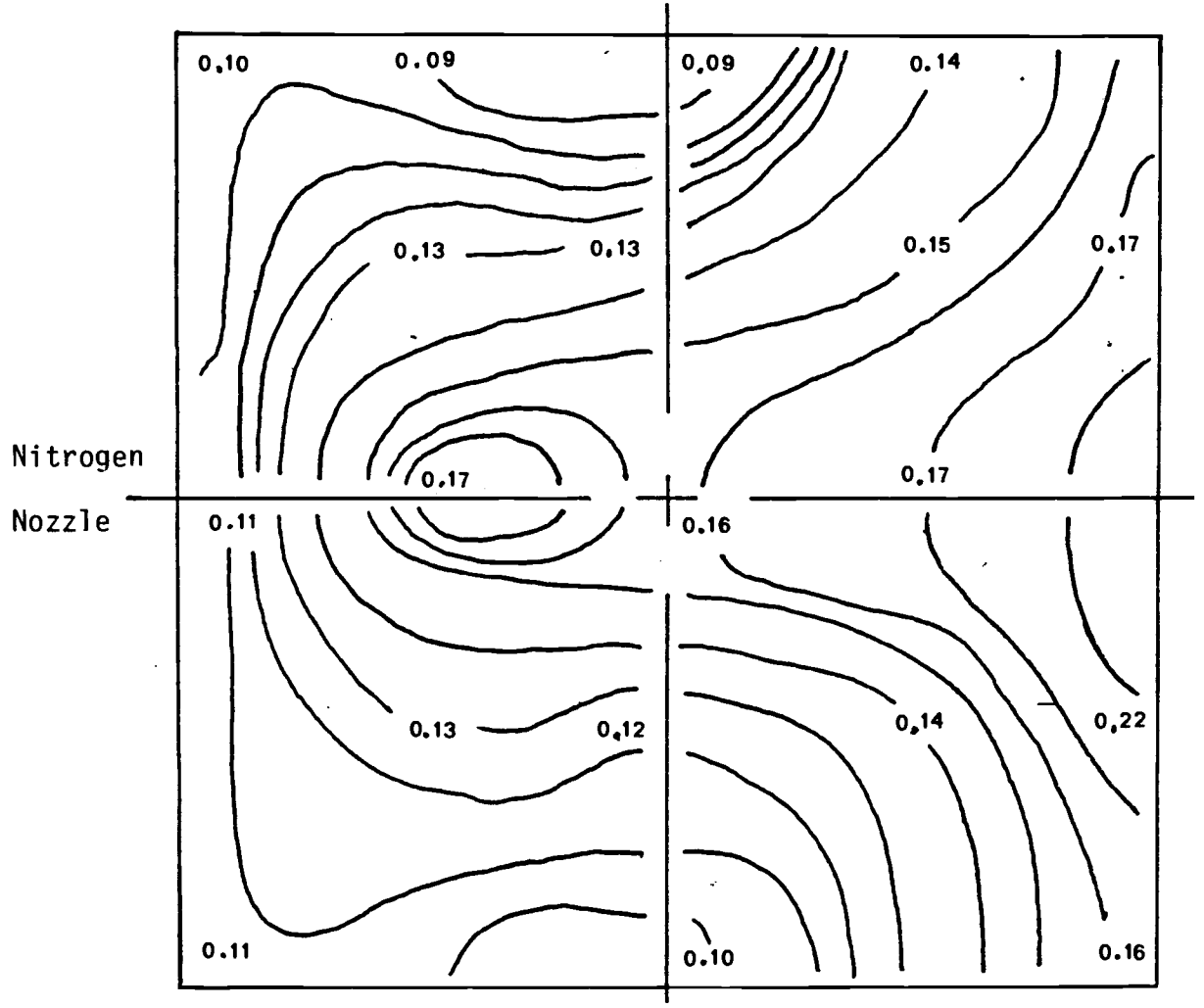

Note: Ice thicknesses in inches.

Figure 5.2 Ice thickness map with contour lines showing nonuniformities of second ice sheet.

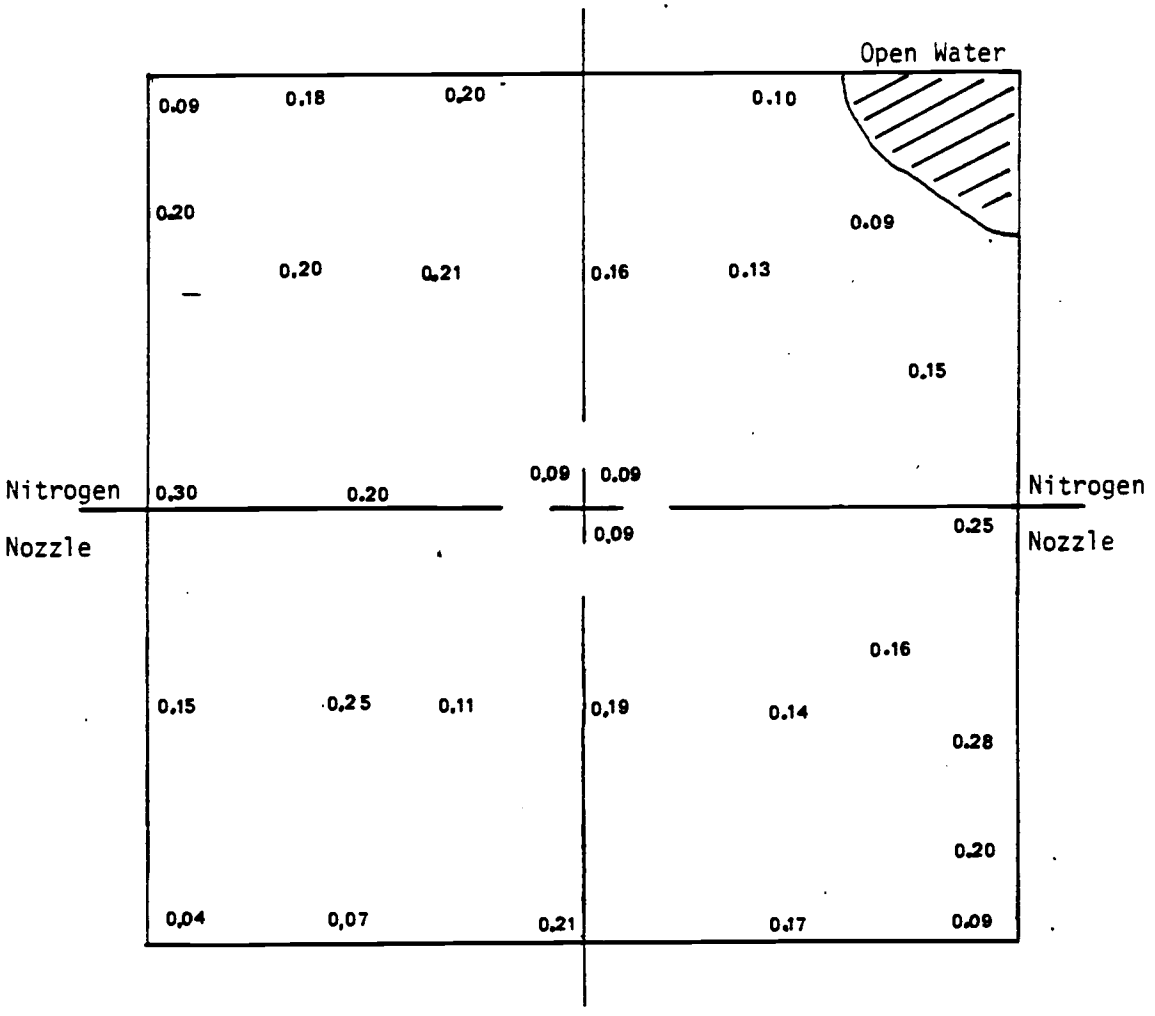

Note: Ice thicknesses in inches.

Figure 5.3 Ice thickness measurements of third ice sheet formed with two nitrogen nozzles.

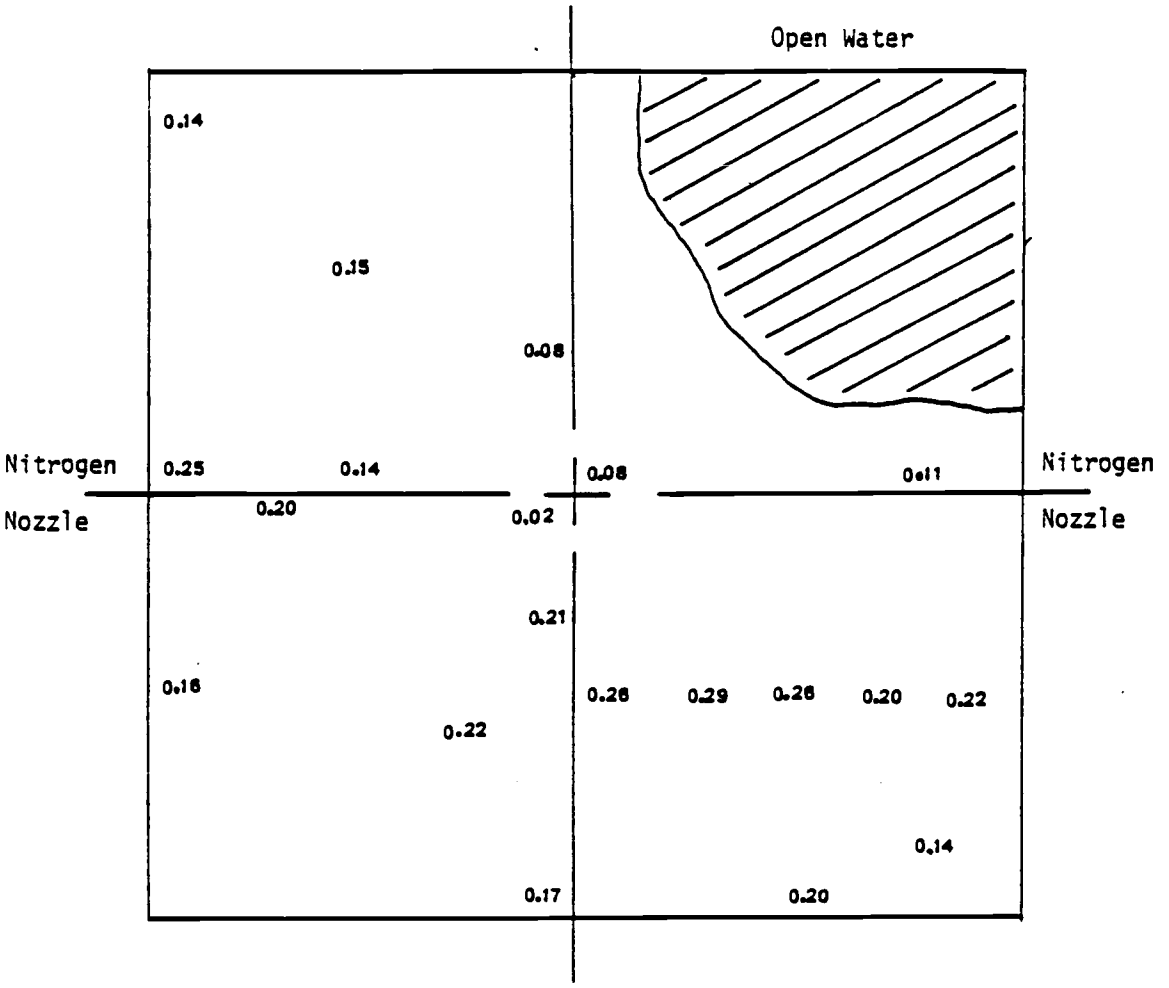

Note: Ice thicknesses in inches.

Figure 5.4 Ice thickness measurements of fourth ice sheet formed with two nitrogen nozzles.

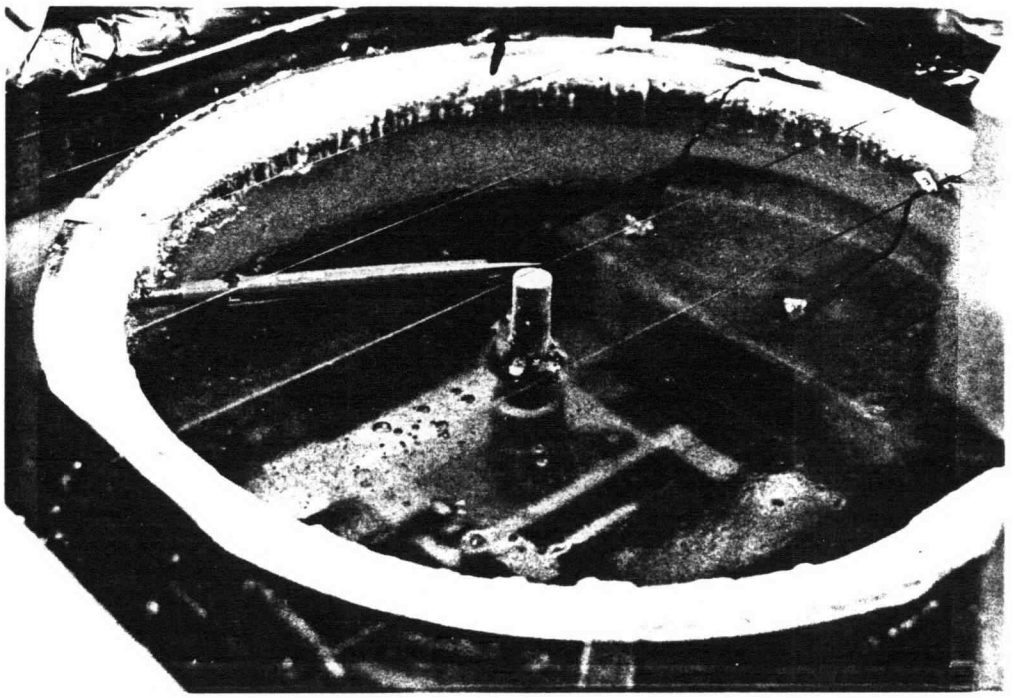

Figure 5.5 Final configuration of nitrogen distribution system.

Considerations of the inertial and gyroscopic forces indicated that if a motor was mounted on the model container such that the axis of rotation of the motor was parallel to the axis of rotation of the centrifuge the gyroscopic forces on the motor would be minimized. It was also recognized that if a motor was mounted adjacent to the hub of the centrifuge the inertial forces would be less than those at the model container.

Two systems were tested in flight to evaluate motor performance. These systems consisted of (1) a motor and lead screw assembly mounted at the centrifuge bucket and, (2) a motor mounted at the centrifuge hub and coupled to a lead screw assembly located at the centrifuge bucket by a flexible drive cable. Both systems were equipped with a model pile instrumented with strain gages and a LVDT. A spring was fixed to the top of the cantilevered pile to apply a force as the pile was moved so that the strain gages located at the base of the pile could be tested. The motor operated satisfactorily in a 100 g inertial field when placed at the bucket. The system with the flexible drive cable produced a periodic drive velocity due to backlash in the cable. The strain gages and LVDT operated satisfactorily at 100 g. One potential problem was identified with the LVDT under a high inertial field, specifically, the LVDT core return spring (to return the core to the fully extended position) was not stiff enough. This problem was easily rectified.

5.3 Freezing Process Test Results

It is necessary to understand the freezing process if a prediction of ice thickness with respect to freezing time is to be made. An

attempt was made to hold as many variables as possible constant during the freezing process. This included precooling the model container and water before applying the liquid nitrogen and also using make-up water between tests that had been chilled to approximately 0°C. During the freezing process the temperature of the atmosphere above the water surface was maintained as closely as possible to -30°C. The only exceptions were the first attempts at forming ice on the centrifuge as discussed in Section - 5.2. Information about the freezing process was gathered with the use of six thermistors, two each located in the air, water and ice. The data acquisition system was used to constantly monitor and record these temperatures throughout the freezing process. The temperature measured in the atmosphere was displayed so that an operator could regulate the liquid nitrogen flow to provide a nearly constant freezing temperature above the water. A freezing index was continuously calculated. When the desired freezing index was reached all nitrogen flow was stopped and the pile was driven into the ice sheet. At the conclusion of each test, following spin down, an ice thickness map was prepared. The ice sheet was thicker around the boundary ring, consequently, the ice thicknesses within a radius of about 3.5 in. (9 cm) around the pile were considered most representative of the sheet thickness associated with the ice sheet failure A typical ice map is shown in Figure 5.6.

A summary of the freezing index data is given in Tables 5.1, 5.2, and 5.3. Included in these tables are values of the g-level, the freezing index, average thicknesses in the overall ice sheet, and average thicknesses within a 3.5 in. (9 cm) radius around the pile.

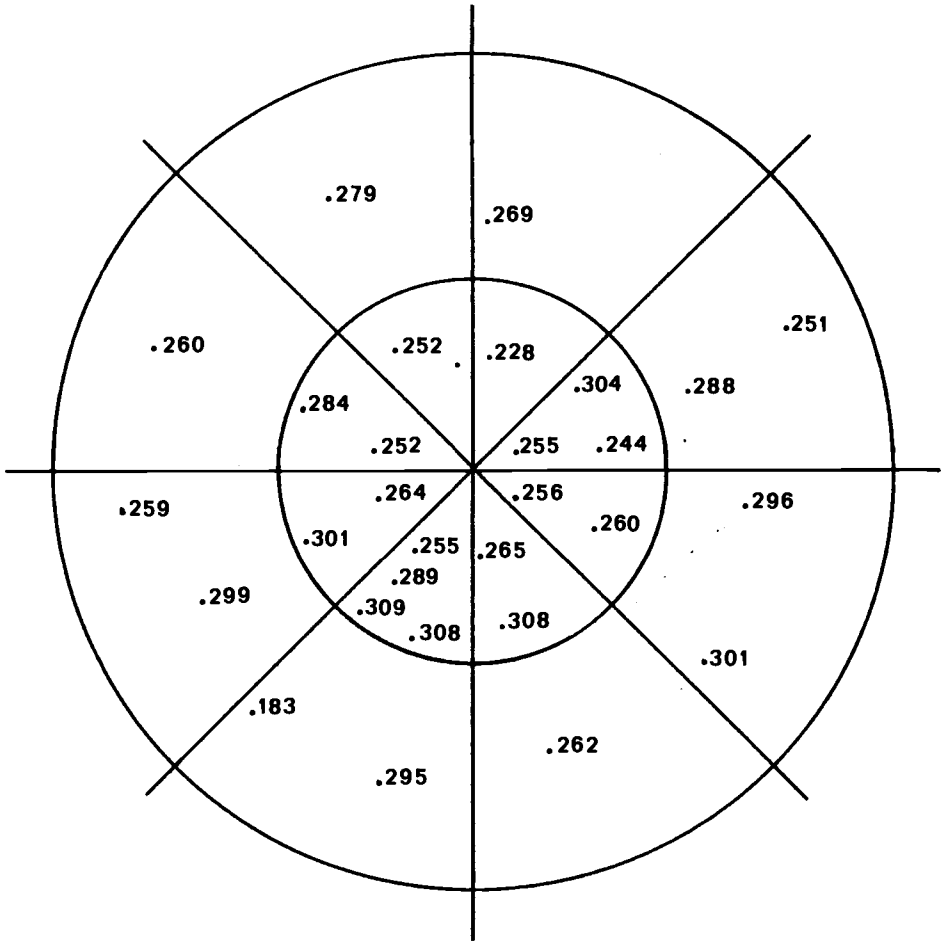

Figure 5.6 Typical ice thickness map for ice sheet formed within circular boundary Condition ring.

Table 5.1 Freezing index and ice thickness data at 1g.

Test Number (1)	g-level (2)	Freezing Index (°C minutes) (3)	Average Overall Ice Sheet Thickness (in.) (4)	(cm) (4)	Average Thickness Within 3.5 in. (9 cm) Radius of Pile (in.) (5)	(cm) (5)
L 2	1	900	.153	.389	.139	.353
L 3	1	1600	.267	.678	.267	.678
L 4	1	1600	.256	.650	.252	.640
L 5	1	1600	.262	.665	.256	.650
L 6	1	1600	.273	.693	.276	.701
L 7	1	1600	.260	.660	.246	.625
L 8	1	1600	.314	.798	.283	.719
L 9	1	1600	.256	.650	.255	.648
L10	1	1600	.272	.691	.273	.693
L11	1	1600	.207	.526	.196	.498
L12	1	900	.142	.361	.141	.358
L13	1	900	.176	.447	.169	.429
L14	1	900	.164	.417	.162	.411
L15	1	900	.160	.406	.149	.378
L16	1	900	.194	.333	.190	.483
L17	1	900	.176	.343	.171	.434
L18	1	900	.160	.406	.144	.366
L19	1	900	.131	.333	.128	.325
L20	1	900	.135	.343	.134	.340
L21	1	900	.121	.307	.105	.267
L22	1	1024	.153	.389	.135	.343
L23	1	900	.158	.401	.139	.353

Table 5.2 Freezing index and ice thickness data at 20 g

Test Number (1)	g-level (2)	Freezing Index (°C minutes) (3)	Average Overall Ice Sheet Thickness (in.) (4)	(cm) (4)	Average Thickness Within 3.5 in. (9 cm) Radius From Pile (in.) (5)	(cm) (5)
C 4	20	529	.176	.447	.162	.411
C 5	20	529	.161	.409	.142	.361
C 7	20	529	.114	.290	.112	.284
C 8	20	529	.113	.287	.113	.287
C 9	20	529	.123	.312	.119	.302
C10	20	784	.167	.424	.161	.409
C11	20	784	.163	.414	.157	.399
C16	20	676	.138	.351	.145	.368
C17	20	729	.226	.574	.204	.518
C18	20	676	.236	.599	.237	.602
C19	20	676	.254	.654	.233	.592
C20	20	576	.222	.564	.216	.549
C21	20	441	.169	.429	.146	.371
C22	20	400	.138	.351	.320	.813
C29	20	784	.149	.378	.143	.363
C30	20	841	.189	.480	.179	.455
C31	20	841	.170	.432	.157	.399
C32	20	1600	.365	.927	.352	.894
C33	20	1225	.292	.742	.270	.686
C34	20	1089	.269	.683	.256	.650

Table 5.3 Freezing index and ice thickness data at 50 g

Test Number (1)	g-level (2)	Freezing Index (°C minutes) (3)	Average Overall Ice Sheet Thickness (in.) (4)	(cm) (4)	Average Thickness Within 3.5 in. (9 cm) Radius From Pile (in.) (5)	(cm) (5)
C 6	50	529	.190	.483	.153	.389
C12	50	784	.252	.640	.260	.660
C13	50	625	.158	.501	.166	.422
C14	50	676	.178	.452	.164	.417
C15	50	676	.179	.455	.175	.445
C23	50	529	.090	.229	.090	.203
C24	50	729	.173	.439	.161	.409
C25	50	254			.062	.157
C26	50	729	.165	.419	.147	.373
C27	50	729	.224	.569	.219	.556
C28	50	729	.159	.404	.144	.366
C35	50	1225	.322	.818	.313	.795
C36	50	1225	.292	.742	.274	.696
C37	50	1225	.399	1.01	.380	.965

5.4 Ice Failure Test Results

Typical ice failures are shown in Figure 5.7. An area of open water behind the pile and broken ice rubble in front of the pile is evident. The corresponding measurements of ice force versus penetration velocity for these events are shown in Figures 5.8 and 5.9.

A summary of the data pertinent to the ice failure events is given in Tables 5.4, 5.5, and 5.6. Values of the g-level, n, average ice thickness around the pile, t, pile diameter, d, penetration velocity, v, maximum measured force, F_{max}, and ice temperature, T_{ice}, are given.

Corrections were made to the measured maximum force to account for the point of application of the ice sheet on the cantilevered pile. The force was assumed to act at the middepth of the ice sheet. Schwartz (1970) substantiates this assumption. Knowing the ice thickness, the distance from the top of the pile to the ice surface, and the influence line for the moment at the base of the pile due to a point load, this correction can be made. Maximum measured pressures were corrected to a temperature of -0.5°C knowing the variation of the compressive strength of freshwater ice with temperature and assuming a direct proportion between measured ice force and compressive strength. The rate at which the compressive strength of ice increases with decreasing temperature for freshwater ice was deduced from the work of Schwarz (re. Figure 3.7). Figure 5.10 is a plot of compressive strength versus temperature for constant values of strain rate. Considering the average slope of the lines shown the compressive strength of ice varies with temperature as 32.44 psi/°C (2.228 kg/cm^2/°C).

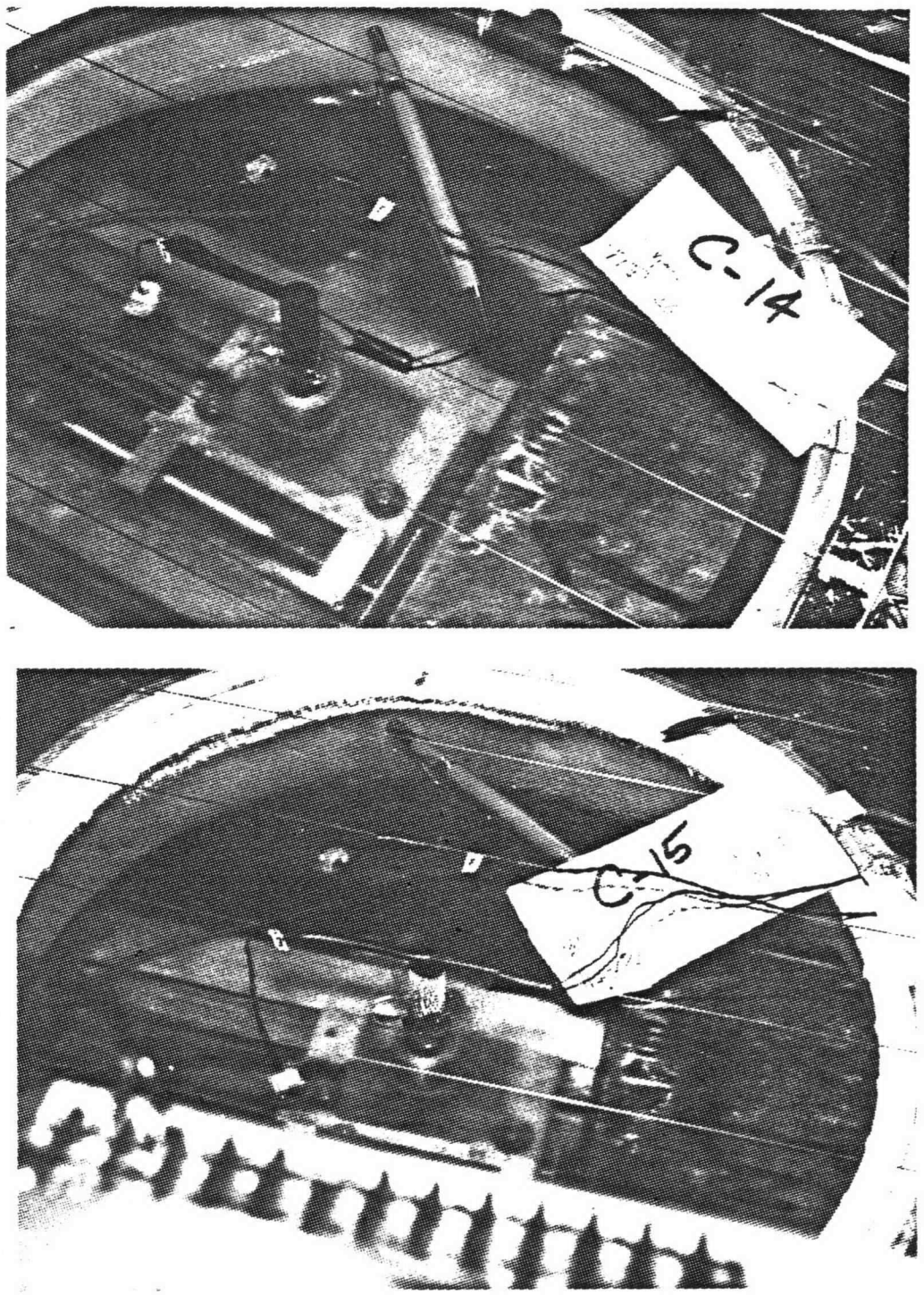

Figure 5.7 Typical ice sheet failures. Note ice rubble in front of the pile and open water behind the pile.

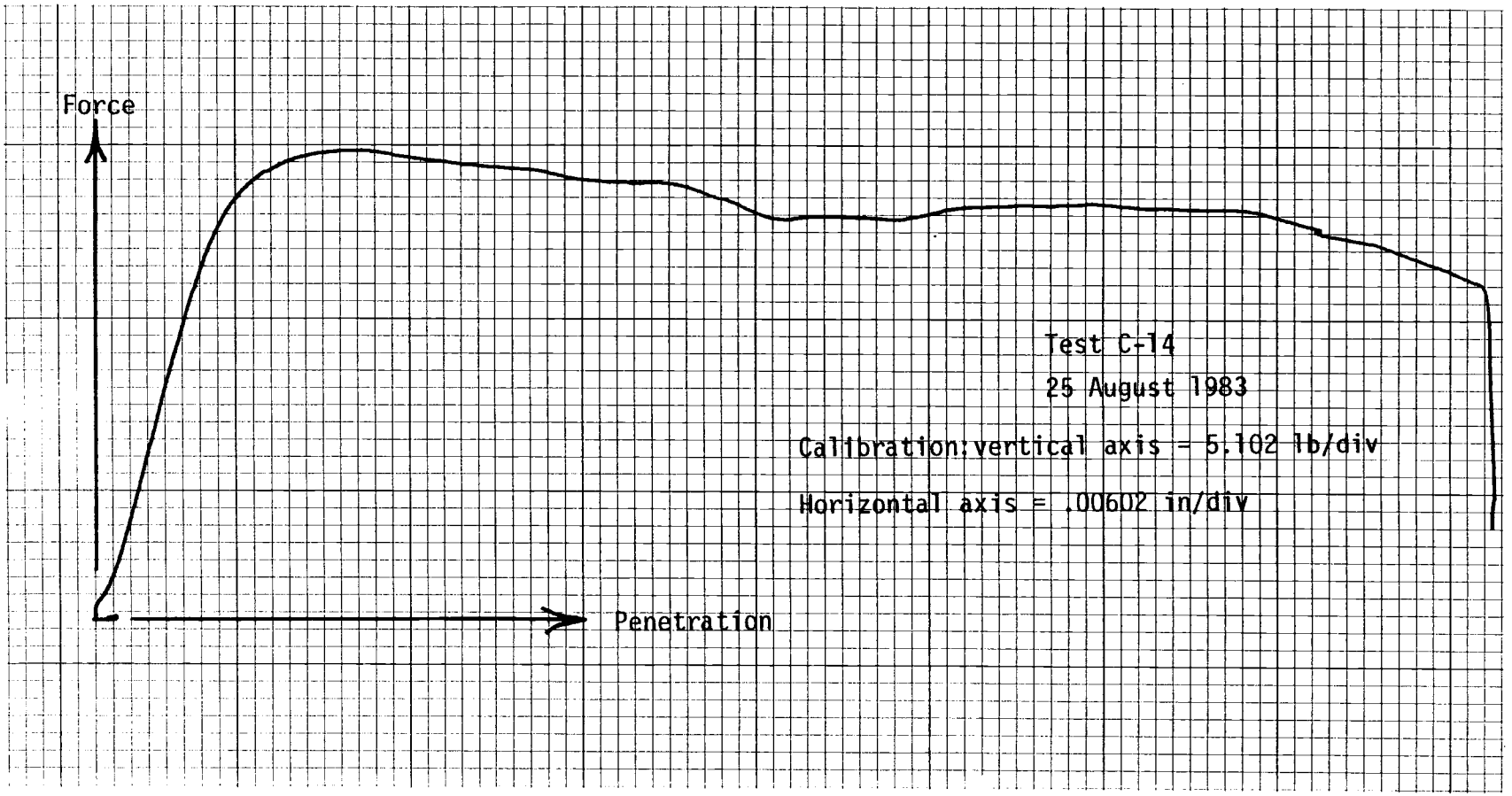

Figure 5.8 Force on pile versus penetration for test C-14.

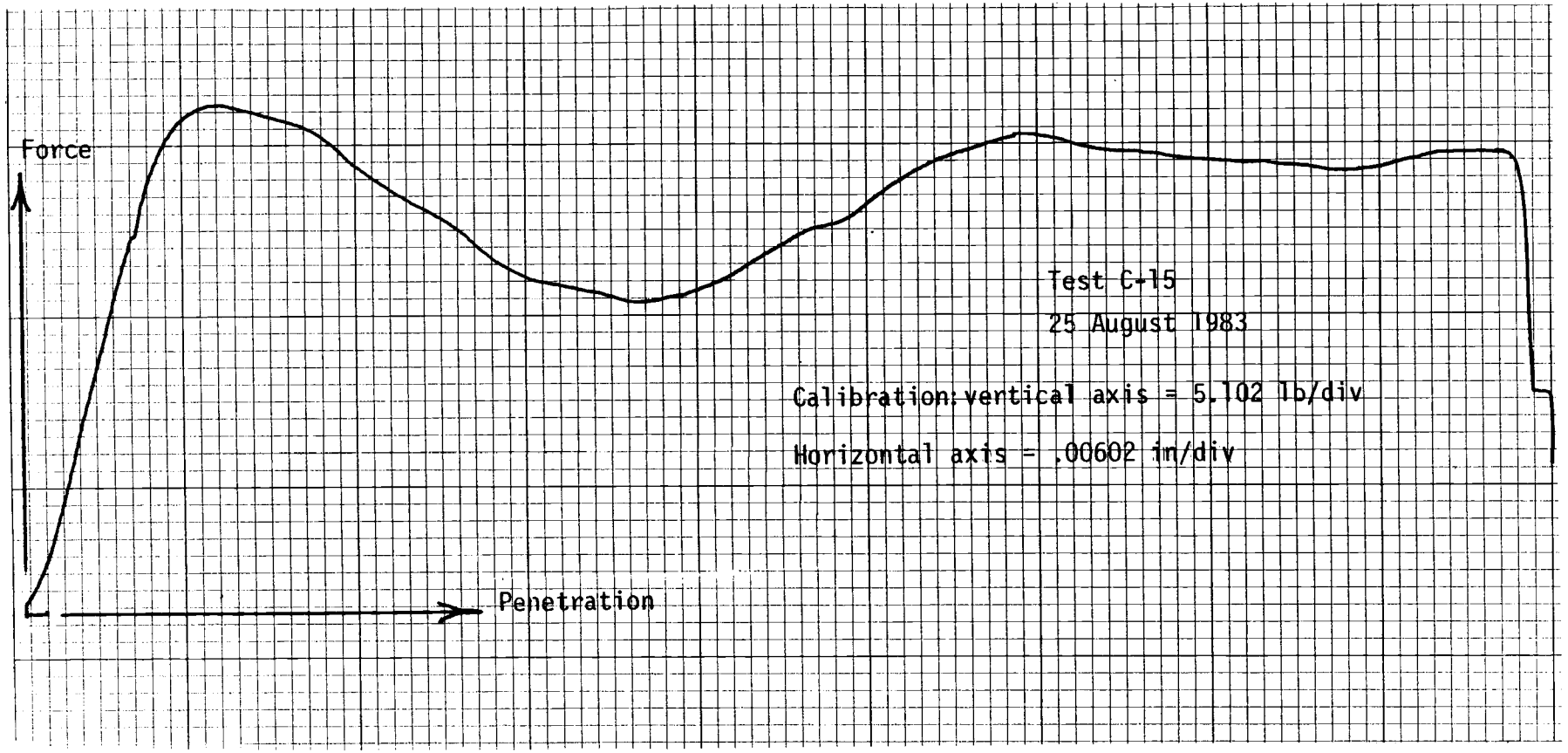

Figure 5.9 Force on pile versus penetration for test C-15.

Table 5.4 Ice failure data at 1 g.

Test Number (1)	g-level (2)	Average Ice Thickness Around Pile (in) (3)	(cm) (3)	Pile Diameter (in) (4)	(cm) (4)	Penetration Velocity (in/min) (5)	(cm/min) (5)	Maximum Force (lbs) (6)	(kg) (6)	T_{ice} (°C) (7)	Maximum @ T_{ice} (psi) (8)	(kg/cm²) (8)	Maximum Pressure @ T = -0.05°C (psi)* (9)	(kg/cm²) (9)
N2	1	.139	.353	.75	1.91	1.50	3.81	110	49.9	-0.5	1056	74.2	1056	74.2
N3	1	.267	.675	.75	1.91	1.50	3.81	240	109	-0.5	1200	84.4	1200	84.4
N4	1	.252	.640	.75	1.91	.750	1.91	212	96.2	-0.5	1123	79.0	1123	29.0
N5	1	.256	.650	.75	1.91	.375	.953	207	94.0	-0.4	1080	75.9	1083	76.1
N6	1	.275	.699	.75	1.91	.175	.445	168	76.3	-0.3	816	57.4	823	57.9
N7	1	.246	.625	.75	1.91	.175	.445	148	67.2	-0.3	803	56.5	810	56.9
N8	1	.283	.719	.75	1.91	.375	.953	222	101	-0.4	1048	73.7	1051	73.9
N9	1	.255	.648	.75	1.91	.050	.127	127	57.7	-0.5	665	46.8	665	46.8
N10	1	.273	.693	.75	1.91	.100	.254	158	71.7	-0.5	773	54.3	773	54.3
N11	1	.196	.498	.75	1.91	.025	.064	71.5	32.5	--	486	34.2	486	34.2
N12	1	.141	.258	.75	1.91	.050	.127	57.2	26.0	-0.3	540	38.0	547	38.5
N13	1	.169	.429	.75	1.91	.500	1.27	133	60.4	-0.4	1050	73.8	1053	74.0
N14	1	.162	.411	.75	1.91	2.00	5.08	143	64.9	-0.5	1178	82.8	1178	82.8
N15	1	.149	.378	.50	1.27	.050	.127	16.2	7.3	-0.4	480	33.7	483	34.0
N16	1	.190	.483	.50	1.27	.500	1.27	73.1	33.2	-0.4	1694	119	1697	119
N17	1	.171	.434	.50	1.27	1.25	3.18	141	64.0	-0.5	1652	116	1652	116
N18	1	.144	.366	.50	1.27	2.00	5.08	65.4	29.7	-0.5	908	63.8	908	63.8
N19	1	.128	.325	.50	1.27	.075	.191	48.0	21.8	-0.4	751	52.8	753	52.9
N20	1	.134	.340	.50	1.27	.500	1.27	77.7	35.3	-0.5	1159	81.5	1159	81.5
N21	1	.105	.267	.50	1.27	2.00	5.08	56.6	25.7	-0.5	1079	75.9	1079	75.9
N22	1	.135	.343	.50	1.27	2.00	5.08	90.9	41.3	-0.5	1346	94.6	1346	94.6
N23	1	.139	.353	.75	1.91	1.00	2.54	102	46.3	-0.5	979	68.8	979	68.8

* Corrected for point of application

Table 5.5 Ice failure data at 20 g.

Test Number (1)	g-level (2)	Average Ice Thickness Around Pile (3)		Pile Diameter (4)		Penetration Velocity (5)		Maximum Force (6)		T_{ice} (°C) (7)	Maximum @ T_{ice} (8)		Maximum Pressure @ T = -0.05°C (9)	
		(in)	(cm)	(in)	(cm)	(in/min)	(cm/min)	(lbs)	(kg)		(psi)	(kg/cm^2)	(psi)*	(kg/cm^2)*
C4	20	.162	.441	0.50	1.27	.800	2.03	108	49.0	-1.2	1337	94.0	1314	92.4
C5	20	.142	.361	0.50	1.27	.150	.381	20.3	9.22	-0.7	991	69.7	984	69.2
C7	20	.112	.284	0.50	1.27	.150	.381	105	47.7	-0.7	1892	133	1885	133
C8	20	.113	.287	0.50	1.27	.150	.381	73.6	33.4	-0.9	1303	91.6	1289	90.6
C9	20	.119	.302	0.50	1.27	.450	1.14	96.6	43.8	-0.8	1523	114	1613	113
C10	20	.161	.409	0.50	1.27	.800	2.03	158	71.7	-1.2	1957	138	1934	136
C11	20	.157	.399	0.50	1.27	1.50	3.81	129	58.6	-1.4	1544	116	1615	114
C16	20	.145	.368	0.50	1.27	1.50	3.81	129	58.6	-1.4	1544	116	1615	114
C17	20	.204	.518	0.50	1.27	.200	.508	126	57.2	-2.2	1236	86.9	1180	83.0
C18	20	.237	.602	0.50	1.27	.800	2.03	138	62.7	-0.7	1166	82.0	1159	81.5
C19	20	.233	.592	0.50	1.27	2.00	5.08	149	67.6	-1.2	1278	89.9	1256	88.3
C20	20	.216	.549	0.50	1.27	2.00	5.08	139	63.1	-0.7	1287	90.5	1281	90.1
C21	20	.146	.371	0.50	1.27	2.00	5.08	112	50.8	-1.2	1541	108	1517	107
C22	20	.132	.335	0.50	1.27	.800	2.03	94.3	42.8	-0.7	1428	100	1422	100
C29	20	.142	.363	0.75	1.91	.075	.191	119	54.0	-0.6	1107	77.8	1103	77.5
C30	20	.179	.455	0.75	1.91	.500	1.27	168	76.3	-0.7	1253	88.1	1247	87.7
C31	20	.157	.399	0.75	1.91	2.00	5.08	175	79.5	-0.8	1483	104	1474	104
C32	20	.352	.894	0.75	1.91	.075	.191	293	133	-0.9	1112	78.2	1099	77.3
C33	20	.270	.686	0.75	1.91	.500	1.27	269	122	-0.8	1331	93.6	1321	92.9
C34	20	.256	.650	0.75	1.91	2.00	5.08	240	109	-1.3	1249	87.8	1225	86.1

* Corrected for point of application

Table 5.6 Ice failure data at 50 g's.

Test Number (1)	g-level (2)	Average Ice Thickness Around Pile (in) (3)	(cm) (3)	Pile Diameter (in) (4)	(cm) (4)	Penetration Velocity (in/min) (5)	(cm/min) (5)	Maximum Maximum Force (lbs) (6)	(kg) (6)	T_{ice} (°C) (7)	Maximum @ T_{ice} (psi) (8)	(kg/cm²) (8)	Pressure @ T = -0.05°C (psi)* (9)	(kg/cm²)* (9)
C6	50	.153	.389	0.50	1.27	.150	.381	97.7	44.4	-0.9	1277	89.8	1263	88.8
C12	50	.250	.635	0.50	1.27	.150	.381	164	74.5	-0.9	1263	88.8	1251	88.0
C13	50	.166	.422	0.50	1.27	.450	1.14	133	60.4	-0.5	1508	113	1504	113
C14	50	.154	.417	0.40	1.27	.800	2.03	154	69.9	-0.7	1881	132	1878	132
C15	50	.175	.445	0.50	1.27	1.50	3.81	155	70.3	-1.0	1000	70.3	1884	133
C32	50	.080	.203	0.50	1.27	.075	.191	80.2	36.4	-1.0	2005	141	1963	138
C24	50	.151	.409	0.50	1.27	.075	.191	122	55.3	-0.7	1390	97.7	1384	97.3
C25	50	.052	.157	0.50	1.27	.500	1.27	44.2	20.1	-0.9	1427	100	1413	99.3
C26	60	.147	.373	0.50	1.27	.500	1.27	130	59.0	-1.8	1759	124	1727	121
C27	50	.219	.556	0.40	1.27	2.00	5.08	152	69.0	-7.5	1390	97.7	1152	81.7
C28	50	.144	.366	0.50	1.27	2.00	5.08	127	57.7	-0.8	1758	124	1747	123
C35	50	.313	.795	0.75	1.91	.075	.191	295	134	-0.9	1255	88.2	1242	87.3
C36	50	.274	.595	0.75	1.91	.500	1.27	353	160.1	-0.6	1719	121	1716	121
C37	50	.399	1.01	0.75	1.91	1.50	3.81	356	162	-1.0	1248	87.7	1231	86.5

* Corrected for point of application

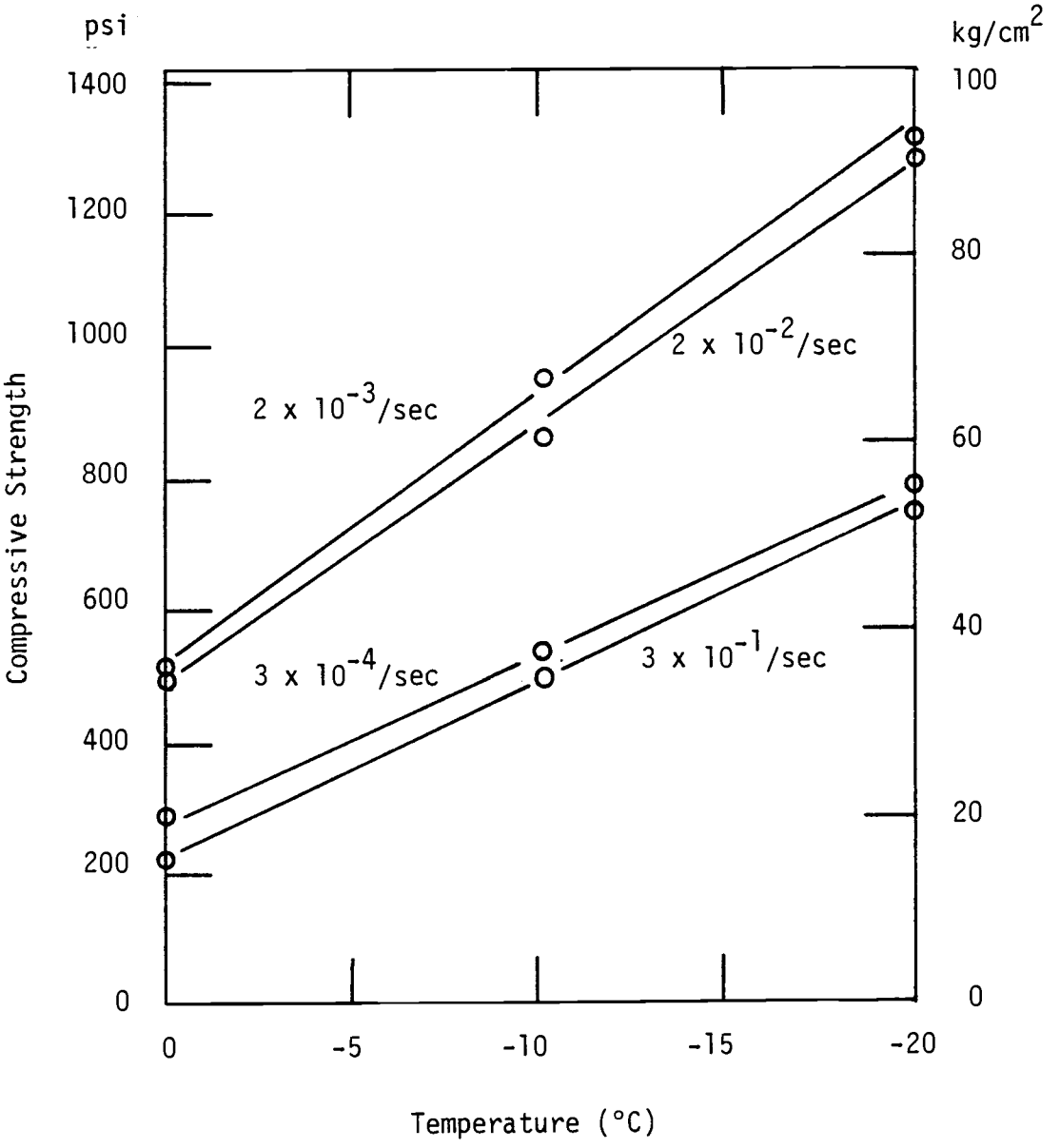

Figure 5.10: Ice compressive strength versus temperature at constant strain rate (modified after Schwart, 1970).

6.0 DISCUSSION OF RESULTS

6.1 General

A theory relating ice thickness to time and temperature below freezing is given to allow the experimental results associated with the freezing of an ice sheet in the environmental model container to be interpreted. Dimensional analysis is used to analyze the results of the ice failure experiments. An empirical equation is given that describes the ice failure data obtained at 1, 20 and 50 g. Possible sources of experimental error are discussed. The results of this study are compared with the results of others in an attempt to validate the use of the centrifugal modeling technique to investigate ice forces and ice floe failure mechanisms on a vertical pile. The effect of the high inertial acceleration field on the results obtained in this study are discussed.

6.2 Freezing Process

Stefan (1890) related the thickness of an ice sheet to the square root of the product of subfreezing step temperature and time (or the square root of the freezing index). The assumptions made to facilitate the solution include:

(1) The temperature of ice, T_o, at the isothermal boundary between the frozen and unfrozen zone and below this boundary is 0°C.

(2) The subfreezing surface temperature, T_s, is constant.

(3) The temperature in the frozen ice zone varies linearly between T_s and T_o.

(4) The density of ice is the same as the density of water.

Fig. 6.1 represents the situation for which the solution is derived.

Considering conductive heat transfer only:

$$q = -kA \frac{T}{x} = kA\left(\frac{T_s - T_o}{x} \right) \tag{6.1}$$

in which,

q = heat transfer per unit time

A = area normal to the direction of heat transfer

$$Q = q\, dt = kA \left(\frac{T_s - T_o}{x}\right) dt \tag{6.2}$$

in which,

Q = heat transfer during time dt

$$Q = Ldv = L\, A\, dx \tag{6.3}$$

in which,

L = latent heat of water
dv = differential volume of ice

equating equations 6.2 and 6.3:

$$\frac{kA\,(T_s - T_o)}{x} dt = L\, A\, dx \tag{6.4}$$

separating variables:

$$\frac{k}{L} \frac{(T_s - T_o)}{x} dt = x\, dx \tag{6.5}$$

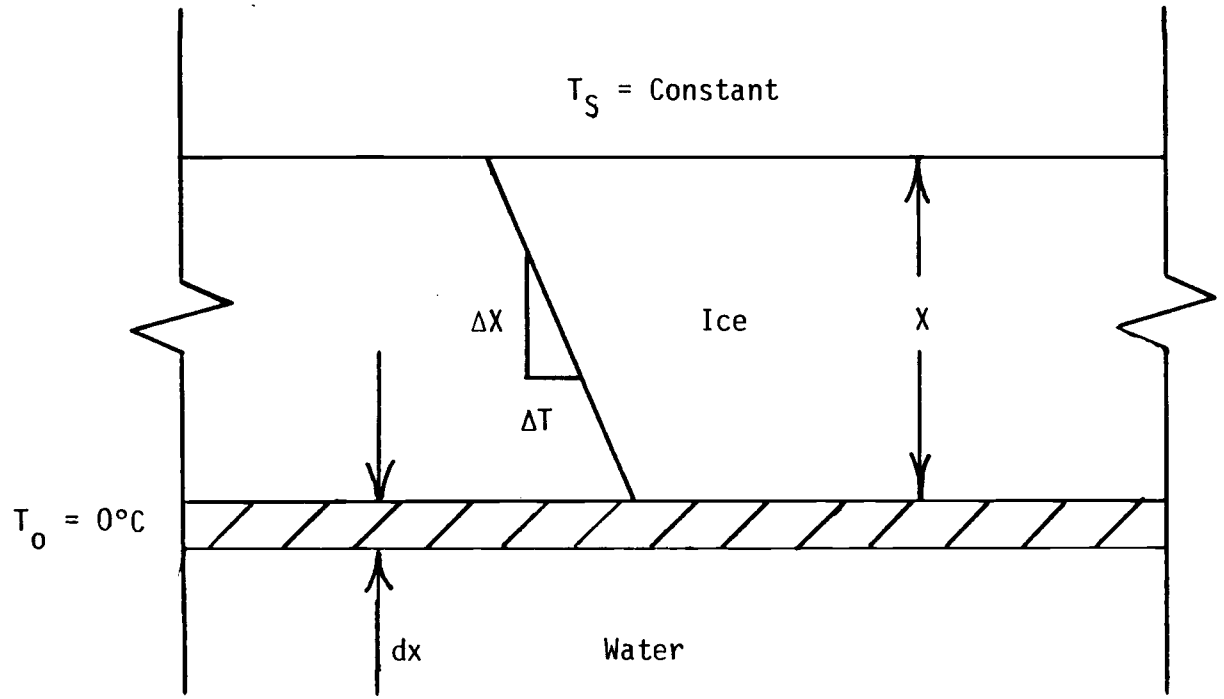

Figure 6.1 Definition sketch representing the Stefan solution

integrating and solving for x:

$$\frac{k}{L} \quad (T_s - T_o)t = \frac{x^2}{2} \tag{6.6}$$

$$x = \left(\frac{2k}{L} \quad (T_s - T_o)t \right)^{\frac{1}{2}} \tag{6.7}$$

this can also be written as:

$$x = \left(\frac{2k}{L}\right)^{\frac{1}{2}} (FI)^{\frac{1}{2}} \tag{6.8}$$

in which,

FI = freezing index

The results presented in Equations 6.7 and 6.8 suggest it is appropriate to interpret the ice thickness data obtained in the research program with respect to the square root of the freezing index. Figure 6.2 is a plot of average ice thickness around the pile versus the square root of the freezing index for the data presented in Tables 5.1 through 5.3.

Adopting values of 3.208×10^{-3} Btu/in. min °C and 5.173 Btu/in.^{3} for the thermal conductivity of ice and the volumetric latent heat of fusion of water, respectively, the Stefan solution predicts a relationship between ice thickness and the square root of the freezing index of:

$$x = 3.52 \times 10^{-2} \left(\frac{\text{inches}}{(°C \text{ min})^{\frac{1}{2}}}\right) (FI)^{\frac{1}{2}} \tag{6.9}$$

The best straight line fit through the experimental data yields the following relationship:

$$x = 7.97 \times 10^{-3} \left(\frac{\text{inches}}{(°C \text{ min})^{\frac{1}{2}}}\right) (FI)^{\frac{1}{2}} - 4.89 \times 10^{-2} \text{ inches} \tag{6.10}$$

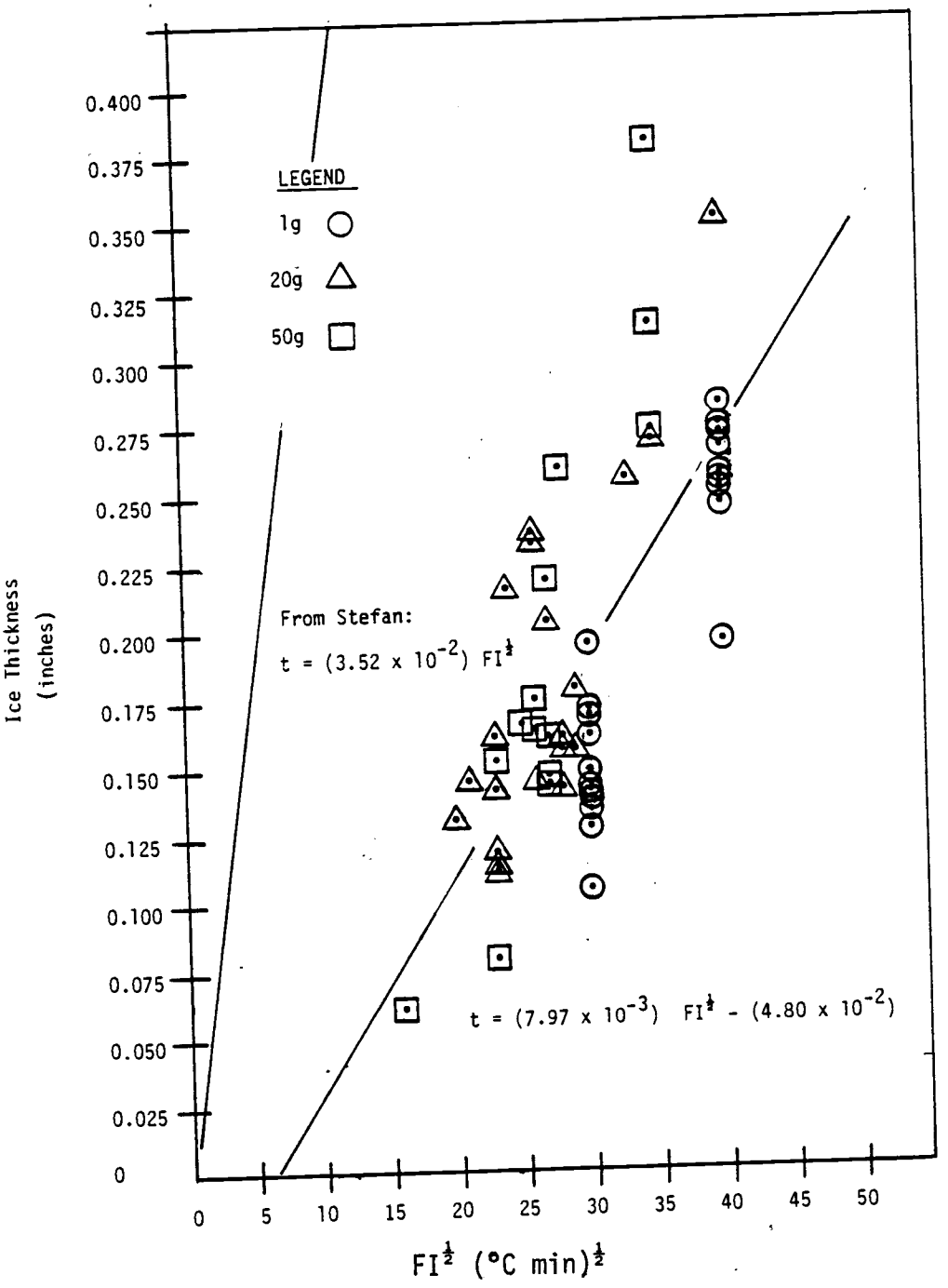

Figure 6.2 Comparison of freezing process results and the Stefan solution.

These relationships are shown in Figure 6.2.

The differences between the theoretical and experimental results may be attributed to the following factors:

(1) the water temperatures in the experiments were warmer than 0°C during the freezing process,

(2) the calculation of the freezing index commenced when nitrogen flow was initiated rather than when ice was beginning to form on the water surface,

(3) the water temperature was warmer than 0°C during the freezing process and, therefore, required that heat be removed from the water prior to the formation of ice owing to the specific heat capacity of the water.

In comparing the experimental results and those predicted by the Stefan solution two discrepancies are noted as follows: (1) the slope of the best fit straight line through the experimental data is flatter than that predicted by Stefan, and (2) the best fit straight line through the experimental data does not pass through the origin. It is believed that the reasons for these discrepancies can be attributed mainly to the fact that the initial water temperature was above 0°C. Before ice can form on the water surface the water at the surface must be cooled for freezing. This would explain the fact that the best straight line fit does not intersect the origin. In order for the freezing front to advance a certain amount of heat capacity must be removed from the water beneath the front. This would explain the fact that the slope of the best fit straight line through the experimental data is flatter than that predicted. The experimental data may be described by a curve which increases in slope with increasing

freezing index until it becomes parallel with the slope of the line predicted by the Stefan equation and remains parallel as the freezing index increases beyond this point. Measurement of the temperature in the water below the ice indicates that as freezing progresses the water temperature approaches 0°C. Unfortunately freezing was not continued for a sufficiently long time period to prove this hypothesis.

6.3 Dimensional Analysis

The available literature indicates that the important parameters influencing the force that an ice sheet exerts on a vertical cylindrical pile include:

(1) pile diameter
(2) ice thickness
(3) penetration velocity
(4) ice temperature
(5) grain size and orientation
(6) ice strength

A discussion of the influence of these parameters on the results developed in the present study follows. Other parameters which might influence and complicate the problem include:

(1) ice mass density
(2) modulus of elasticity
(3) Poisson's ratio

(4) ice viscosity

(5) friction between the ice and pile

(6) adhesion between the ice and pile

These parameters were not considered in the present study.

Dimensional analysis provides a means by which one can consider the effects of several variables in unison. Roberson and Crowe (1980) state that the basic objective of dimensional analysis is to reduce a large number of variables into a smaller group of dimensionless numbers. The Buckingham PI Theorem indicates that to describe a given problem the required number of dimensionless groups is equal to n-m where n is the number of variables and m is the number of basic dimensions represented in the variables.

From the list of parameters known to influence the force that a moving ice sheet exerts on a vertical cylindrical structure and with the addition of the acceleration of gravity a tentative list of PI groups can be established. The parameters of ice temperature, grain size and orientation, and strength deserve further discussion.

In this study ice temperatures were in a range from -0.3° to -2.2°C with the exception of one test with an ice temperature of -7.5°C. All the experimental data has been corrected to reflect an ice temperature of -0.5°C using the relationship of compressive strength versus ice temperature from Schwartz (1970). This has been previously discussed (re. section 5.4). A determination of ice grain size and orientation has been made by Schrieber (1983). It is assumed that ice grain size and orientation is the same in all ice sheets tested and this assumption appears consistent with Schriber's

preliminary results. Schrieber has determined that the average grain size of the ice created in both the 1 g environment and in the 20 and 50 g environments is approximately 0.08 in. (2 mm). He has also determined that the ice tested in this study exhibits a columnar structure and a horizontal crystallographic axis with a random orientation of crystals within this plane.

The compressive strength of ice appears to be the most appropriate parameter to relate to the maximum force that an ice sheet exerts on the model pile. This statement is supported by the experimental observation that the maximum force was always measured soon after ice failure was observed. When the maximum force was reached little or no bending was observed directly in front of the pile while an area of open water was observed directly behind the pile. Crushing of the ice was observed directly in front of the pile. As a test progressed the force on the pile became smaller and bending deformations as well as radial and circumferential cracking were observed in front of the pile. These observations appear to be consistent with the fact that the flexural strength of ice is less than the compressive strength.

It is proposed that under conditions of constant ice sheet temperature and in ice with similar grain size and orientation that the maximum force an ice sheet exerts on a structure is a function of the pile diameter, ice thickness, penetration velocity, ice compressive strength, and the acceleration of gravity. In mathematical terms this may be expressed as:

$$F_{max} = f(d, t, v, \sigma_c, g, n) \tag{6.11}$$

in which,

F_{max} = maximum force the ice exerts on the pile

d = pile diameter

t = ice thickness

v = penetration velocity

σ_c = ice compressive strength

g = acceleration of gravity

n = centrifugal acceleration in units of g

Since there are seven variables and three basic dimensions, mass, length, and time, then the Buckingham PI Theorem indicates that four nondimensional numbers are required to characterize the problem. The nondimensional numbers that appear to be most appropriate are as follows:

$$PI_1 = \frac{F_{max}}{\sigma_c dt}$$

$$PI_2 = \frac{v^2}{gt} \qquad (6.12)$$

$$PI_3 = \frac{d}{t}$$

$$PI_4 = n$$

These nondimensional numbers have physical meaning. PI_1 is the ratio of the peak effective pressure on the pile, F_{max}/dt, to the compressive strength of ice, σ_c. PI_2 is in the form of a Froude number squared and represents the ratio of inertial to gravity forces. Contained within PI_2 is the product of penetration velocity and strain rate. The definition of strain rate is adopted, by convention, as the

ratio of penetration velocity to ice thickness. PI_3 is the aspect ratio, a term commonly employed by ice/structure interaction researchers. PI_4 is the centrifugal acceleration in units of g's.

Mathematically the dependant PI groups are a function of the independent PI groups, or:

$$\frac{F_{max}}{\sigma_c dt} = f\left(\frac{v^2}{gt}, \frac{d}{t}, n\right) \tag{6.13}$$

In this study all parameters except the compressive strength of ice have been determined. A study is currently underway to determine the compressive strength for ice created in the same manner as that which was used in this study. The compressive strength of ice as determined by Schwartz (1970) has been adopted for use in the analysis of the experimental data of this study. It is recognized that the compressive strength of ice is a function of ice temperature, strain rate, and the direction of the applied stress. The relationship between compressive strength and strain rate for a load applied perpendicular to the direction of ice growth near -0.5°C is shown in Figure 3.7.

From the information given in Tables 5.4, 5.5 and 5.6 and knowning the compressive strength of ice at corresponding strain rates as given by Schwartz (re. Figure 3.7) values of the the nondimensional numbers may be determined (re. Eq. 6.12). Tables 6.1, 6.2, and 6.3 present the nondimensional numbers calculated from the test data.

A plot of the normalized force on the pile, $\frac{Fmax}{\sigma_c dt}$, and the Froude

Table 6.1 Nondimensional numbers for 1 g data

Test # (1)	Strain Rate (1/sec) (2)	Compressive Strength (psi)	Compressive Strength (kg/cm^2) (3)	$\frac{F_{max}}{\sigma_c dt}$ (4)	$\frac{v^2}{gt}$ (6)	$\frac{d}{t}$ (6)	n (7)
N2	1.80×10^{-1}	358	25.2	2.95	1.16×10^{-5}	5.40	1
N3	9.36×10^{-2}	415	29.2	2.90	6.06×10^{-6}	2.81	1
N4	4.76×10^{-2}	457	32.1	2.46	1.60×10^{-6}	2.98	1
N5	2.44×10^{-2}	528	37.1	2.04	3.95×10^{-8}	2.93	1
N7	1.19×10^{-2}	528	37.1	1.53	8.95×10^{-8}	3.05	1
N8	2.21×10^{-2}	514	36.1	2.04	3.57×10^{-7}	2.65	1
N9	3.33×10^{-3}	543	38.2	1.23	7.05×10^{-9}	2.94	1
N10	6.11×10^{-3}	528	37.1	1.46	2.63×10^{-8}	2.75	1
N11	2.13×10^{-3}	500	35.2	0.97	2.29×10^{-9}	3.82	1
N12	8.20×10^{-3}	528	37.1	1.04	1.27×10^{-8}	5.32	1
N13	4.93×10^{-2}	464	32.6	2.27	1.06×10^{-6}	4.44	1
N14	2.06×10^{-1}	351	24.7	3.36	1.78×10^{-5}	4.63	1
N15	5.59×10^{-3}	533	37.5	0.41	1.21×10^{-8}	3.36	1

Table 6.1 (continued) Nondimensional numbers for 1 g data

Test # (1)	Strain Rate (1/sec) (2)	Compressive Strength (psi) (3)	Compressive Strength (kg/cm^2) (3)	$\frac{F_{max}}{\sigma_c dt}$ (4)	$\frac{v^2}{gt}$ (6)	$\frac{d}{t}$ (6)	n (7)
N16	4.39×10^{-2}	472	33.2	1.63	9.46×10^{-7}	2.63	1
N17	1.22×10^{-1}	393	27.6	4.20	6.57×10^{-6}	2.92	1
N18	2.31×10^{-1}	349	24.5	2.60	2.00×10^{-5}	3.47	1
N19	9.77×10^{-3}	528	37.1	1.43	3.16×10^{-8}	3.91	1
N20	6.22×10^{-2}	543	38.2	2.14	1.34×10^{-6}	3.73	1
N21	3.17×10^{-1}	329	23.1	3.28	2.74×10^{-5}	4.76	1
N22	2.47×10^{-1}	343	24.1	3.92	2.13×10^{-5}	3.70	1
N23	1.20×10^{-1}	386	27.1	2.54	5.17×10^{-6}	5.40	1

Table 6.2 Nondimensional numbers for 20 g data

Test # (1)	Strain Rate (1/sec) (2)	Compressive Strength (psi) (3)	Compressive Strength (kg/cm^2) (3)	$\frac{F_{max}}{\sigma_c dt}$ (4)	$\frac{v^2}{gt}$ (6)	$\frac{d}{t}$ (6)	n (7)
C4	8.23×10^{-2}	450	31.6	2.96	2.84×10^{-6}	3.08	20
C5	1.76×10^{-2}	521	36.6	0.55	1.14×10^{-7}	3.52	20
C7	2.23×10^{-2}	521	36.6	3.62	1.44×10^{-7}	4.46	20
C8	2.21×10^{-2}	443	31.1	2.91	1.43×10^{-7}	4.42	20
C9	6.30×10^{-2}	443	31.1	3.66	1.22×10^{-6}	4.20	20
C10	8.28×10^{-2}	415	29.2	4.73	2.86×10^{-6}	3.11	20
C11	1.59×10^{-1}	372	26.2	4.34	1.03×10^{-5}	3.18	20
C16	1.72×10^{-3}	528	37.1	3.37	2.78×10^{-8}	3.45	20
C17	1.63×10^{-2}	528	37.1	2.34	1.41×10^{-7}	2.45	20
C18	5.63×10^{-2}	443	31.1	2.62	1.54×10^{-6}	2.17	20
C19	1.43×10^{-1}	386	27.1	3.31	1.23×10^{-5}	2.15	20
C20	1.54×10^{-1}	372	26.2	3.44	1.33×10^{-5}	2.31	20
C21	2.28×10^{-1}	343	24.1	4.47	1.97×10^{-5}	3.42	20
C22	1.01×10^{-1}	400	28.1	3.55	3.48×10^{-6}	3.78	20

Table 6.2 (continued) Nondimensional numbers for 20 g data

Test # (1)	Strain Rate (1/sec) (2)	Compressive Strength (psi) (3)	Compressive Strength (kg/cm^2) (3)	$\frac{F_{max}}{\sigma_c dt}$ (4)	$\frac{v^2}{gt}$ (6)	$\frac{d}{t}$ (6)	n (7)
C29	8.74×10^{-3}	528	37.1	2.09	2.82×10^{-8}	5.28	20
C30	4.65×10^{-2}	472	33.2	2.64	1.00×10^{-6}	4.19	20
C31	2.13×10^{-1}	343	24.1	4.29	1.83×10^{-5}	4.78	20
C32	3.55×10^{-3}	543	38.2	2.03	1.15×10^{-8}	2.14	20
C33	3.00×10^{-2}	500	35.2	2.64	6.66×10^{-7}	2.78	20
C34	1.30×10^{-1}	386	27.1		1.12×10^{-5}	2.93	20

Table 6.3 Nondimensional numbers for 50 g data

Test # (1)	Strain Rate (1/sec) (2)	Compressive Strength (psi) (3)	Compressive Strength (kg/cm^2) (3)	$\frac{F_{max}}{\sigma_c dt}$ (4)	$\frac{v^2}{gt}$ (6)	$\frac{d}{t}$ (6)	n (7)
C 6	1.63×10^{2}	528	37.1	2.39	1.06×10^{-7}	3.27	50
C12	9.63×10^{-3}	528	37.1	2.48	6.20×10^{-8}	2.00	50
C13	4.52×10^{-2}	472	33.2	3.19	8.75×10^{-7}	3.01	50
C14	8.13×10^{-2}	415	29.2	4.82	2.81×10^{-6}	3.25	50
C15	1.43×10^{-1}	372	26.2	4.76	9.25×10^{-6}	2.86	50
C23	1.54×10^{-2}	514	36.1	2.90	5.05×10^{-8}	6.25	50
C24	8.28×10^{-3}	543	38.2	2.98	2.51×10^{-8}	3.31	50
C25	1.60×10^{-1}	385	27.1	3.67	2.90×10^{-6}	9.62	50
C26	5.67×10^{-2}	443	31.1	3.99	1.23×10^{-6}	3.40	50
C27	1.52×10^{-1}	372	26.2	3.73	1.32×10^{-5}	2.28	50
C28	2.31×10^{-1}	343	24.1	5.14	2.00×10^{-5}	3.47	50
C35	3.99×10^{-3}	543	38.2	2.29	1.29×10^{-8}	2.40	50
C36	3.56×10^{-2}	500	35.2	3.44	5.49×10^{-7}	2.74	50
C37	6.29×10^{-2}	429	30.2	2.77	8.51×10^{-8}	1.88	50

number squared, $\frac{v^2}{gt}$, is shown in Figure 6.3. The aspect ratio, d/t, for each data point is shown on the plot. The data points are also grouped in terms of the g level, n. There appears to be a strong correlation between the normalized force, the Froude number squared, and the g level. Families of curves can be drawn at the three g levels using linear regression. These lines are shown in Figure 6.3. The equations describing these lines are:

$$\text{At } n = 1: \quad \frac{F_{max}}{\sigma_c dt} = (.6135)\log(\frac{v^2}{gt}) + 6.072 \tag{6.14}$$

$$\text{At } n = 20: \quad \frac{F_{max}}{\sigma_c dt} = (.6793)\log(\frac{v^2}{gt}) + 7.190 \tag{6.15}$$

$$\text{At } n = 50: \quad \frac{F_{max}}{\sigma_c dt} = (.6336)\log(\frac{v^2}{gt}) + 7.389 \tag{6.16}$$

Assuming that these lines should be parallel and adopting the average slope leads to a set of relationships as follows.

$$\text{At } n = 1: \quad \frac{F_{max}}{\sigma_c dt} = (.6427)\log(\frac{v^2}{gt}) + 6.072 \tag{6.17}$$

$$\text{At } n = 20: \quad \frac{F_{max}}{\sigma_c dt} = (.6427)\log(\frac{v^2}{gt}) + 7.190 \tag{6.18}$$

$$\text{At } n = 50: \quad \frac{F_{max}}{\sigma_c dt} = (.6427)\log(\frac{v^2}{gt}) + 7.389 \tag{6.19}$$

The values of the y intercept can be plotted against the log of the g level, n, as shown in Figure 6.4.

The least squares best straight line through these points leads to

$$y = .7960 \log(n) + 6.088 \tag{6.20}$$

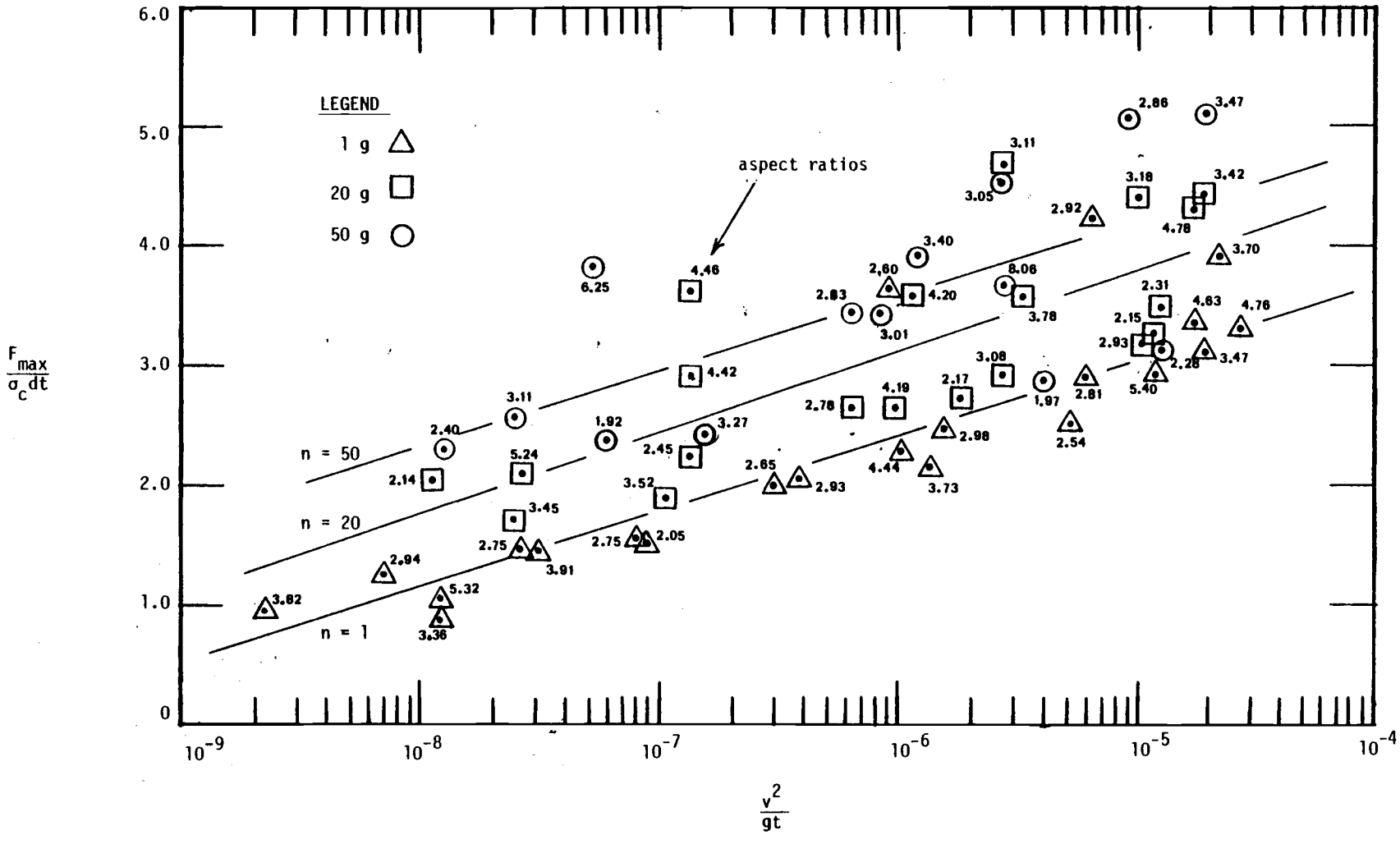

Figure 6.3 Normalized force on the pile versus the Froude number squared.

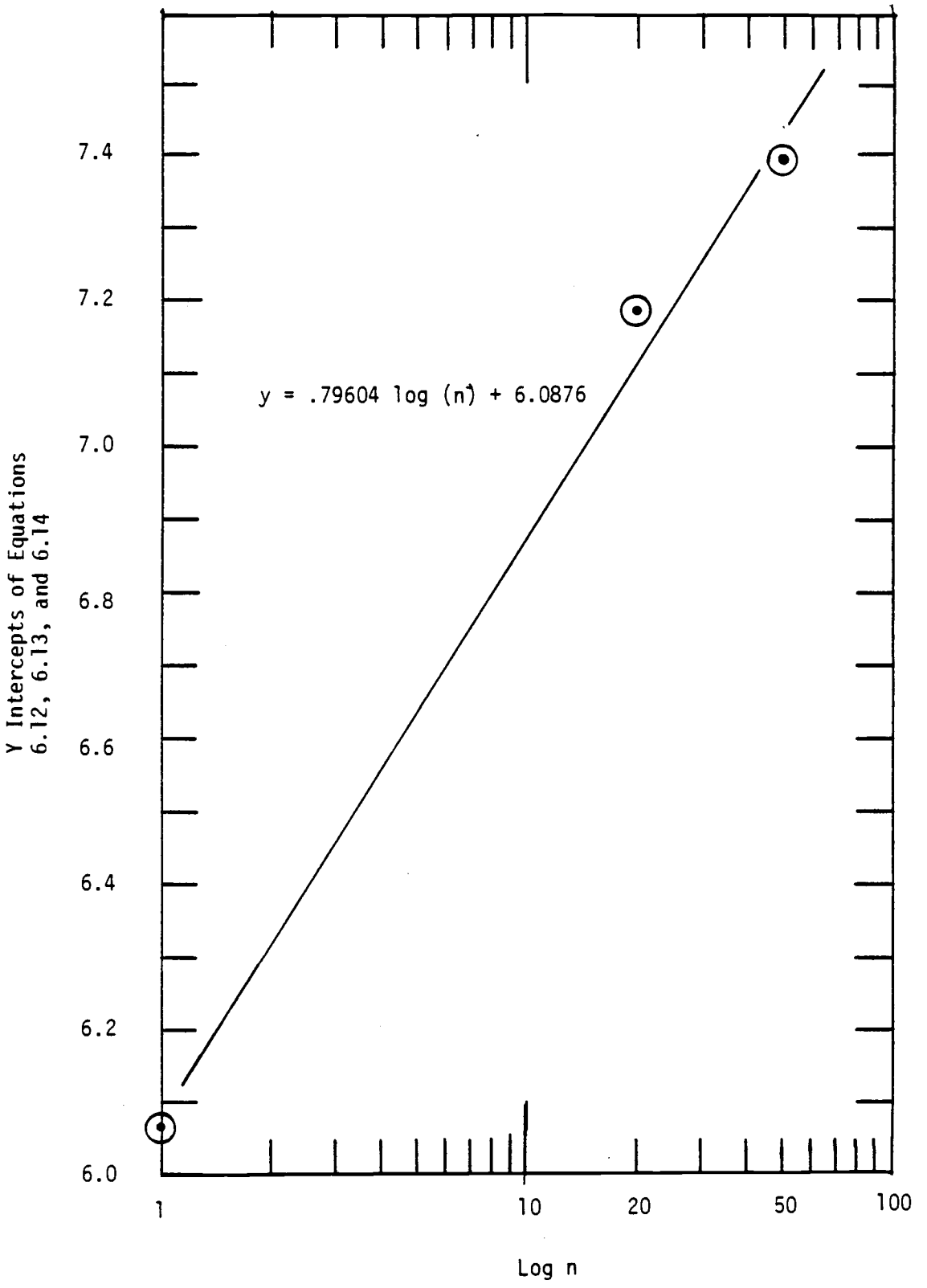

Figure 6.4. Y intercept of equations 6.17, 6.18, and 6.19 versus g level, n.

Equations 6.17 through 6.19 may be reduced to:

$$\frac{F_{max}}{\sigma_c dt} = .6427 \log \left(\frac{v^2}{gt}\right) + .7960 \log(n) + 6.088 \qquad (6.21)$$

This relationship may be plotted for various values of n and is shown in Figure 6.5.

As shown in Figure 6.3 the effect of aspect ratio d/t is difficult to interpret. In an attempt to ascertain the effect of aspect ratio the relationship between normalized force and aspect ratio was plotted at various g levels as shown in Figures 6.6 through 6.8. Shown in the legend is the order of magnitude of the Froude number squared for each data point. As seen in these figures it is difficult to interpret the exact relationship between normalized force, aspect ratio, and the square of the Froude number. It may be generalized, however, that as aspect ratio increases the normalized force decreases. Furthermore, as the square of the Froude number increases or as the g level increases the normalized force increases.

6.4 Experimental Errors

It is appropriate to discuss possible sources of error which may be represented in the results of this study before a comparison with the results of others is made.

The greatest source of error is probably due to the nonuniformity of the ice sheets employed in the study. As previously mentioned thicker sections of ice existed directly adjacent to the pile and at the boundaries of the ice sheet. This was accounted for by taking the average of the thicknesses within a radius of about 3.5 in. (9 cm)

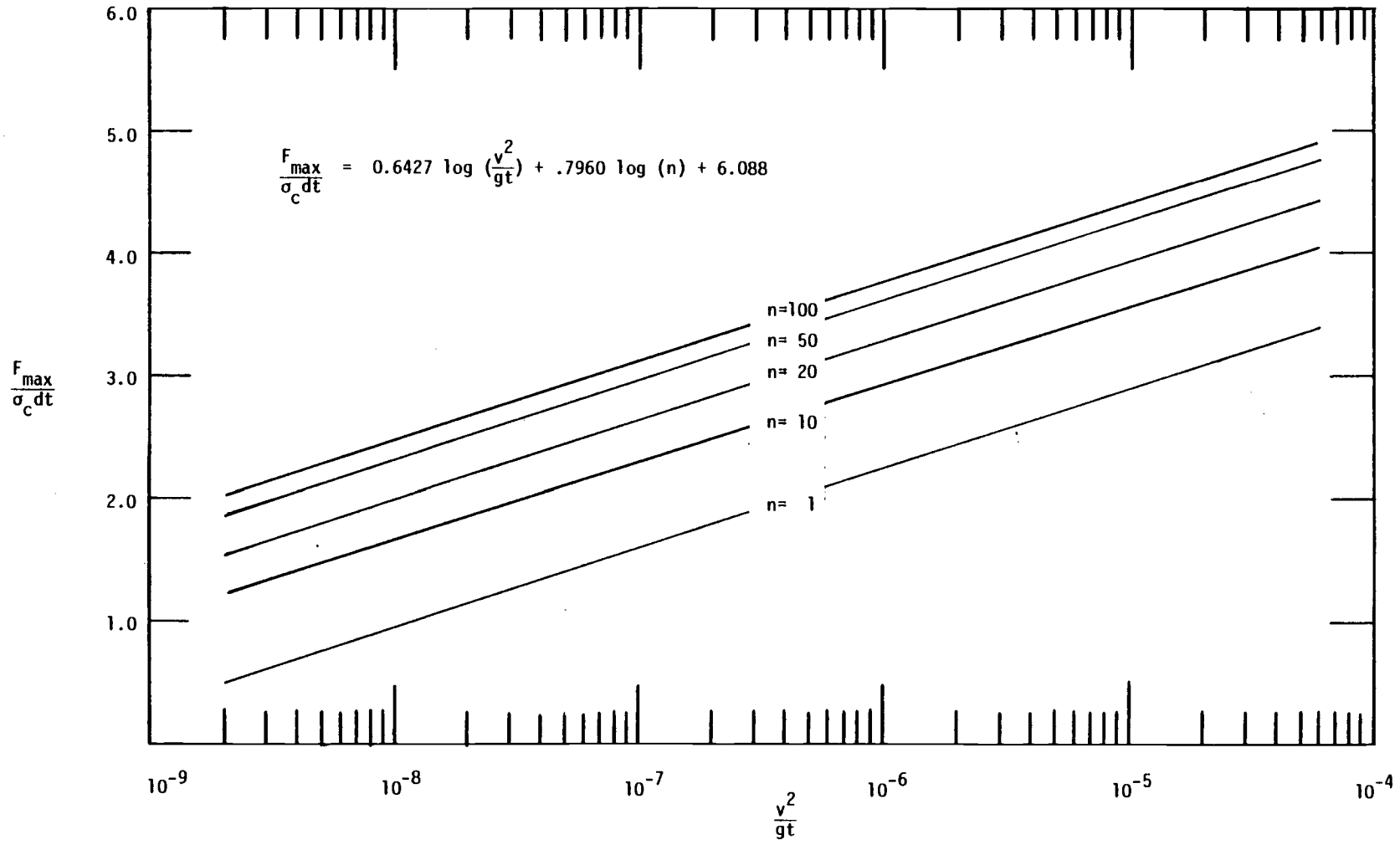

Figure 6.5 Normalized force versus the Froude number squared for several values of the g level, n.

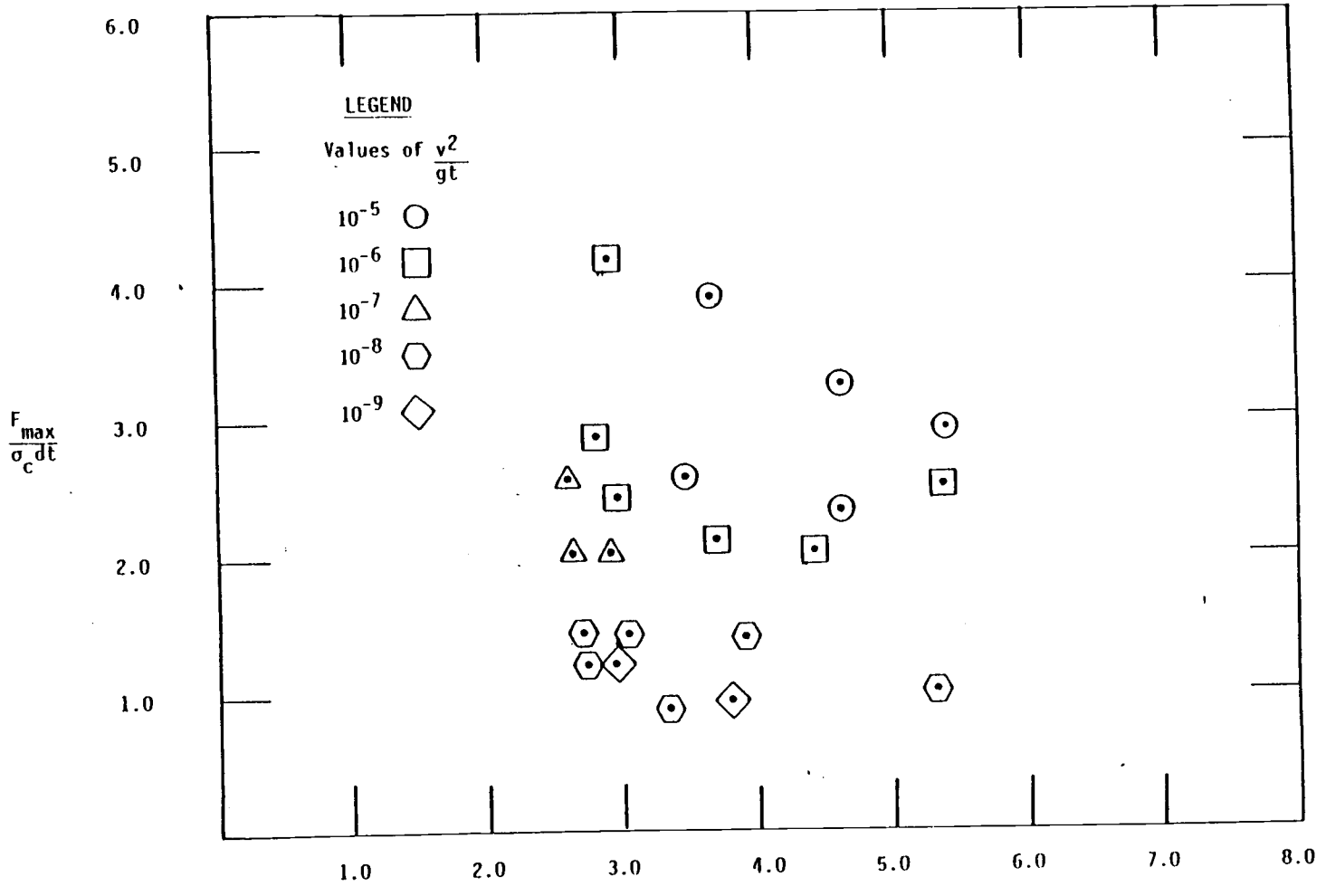

Figure 6.6 Normalized force versus the aspect ratio at 1 g.

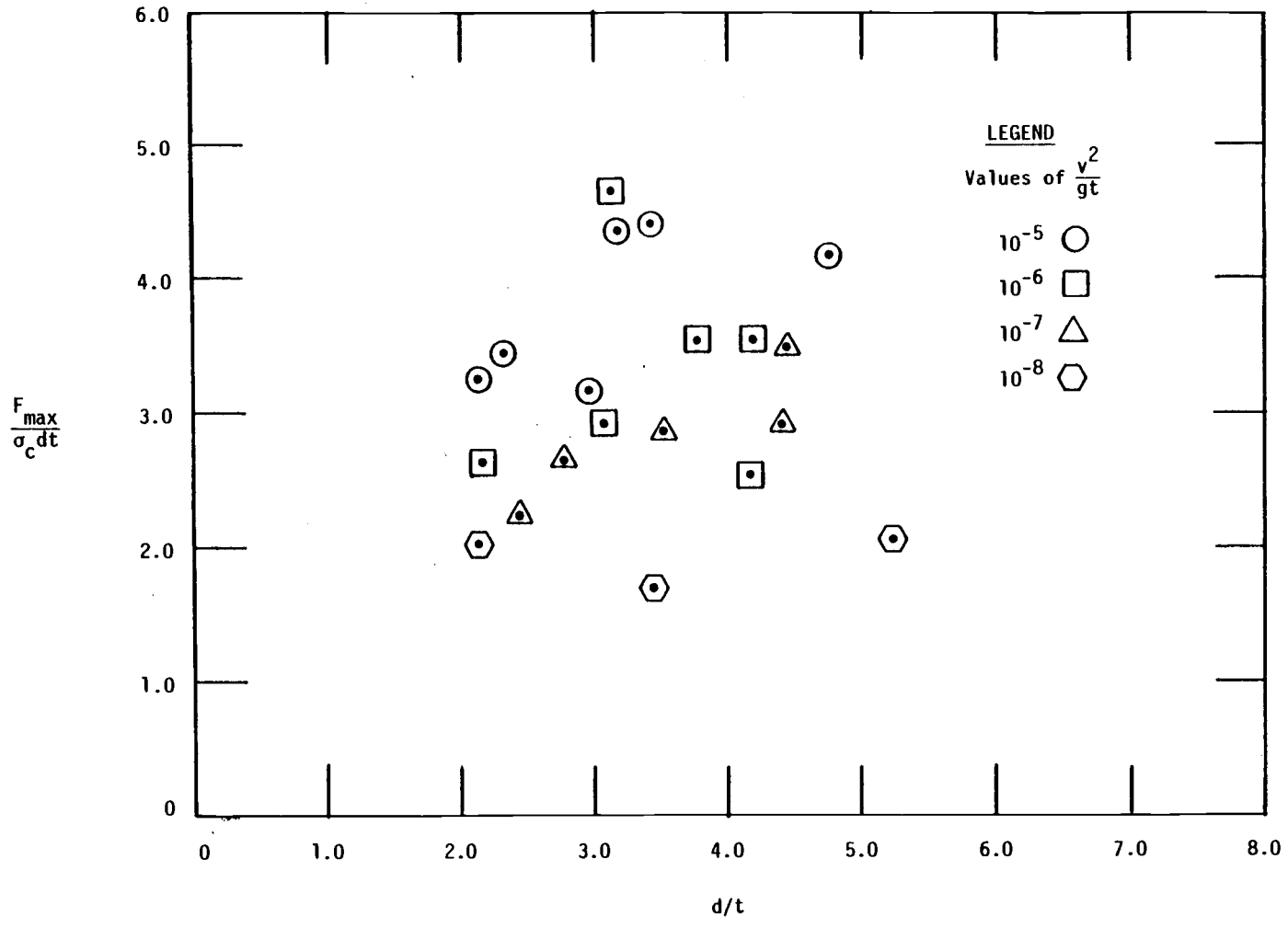

Figure 6.7 Normalized force versus the aspect ratio at 20 g.

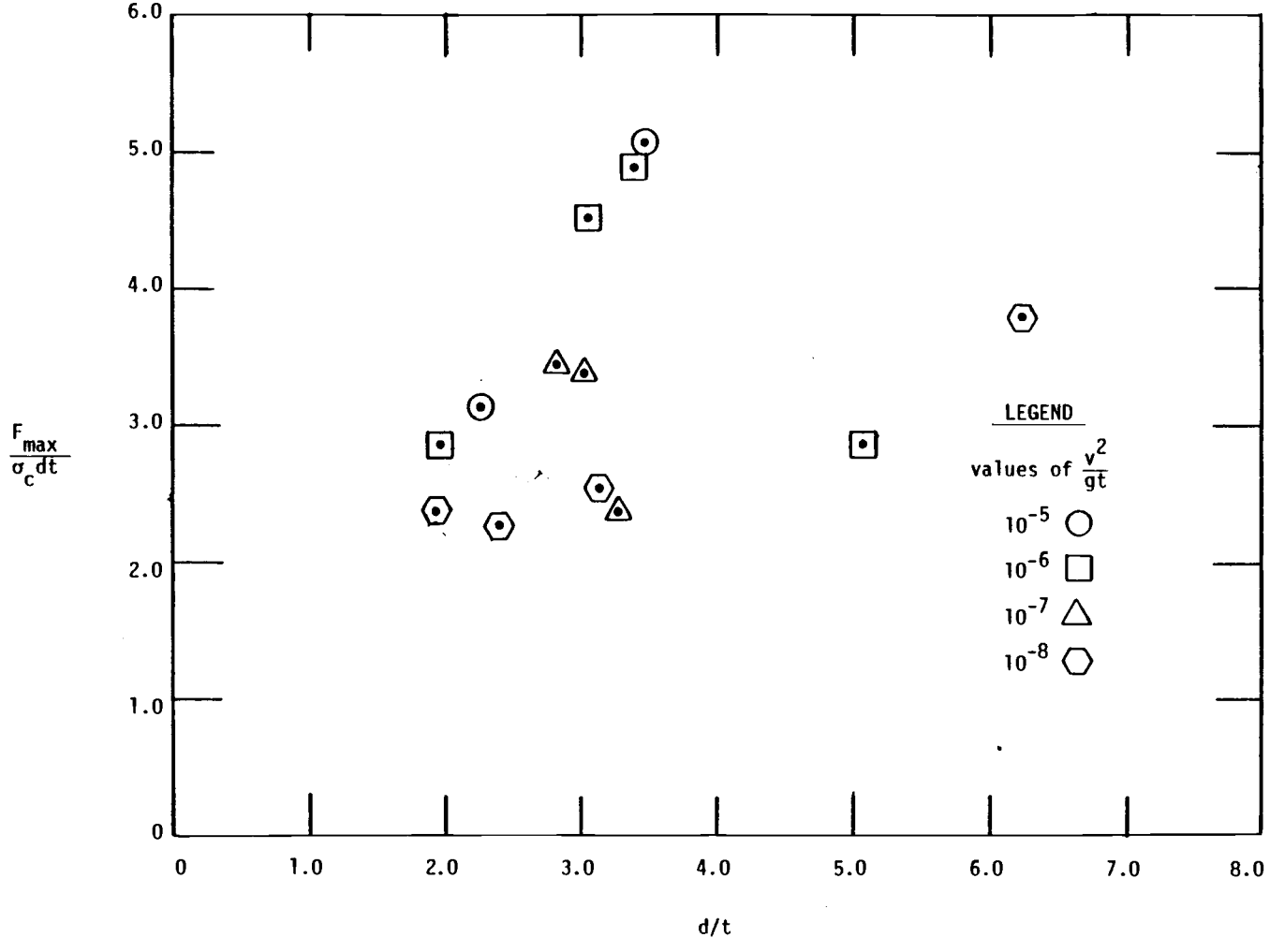

Figure 6.8 Normalized force versus the aspect ratio at 50 g.

around the pile. The ice within this radius corresponded to that maximum area of ice which was observed to participate in the failure. Within the 3.5 in. (9 cm) radius areas of thicker or thinner ice than the average existed. If the pile encountered an area of ice thicker than the average then the normalized ice force calculated would be greater than the actual value. The reverse would be true if the pile encountered a thinner section of ice.

Another source of error could be associated with the fact that all the ice failure data was normalized to represent an ice temperature of -0.5°C. The correction factor was taken from Schwartz (1970) and it is assumed that his data correctly represents the variation of ice compressive strength with respect to temperature. However, since the variation in temperatures were not large and the correction factor is not large the error associated with this correction should be small.

Errors could be introduced due to the flexure in the model pile under load. This flexure caused the model pile to deflect from a true vertical orientation during the tests. Furthermore, since the measured forces varied the flexure would vary as well and greater flexure would exist in the 1/2 in. diameter pile than in the 3/4 in. model pile under the same load. Since the pile length is short this error should be small as far as the measured force is concerned. This flexure causes the contact face between the ice and the pile to be inclined and this may promote a flexural failure in the ice rather than a crushing failure as pile penetration into the ice continues.

There is a possibility that the boundary conditions at the edge of the ice sheet could also influence the results. Since in no case

did the ice failure extend to the ice sheet boundary it is assumed that boundary conditions did not enter the problem and that the testing approximated a semi-infinite ice sheet. No attempts were made to change the boundary conditions in the study.

6.5 Comparison of Results with Previous Studies

The results of this study may be compared to the results obtained by previous researchers in an attempt to validate the use of the centrifugal modeling technique to study ice forces and ice floe failure mechanisms on a vertical pile. The results presented in the work of Kry (1981), Taylor (1981), Iyer (1983), Lipsett and Gerard (1980) and Schwartz (1970) may be used for purposes of comparison. The results of Kry and Taylor are presented in terms of pile diameter, ice thickness, penetration velocity, and the maximum pressure the ice exerted on the pile and can be compared directly to the results of this study. Kry and Taylor considered ice at temperatures of -2 and -10°C. Their data for ice at a temperature of -10°C is considered to represent a brittle failure. The warmer ice considered in this study exhibited a ductile failure mode. For this reason it is inappropriate to extrapolate their results at this colder temperature to reflect a warmer temperature. Only their results for ice at -2°C will be considered. Kry and Taylor's results are given and have been corrected to reflect an ice temperature of -0.5°C and are shown in Table 6.4. Dimensionless numbers in the form of those used to analyze the data of this study (re. Eq. 6.12) may be calculated and are shown in Table 6.5.

Table 6.4 Kry and Taylor's results corrected to -0.5 °C

Researcher (1)	Ice Thickness (in.) (2)	(cm)	Pile Diameter (in.) (3)	(cm)	Penetration Velocity (in./min) (4)	(cm/min)	Strain Rate (1/sec) (5)	Max. Ice Pressure @ -2°C (psi) (6)	(MPa)	Max. Ice Pressure @ -0.5°C (psi) (7)	(MPa)
Kry	1.01	2.57	5.0	12.7	.485	1.23	8×10^{-3}	580	4.00	531	3.66
Kry	1.00	2.54	10.0	25.4	.478	1.21	8×10^{-3}	421	2.90	372	2.56
Kry	11.9	30.2	48.0	122	.500	1.27	7×10^{-4}	435	3.00	386	2.66
Kry	11.7	29.7	48.0	122	1.40	3.56	2×10^{-3}	348	2.40	299	2.06
Kry	10.6	26.9	48.0	122	4.45	11.3	7×10^{-3}	508	3.50	459	3.16
Kry	9.29	23.6	48.0	122	11.2	28.5	2×10^{-2}	363	2.50	314	2.17
Taylor	32.0	81.3	12.0	30.5	4.80	12.2	2.5×10^{-3}	515	3.55	466	3.21
Taylor	31.0	78.7	24.0	70.0	6.42	16.3	3.4×10^{-3}	510	3.52	461	3.18

Table 6.5 Nondimensional numbers representing Kry and Taylor's results.

Recorder (1)	Strain Rate (1/sec) (2)	Compressive Strength of Ice (psi) (3)	(MPa) (3)	$\frac{F_{max}}{\sigma_c dt}$ (4)	$\frac{v^2}{gt}$ (5)	$\frac{d}{t}$ (6)	n (7)
Kry	8×10^{-3}	512	3.53	1.04	1.67×10^{-7}	4.95	1
Kry	8×10^{-3}	512	3.53	0.727	1.65×10^{-7}	10.0	1
Kry	7×10^{-4}	341	2.35	1.13	1.51×10^{-8}	4.03	1
Kry	2×10^{-3}	484	3.34	0.62	1.21×10^{-7}	4.10	1
Kry	7×10^{-3}	498	3.43	0.92	1.34×10^{-6}	4.53	1
Kry	2×10^{-2}	512	3.43	0.61	9.62×10^{-6}	5.17	1
Taylor	2.5×10^{-3}	498	3.53	0.94	5.18×10^{-7}	0.37	1
Taylor	2.4×10^{-3}	526	3.63	0.88	9.56×10^{-7}	0.75	1

Schwartz presents an empirical equation to calculate the pressure an ice sheet exerts on a vertical pile (re Eq. 3.3). Unfortunately, Schwartz has not presented the data which substantiates this relationship nor has he considered the effect of penetration velocity. The relationship which Schwartz presents is believed to be valid at a strain rate of 2×10^{-3}/sec. For comparison consider an aspect ratio of 4 and a 3/4 in. diameter pile. The compressive strength of ice at a strain rate of 2×10^{-3}/sec is 526 psi as taken from Schwarz. At a temperature of -0.5°C the effective pressure as calculated from Schwartz is 190 psi. The dimensionless numbers representing this are:

$$\frac{F}{c^{dt}} = .362 \qquad \frac{d}{t} = 4$$

$$\frac{2}{gt} = 4.37 \times 10^{-9} \qquad n = 1$$

These values obtained from Kry, Taylor, and Schwarz are compared to the results obtained in the present study in Figure 6.9.

The work of Lipsett and Gerard (1980) offers another data set with which the results of this study may be compared. They studied forces on bridge piers during the spring ice breakup. Specifically, they measured ice forces which were the result of ice floes carried by river currents impacting bridge piers. The ice floes could not be considered as a semi-infinite ice sheet and the ice floe velocities were considerably greater than the velocities measured in this study. Nevertheless, it appears that their results may be a function of the Froude number squared as were the results of this study. The data

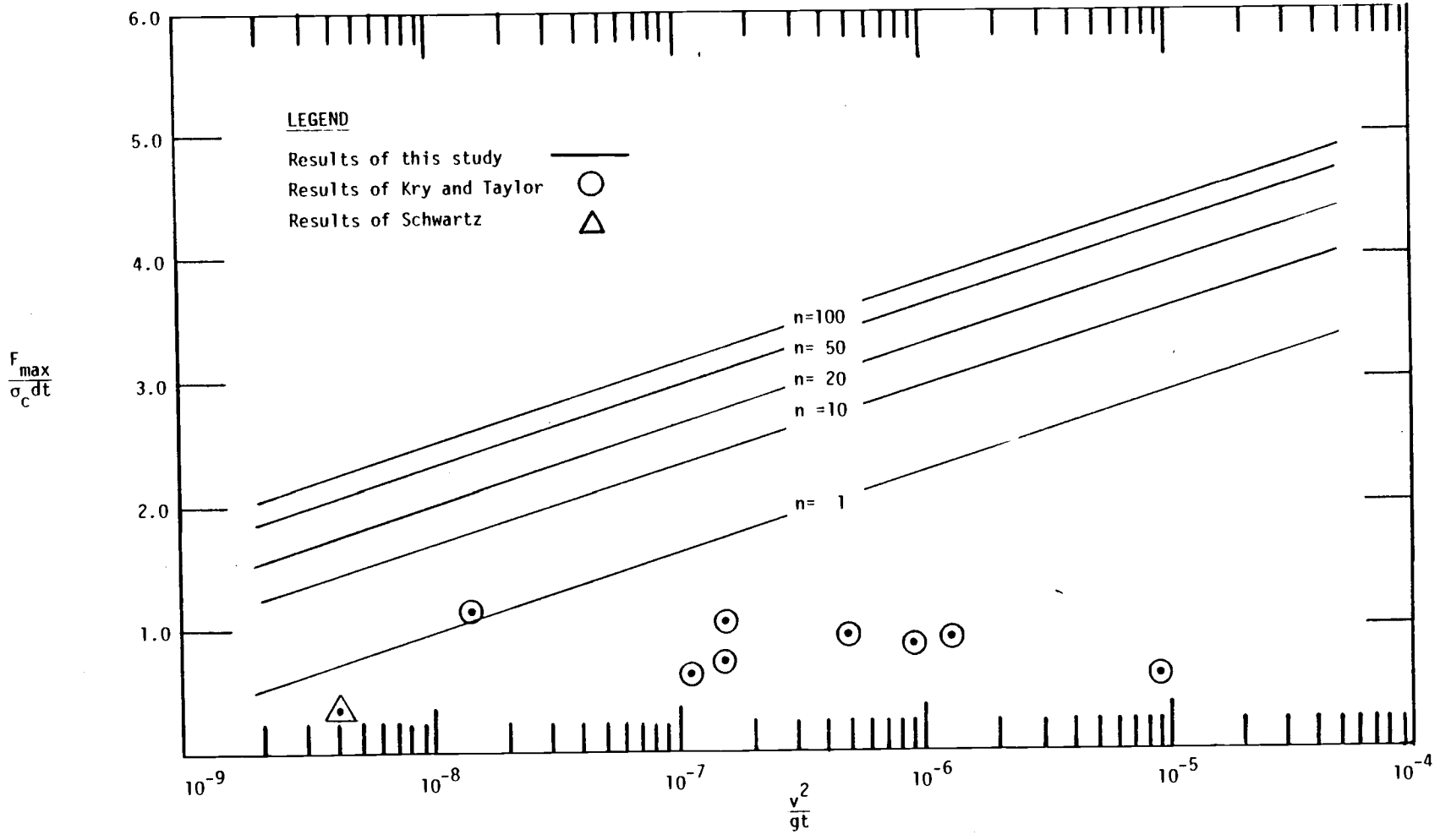

Figure 6.9 Comparison of the results of present study to the results of Kry, Taylor and Schwarz.

which included a measurement of the floe velocity is shown in Table 3.2 (re. section 3.3). Non-dimensional numbers for this data have been calculated and are shown in Table 6.6. The compressive strength of ice assumed for calculation of the normalized ice force is 697 psi which has been taken from Figure 6.10. Lipsett and Gerard did not report the ice temperature. The relationship between normalized force versus Froude number squared based on Lipsett and Gerards results is shown in Figure 6.11. Although the correlation is not strong, the normalized force appears to increase as the Froude number squared increases. This is consistent with the trends observed in this study. Since the square of the Froude number for the data of Lipsett and Gerard is several orders of magnitude greater than the results of this study a more direct comparison is not justified.

Lipsett and Gerard present a relationship between normalized ice force and aspect ratio from a compilation of the results of several researchers. This relationship was shown in Figure 3.9 (re. Section 3.3). In Figure 3.8 Iyer has shown a relationship similar to that shown in Figure 3.9. The results as presented by Lipsett and Gerard and Iyer may be combined and compared with the results of this study. Figure 6.12 shows the combination of these results together with the results of this study at 1 g. There is agreement between the results of this study and those published by Iyer and Lipsett and Gerard. Those studies do not report the penetration velocities their data represents.

Table 6.6 Nondimensional numbers for events at Pembridge

Event (1)	$\frac{F_{max}}{\sigma_c dt}$ (2)	$\frac{v^2}{gt}$ (3)	$\frac{d}{t}$ (4)	n (5)
P74.04.17.22.07.28	.188	2.45×10^{-1}	1.91	1
.22.10.16	.435	$.3.95 \times 10^{-1}$	1.91	1
.22.13.07	.306	3.54×10^{-1}	1.91	1
.22.15.31	.275	5.80×10^{-1}	1.91	1
.22.40.05	.280	7.34×10^{-1}	1.91	1
.22.41.50	.297	8.17×10^{-1}	1.91	1

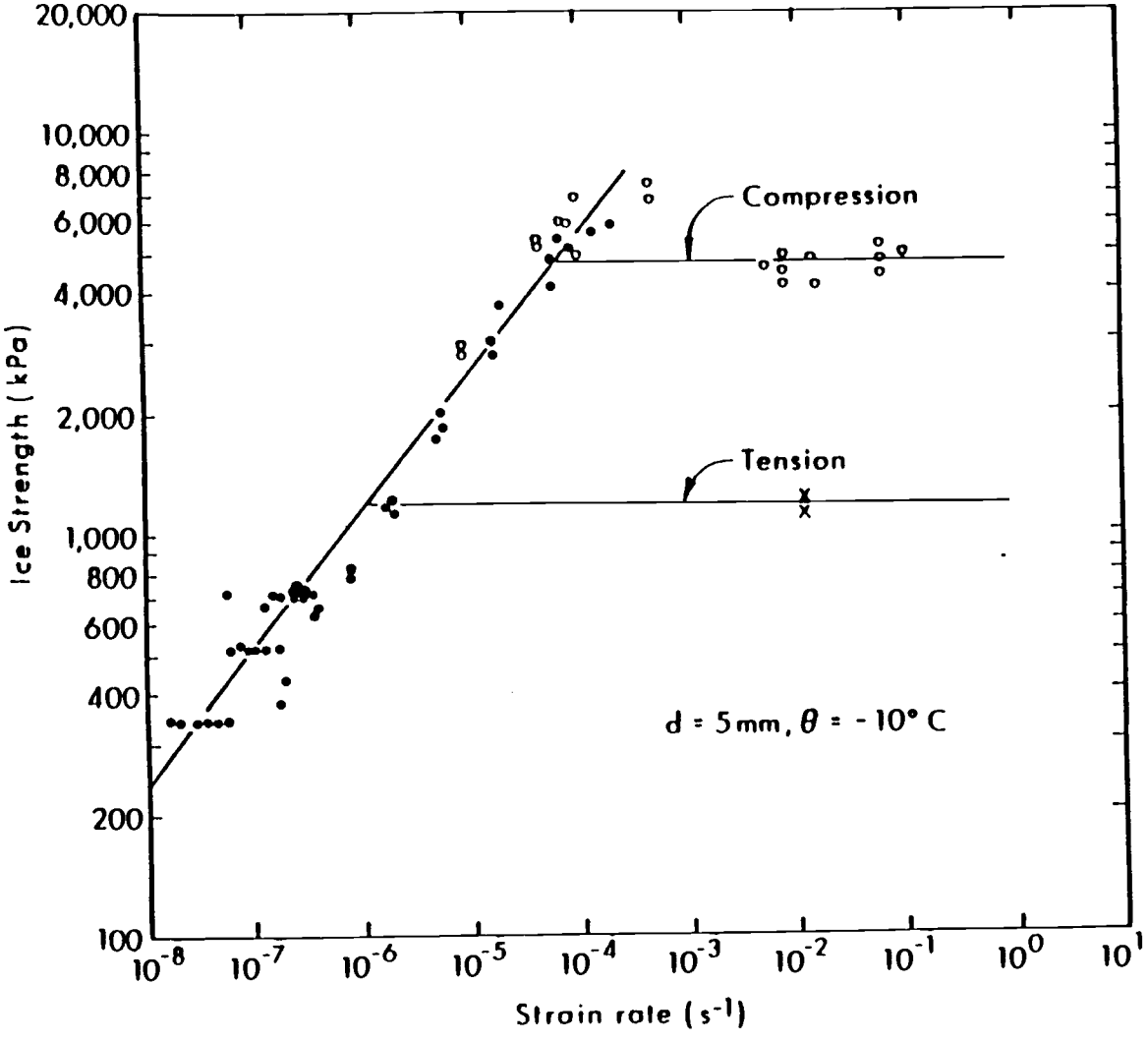

Figure 6.10 Freshwater ice compressive strength at a temperature of -10°C versus strain rate (after Michel, 1978).

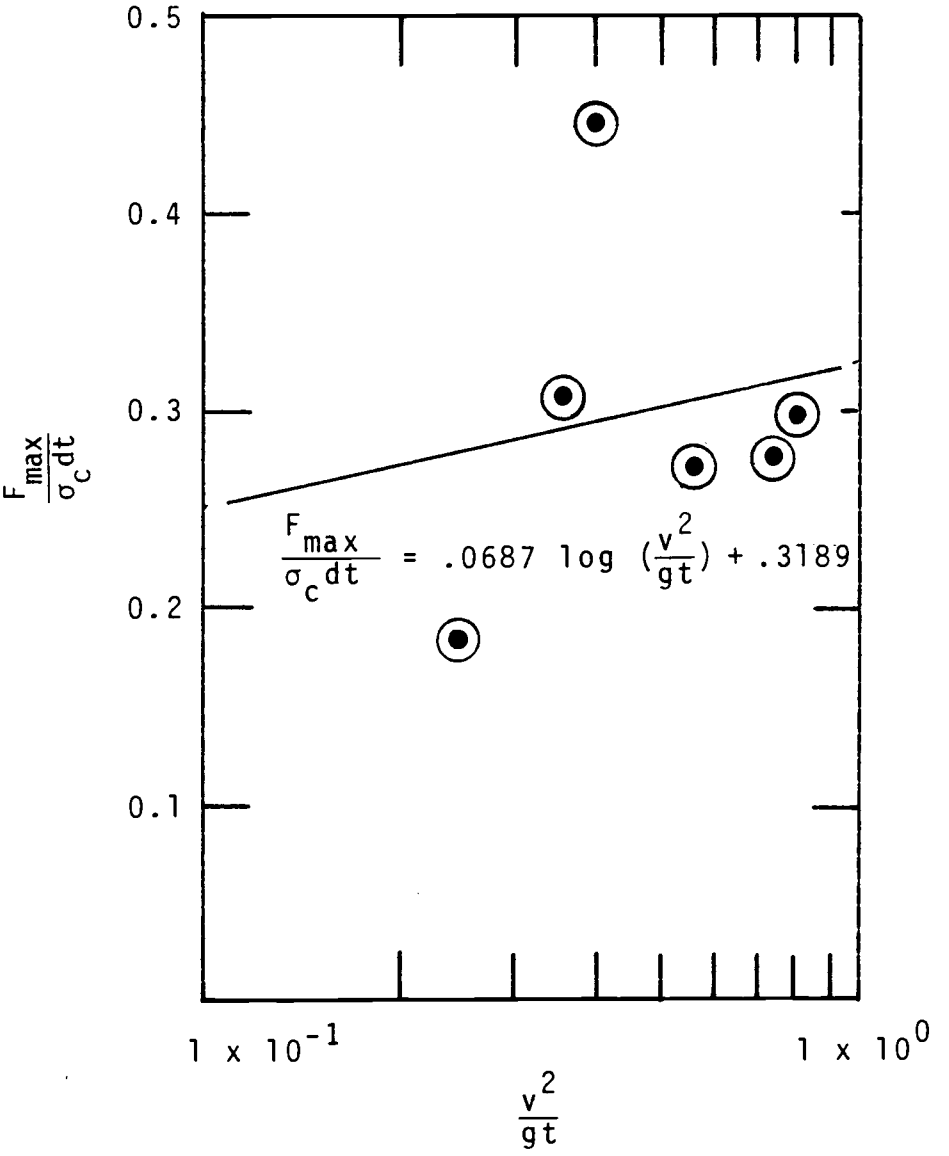

Figure 6.11 Normalized force versus Froude number squared for events at Pembridge.

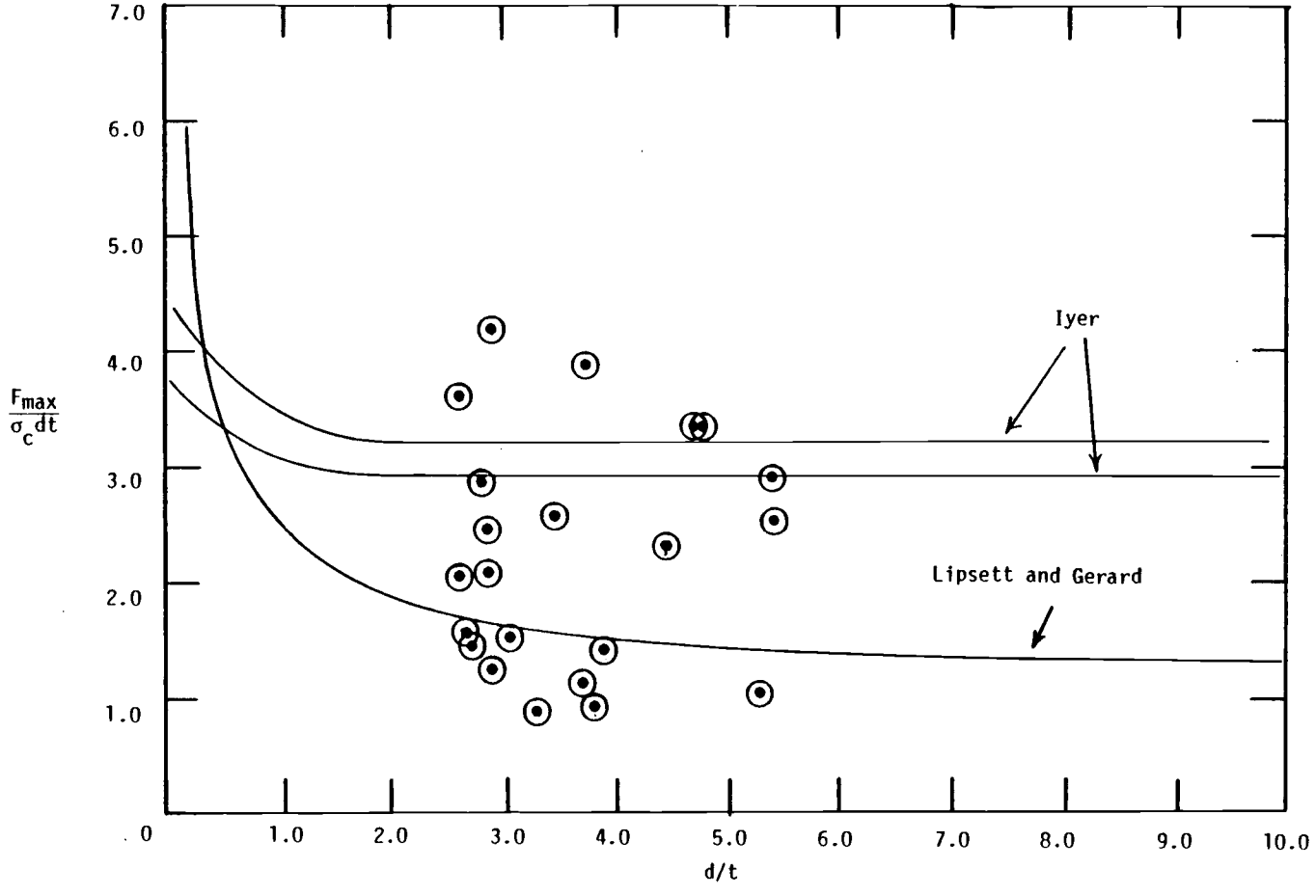

Figure 6.12 Normalized force versus aspect ratio from Lipsett and Gerard (1980) and Iyer (1983) compared to the results of the present study at 1g.

6.6 Inertial Field Effects on Test Results

In order to further study ice forces and ice floe failure mechanisms and to eventually address the ice, structure, and geologic foundation interaction problem it is important to understand the dependance of ice forces on the magnitude of inertial acceleration. It has been observed that as the g level increases the normalized ice force increases. This increase in normalized force appears to be a linear function of the logarithm of the g level (re. Figure 6.4).

Three reasons which may explain this phenomena can be offered. The first assumes that the ice behaves somewhat like an axially loaded beam elastically braced against buckling. While the self weight of the ice increases the bouyant force of the water increases so that the ice sheet remains in equilibrium and floats at the same depth on the water surface. Bouyancy and the weight of the ice may be considered as restoring forces acting to prevent the ice sheet from bending or buckling. As the g level increases the effect of this lateral bracing would be more pronounced. It seems reasonable to expect that if the ice is constrained against buckling the axial load it could carry would be greater.

The second reason that may be offered to explain the increase in ice forces with increasing g level is associated with the fact that the structure of ice contains cracks. These cracks may begin to close due to the increased body weight of ice. If these cracks close then the compressive strength of ice would increase. Since the variation of normalized force on the pile appears to be a linear function of the

logarithm of the g level a threshold g level may be reached at which an increase in the g level produces a negligible increase in the compressive strength of ice. Unfortunately tests were not conducted at high enough g levels to substantiate this hypothesis.

The third reason assumes that splitting of the ice may be the controlling failure mechanism. It was observed that radial and tangential cracking of the ice occurred as the penetration of the pile into the ice sheet continued (re. section 6.3). The formation of these cracks would be controlled by the tensile strength of the ice. The tensile strength of the ice would increase as the centrifugal acceleration increased the overall compressive stress state within the ice. The effect would be that the measured force on the pile would increase as the g level increased because it became more difficult for these cracks to initiate and propagate. A continuum mechanics approach may be a means to further investigate this hypothesis.

6.7 Grain Size Effect on Test Results

The differences observed between the results of this study and the results of others could be due to grain size effects. Results presented by Lipsett and Gerard (1980) and reproduced in Figure 6.15 show a decrease in compressive strength with an increase in grain size. Weeks (1969) found that as the cross-sectional area of a specimen is increased and, hence, represents a greater number of crystals, unconfined compressive strength decreases. Kry reports that the ice tested in his study exhibited a grain size from 1 to 5 mm. The average grain size of the ice tested in the present study is approximately

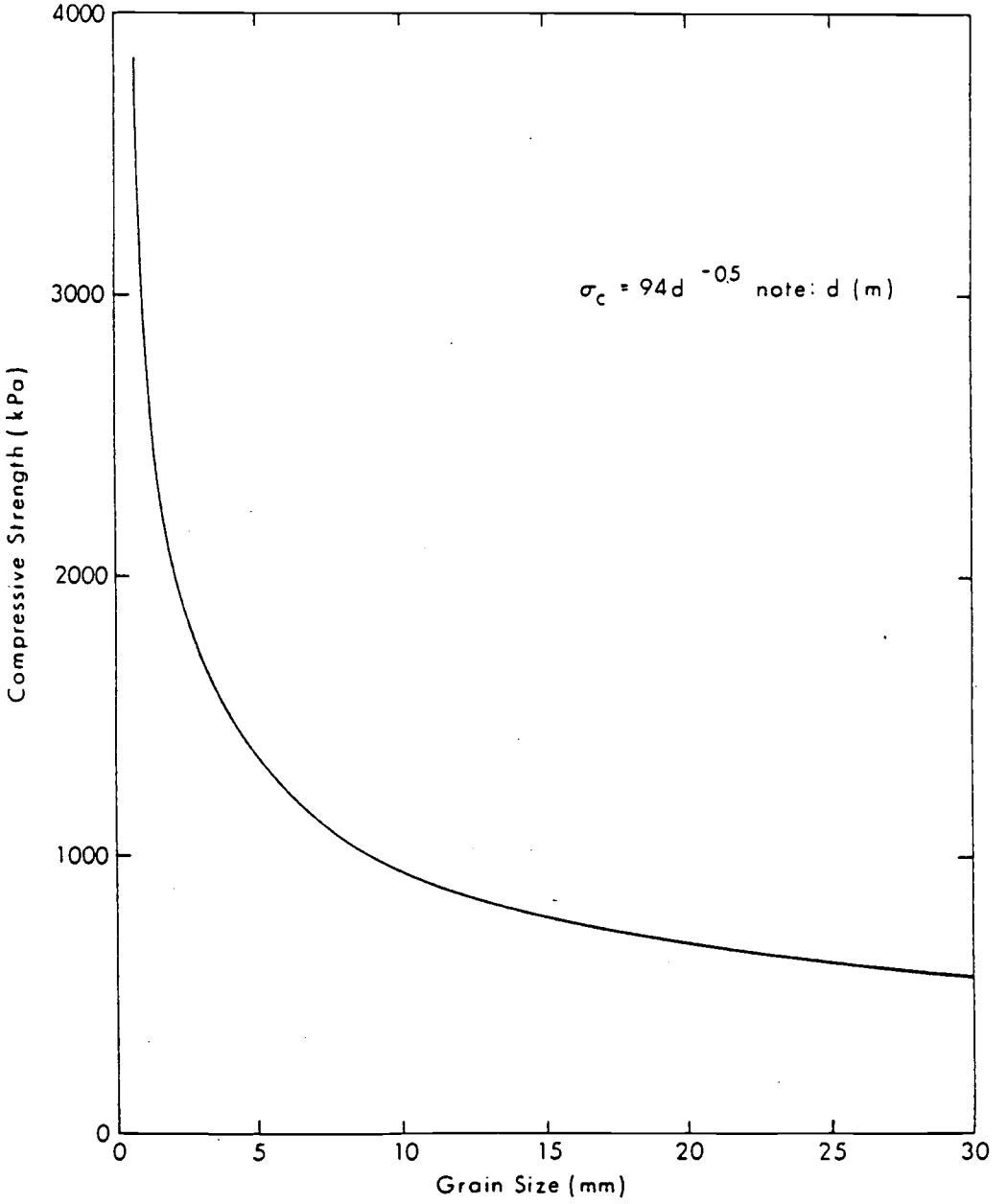

Figure 6.13 Grain size dependance of the strength of polycrystalline ice at 0°C (after Lipsett and Gerard, 1980).

2 mm. Kry considered pile diameters much larger than those considered in this study and consequently the ratio of grain size to pile diameter would be much smaller than the corresponding ratio in this study. Furthermore, the normalized force measured in the present study is greater than that measured by Kry. This observation appears consistent with the observation made by Weeks that as the number of grain boundaries at the contact face increases the apparent strength of ice decreases. It appears that an appropriate nondimensional number to be included in the dimensional analysis of the ice force problem would be the ratio of grain size to either the pile diameter or the ice sheet thickness. Consideration of the crystal orientation, either vertical or horizontal, may influence the selection of either the pile diameter or the ice thicknesses as the important parameter with which to nondimensionalize the grain size.

7.0 SUMMARY AND CONCLUSIONS

7.1 Summary

In response to the need to (1) determine ice forces on offshore structures, and (2) improve our understanding of ice structure interaction phenomena, a physical model study was conducted using the technique of centrifugal modeling. An experimental apparatus was designed and fabricated to allow ice sheets to be created and failed under conditions of 1 g and high inertial accelerations of 20 and 50 g's. The forces exerted on a vertical cylindrical model pile were measured under conditions of constant penetration velocity and ice sheet temperature. The effects of ice thickness, pile diameter, penetration velocity, and inertial acceleration were considered in the research program.

The experimental results were analyzed using the method of dimensional analysis. This provided a means with which to consider the effects of several variables in unison. The dimensionless numbers which appeared to be most appropriate in the analysis included:

(1) Normalized maximum force = $\frac{F_{max}}{\sigma_c dt}$

(2) Froude number squared = $\frac{v^2}{gt}$

(3) Aspect ratio = d/t

(4) g level = n

7.2 Conclusions

The following conclusions are made as a result of this study:

(1) It is possible to create and fail model ice sheets in the high inertial acceleration field of a geotechnical centrifuge.

(2) The thickness of ice sheets formed under high inertial accelerations is proportional to the square root of the freezing index. Discrepancies between the experimental results and predictions by the Stefan solution are due primarily to the fact that the initial water temperatures are above 0°C.

(3) Ice forces in the case of freshwater ice and a vertical cylindrical pile are a function of the pile diameter, ice thickness, penetration velocity, and ice temperature.

(4) Maximum ice forces were measured when the ice was failing in compression. This maximum force was measured immediately after beginning to penetrate the ice with the pile. As penetration continued the ice force decreased and the failure mode transitioned to that of flexural failure.

(5) Measured ice forces normalized with respect to ice compressive strength increase as the square of the Froude number increases, the centrifugal acceleration increases, and the aspect ratio decreases.

(6) Reasonable agreement exists between the results of the present study and the results of other researchers who considered similar problems.

7.3 Recommendations for Further Research

The following recommendations are made as a result of this study:

(1) The results of this study should be reappraised when the ice compressive strength, crystal size, structure, and orientation for the ice employed in the study become available.

(2) A nondimensional number in the form of average crystal size normalized by pile diameter or ice thickness should be incorporated in an analysis of the test results.

(3) A determination of the ice viscosity should be made to consider effects of the Reynold's number.

(4) The influence of pile spacing (for multiple piles), pile inclination, and saline ice on ice forces and ice floe failure mechanisms should be investigated with the centrifugal modeling technique.

BIBLIOGRAPHY

1. Al-Hussaini, M.M., "Centrifuge Model Testing of Soils: A Literature Review", Soils and Pavements Laboratory, U.S. Army Engineer Waterways Experiment Station, Vicksburg, MS. 1976.

2. Allyn, N., and Charpentier, K., "Modeling Ice Rubble Fields Around Arctic Offshore Structures," Proceedings, Offshore Technology Conference, Houston, TX, May, 1982.

3. Bucky, P.B., "Use of Models for the Study of Mining Problems," Technical Publication No. 425, Feb. 1931, American Institute of Mining and Metallurgical Engineering, NY, 1931.

4. Cheney, J., "Introduction to Geotechnical Centrifuge Modeling," High Gravity Simulation for Research in Rock Mechanics Workshop held at Colorado School of Mines, Department of Mining Engineering, Golden, CO, May 13-14, 1982.

5. Clough, H. "User Manual for Data Acquisition Programs for Centrifugal Ice Modeling Studies," Research Report submitted to Dept of Civil Engineering, Oregon State University, 1983.

6. Gold, L.W., "Engineering Properties of Fresh-Water Ice," Journal of Glaciolgoy, Vol. 19, No. 81, 1977, pp 197-212.

7. Haynes, F.D., et al., "Ice Forces on Model Bridge Piers," CRREL Report 83-19, U.S. Army Corps of Engineers Cold Regions Research and Engineering Laboratory, July 1983.

8. Jazrawi, W., and Khauna, J., "Monocone, a Mobile Gravity Platform for the Arctic Offshore," Fourth International Conference on Port and Ocean Engineering under Arctic Conditions, September 1977.

9. Iyer, S.H., "Size Effects in Ice and Their Influence on the Structural Design of Offshore Structures." Gulf Canada Research, Inc., Calgary, Canada, 1983.

10. Kato, K., and Sodhi, D.S., "Ice Action on Pairs of Cylindrical and Conical Structures," CRREL Report 83-75, U.S. Army Corps of Engineers Cold Regions Research and Engineering Laboratory, September 1983.

11. Ko, H., "Centrifuges and Soil Mechanics," High Gravity Simulation for Research in Rock Mechanics Workshop held at Colorado School of Mines, Department of Mining Engineering, Golden, Colorado, May 13-14, 1982.

12. Kry, P.R., "Scale Effects in Continous Crushing of Ice," IAHR/AIRH International Symposium on Ice, Volume II, 1981.

13. Lewis, J.W., "Recent Developments in Physical Ice Modeling," Proceedings, Offshore Technology Conference, Houston, TX, May 1982.

14. Lipsett, A.W. and Gerard, R., "Field Measurements of Ice Forces on Bridge Piers 1973-1979," Alberta Research Council, Report SWE 80-3, Edmonton, Alberta, Canada, December, 1980.

15. Maattanen, M., "Dynamic Ice-Structure Interaction During Continous Crushing," CRREL Report 83-5, U.S. Army Corps of Engineers Cold Regions Research and Engineering Laboratory, February, 1983.

16. Maattanen, M., "Modelling the Interaction Between Ice and Structures," Proceedings of the 7th International Conference on Port and Ocean Engineering Under Arctic Conditions, Volume II, 1983, pp 745-769.

17. Morris, D.V., "The Centrifugal Modeling of Dynamic Soil-Structure Interaction and Earthquake Behavior," Ph.D. Thesis, Cambridge University, 1979.

18. Nakajima, H., Koma, N., and Inoue, M., "The Ice Force Acting on a Cylindrical Pile," Proceedings of the 6th International Conference on Port and Ocean Engineering Under Arctic Conditions, Volume 1, 1981.

19. Nevel, D.E., Perham, R.E., and Hogue, G.B., "Ice Forces on Vertical Piles," CRREL Report 77-10, U.S. Army Corps of Engineers Cold Regions Research and Engineering Laboratory, April 1977.

20. Noble, P.G., and Singh, D., "Interaction of Ice Floes with the Columns of a Semi-Submersible," Proceedings, Offshore Technology Conference, Houston, TX, May, 1982.

21. Roberson, J.A., and Crowe C.T., "Engineering Fluid Mechanics," 2nd Edition, Houghton Miffun Company, Boston, MA, 1980, pp. 274-287.

22. Saeki, H., and Ozaki,A., "Ice Forces on Piles". Proceedings of the Fourth International Conference on Port and Ocean Engineering Under Arctic Conditions, September 1977.

23. Schwarz, J., "The Pressure of Floating Ice Fields on Piles," IAHR/AIRH International Symposium on ice, 1970.

24. Schrieber, M., "Stress-Strain Strength and Crystallography of Thin Ice Sheets Formed with Vaporized Nitrogen", M.S. Project Report, Dept. of Civil Engineering, Oregon State University, 1983 (in progress).

25. Scott, R.F., and Morgan, N.R., "Feasibility and Desirability of Constructing a Very Large Centrifuge for Geotechnical Studies," California Institute of Technology, December 1975.

26. Shide, S.B., and Wards, R.D., "Ice Rubble Field Stability," Proceedings, Offshore Technology Conference, Houston, TX, May 1982.

27. Sutherland, H.J., "Centrifuge Simulations of the Subsidence over Coal Mines and the Stability of Tailings Dams," High Gravity Simulation for Research in Rock Mechanics Workshop held at Colorado School of Mines, Department of Mining Engineering, Golden, CO, May 13-14, 1982.

28. Taylor, T.P., "An Experimental Investigation of the Crushing Strength of Ice," Proceedings of the 6th International Conference on Port and Ocean Engineering Under Arctic Conditions, Volume 1, 1981, pp. 332-345.

29. Vinson, T.S., "Centrifugal Modeling to Determine Ice/Structure/Geologic Foundation Interactive Forces and Failure Mechanisms," Proceedings of the 7th International Conference on Port and Ocean Engineering Under Arctic Conditions, Volume II, 1983, pp 845-854.

30. Wang, Y.S., "Sea-Ice Properties," Proceedings of Technical Seminar on Alaskan Beaufort Sea Gravel Island Design, Exxon Corporation, October, 1979.

31. Weeks, W.F., "Sea Ice Conditions in the Arctic," Arctic Ice Dynamics Joint Experiment Bulletin Number 34, December, 1976.

Appendix

User Manual for Data Acquisition Programs for Centrifugal Modeling Ice Mechanics Studies

The documentation and computer program described herein was developed by Clough (1983).

1. Initialization

To execute these programs the HP 85 must be connected to the HP 3054 Data Logger through the interface card. The connection is between the bottom slot of the four slots on the back of the HP85 and the back of the Data Logger. In addition, one 16K memory module and I/O ROM must be plugged into the back of the HP85. A power card from the Data Logger must also be plugged into the HP85.

Program "FI": Program "FI" requires thermistors wired into the back of the Data Logger together with a current source. Refer to the manuals supplied with the Data Logger for the proper procedure. This program requires that all thermistors be grouped together on successive channel numbers (e.g. channels 11 through 16). The number of thermistors and the initial channel number of the thermistors must be input during the execution of the program. The thermistor calibrations should be available to input during the execution of the program. Finally, a data tape should be ready for use to record temperature data if this is desired. When setting up the hardware the operator should keep in mind that he/she is limited to 30 thermistors by the program and may be limited to fewer than that by the number of hardware hook-ups on the back of the Data Logger.

Program "LOAD": The information previously presented also applies to program "LOAD". In addition, the operator must wire in one strain gage and one LVDT. These should be calibrated prior to execution of the program. The channel number and calibration must be

input for each. The correction factor for the strain gage at zero load will be generated by the program and need not be input.

2. Purpose

"FI": "FI" calculates the freezing index and temperatures using resistance thermistors. The experiment can be controlled by time or freezing index. Temperatures are recorded on tape and the freezing index is printed on paper.

"LOAD": This program records the time, load, and displacement related to the pile or other instrumented structure. Periodically (every 15 seconds for the first minute and every 30 seconds for the remaining time), the temperatures are recorded. The data is stored on tape.

3. Procedure

Program "FI": The following should be readily available:

* A list of the calibration constants for the thermistors
* The initial channel number of the thermistors
* The number of thermistors in air, water, and ice.
* A data tape with the number of records already used known. (This can be easily found by inserting the tape and typing CAT. The screen will display what is on the tape. Look in the column marked RECS and add up the numbers. This is the number of records already used. Note: A NULL file may be listed. Do not count these as used records.)

The following notation is used in the explanation of the procedure to execute the program: (1)Statements preceded with an arrow indicate data to be entered. (2) EL means press the "endline" key. In all cases check the input carefully because once EL is pressed it can't be corrected without starting over (unless you make a format error in which case the computer may let you try again).

The procedure will be demonstrated by presenting a complete example. The situation illustrated as follows: six thermistors are wired into the Data Logger on channels 11 through 16; all thermistors are in the air and it is desired to conduct a 2 minute experiment in which the freezing index will be printed out approximately every 20 seconds and the temperatures will be recorded on tape; this is Test #3.

In the format that follows the information on the left will appear on the screen;comments (that do not appear on the screen) are given.

Screen	Comments
	Turn on the HP 85 with the switch at the right rear. Turn on the Data Logger with the switch on the front. Insert the tape with program "FI" and type:
LOAD "FI" EL	
	When the program is loaded, remove the tape and press:
RUN	
Input number of thermistors in air, water, and ice, separated by commas (= 110 ea).	air: 6 water: 0 ice: 0
?	
6, 0, 0 EL	

Screen	Comments
Input initial channel number of thermistors ? 11 EL	Thermistors are on channels 11-16.
Input therm corr fact by increasing channel number, separated by END LINE. ? 0 EL ? 0 EL ? 0 EL ? 0 EL ? 0 EL ? 0 EL	In this experiment the thermistors do not have correction factors, hence, the entry is zero. In other experiments just type the thermistor corection factors from a prepared list.
If you want to see temps, press K1, otherwise press K2. K2	Anytime during the program, pressing K1 will printout the temperatures. The K1 and K2 refer to the special function keys at the top of the keyboard. In this example just continue.
Does freeze index (FI) or time (T) control the period of freezing? Type PI or T. T EL	This program allows the operator to terminate freezing when either a certain FI is reached corresponding to an ice thickness, or a certain time is reached. In this example the freezing period time is controlled by time.
Input freezing period time limit in minutes. ? 2 EL	This example: 2 minutes
Input time interval for FI printout in seconds. ?	

Screen	Comments
20 EL	This example: every 20 sec.
Input test #, 1 through 10. ? 3 EL	This example: 3 This number is important to distinguish between tests; also, if you are recording temperatures, never use the same test number because the computer will attempt to create two files with the same name and an error will result.
Do you want to record temps, Type yes or no. ? YES EL	This example: yes
Insert data tape and press cont. CONT	Insert the data tape with the "record" tab pushed outward to the left.
Input number of data records already used on data tape. ? / EL	This number is obtained from the tape catalogue before executing the program. This example: tape blank.
When liquid nitrogen is on, press freezing process, press cont. CONT	When ready to begin the cont.
Control Temperature -20.6 -20.6 -20.7 . . . -22.4 -22.6	The average temperature in the air is displayed on the screen and updated every few seconds At this point the experiment is over. Another experiment may be conducted without having to input thermistor constants or channel numbers. The length of the experiment, the control, and the FI printout frequency may be changed. In this example: No.
Do you want to conduct another experiment? Type yes or no ?	

Screen	Comments
NO EL	

This completes the procedure for program "FI". The printout for this example follows. To retrieve the temperatures stored on the tape, refer to the HP85 owner's manual pp 183-187. A knowledge of simple programming is required. The printout gives the file name of the temperature data.

Program "LOAD". The following should be readily available:

Have readily available:

* All items listed under program "FI"
* Channel numbers and calibration constants for the strain gage and LVDT.

Notation: Same as program "FI".

Example: Test #1. A spring was attached to a model pile and the pile was moved up and back by the motor. A strain gage and LVDT were attached to the pile. In addition, thermistors were wired in as in the previous example.

Screen	Comments
	Insert the tape with program "LOAD". Type:
Load "LOAD" EL	
	When loaded, remove tape and press:
RUN	
	The first 3 inputs are the same as program "FI".
Input test #, 1-5. ?	This example: #1
1 EL	
Input channel numbers of strain gage and LVDT, separated by a comma: ?	This example: 1,2
1,2 EL	
Input calibration constants for strain gage and LVDT, separated by a comma. ?	This example: 28.6, 0.0608
28.6,0.0608 EL	
When motor turned on, press CONT.	

CONT	The experiment will now run and continue to run for approximately 15 to 20 minutes. Once you are through, however, wait for one more temperature measurement and then press:
K1	
Insert data tape and press CONT.	Insert the data tape with the "record" tab pushed out to the left. Then press:
CONT	
Input # of data records already in use on tape.	Input the number of data records already being used. This can be obtained before running the experiment from the catalogue of the data tape. This example: blank tape.
?	
0 EL	

When the printout is complete, the experiment is over and the data is stored on tape. The printout gives the time of the experiment, the maximum load, and the file names of the data files. In addition the number of measurements is given and these will be used to retrieve the data from the tape.

Program "FI": Flowchart

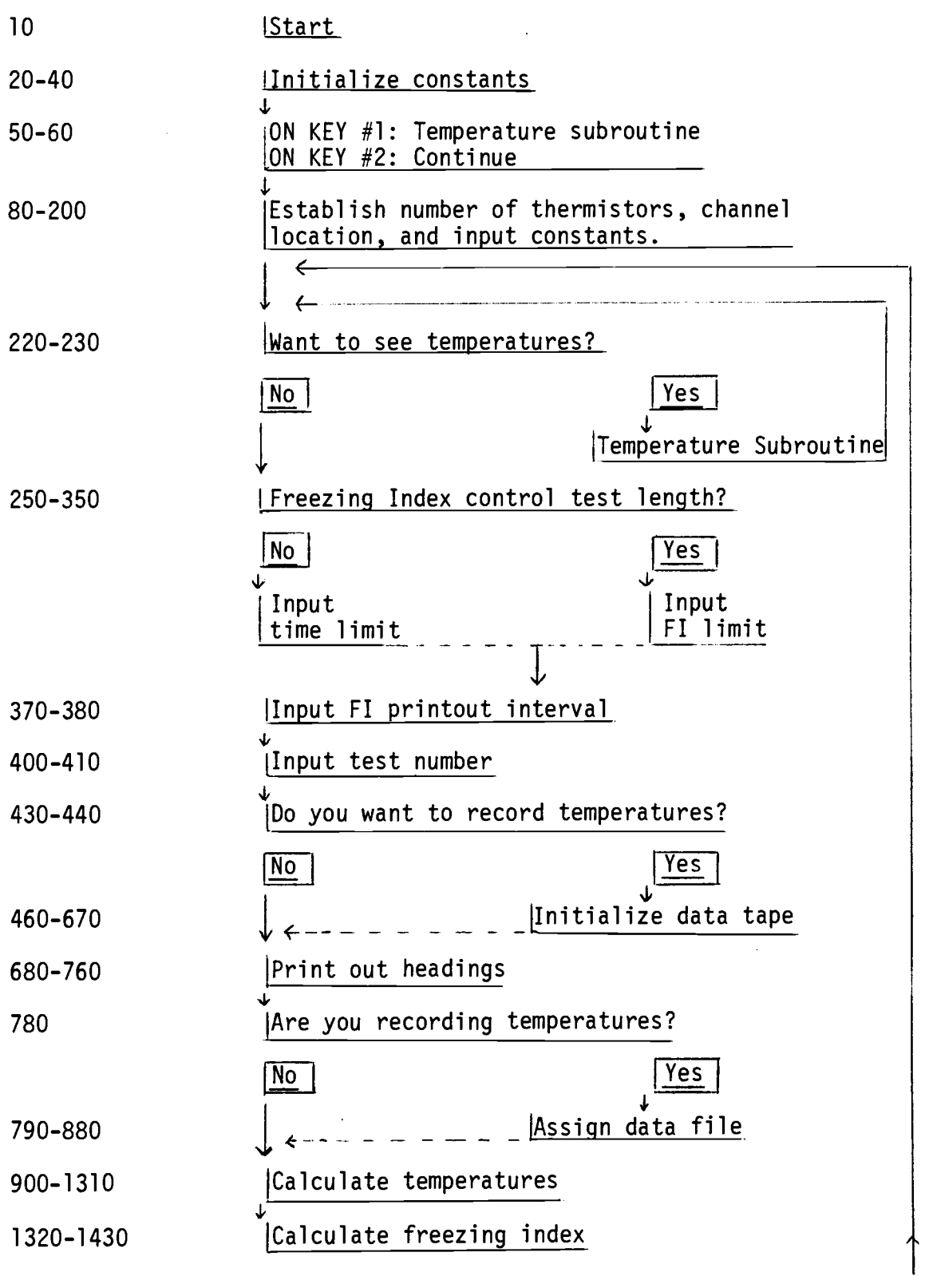

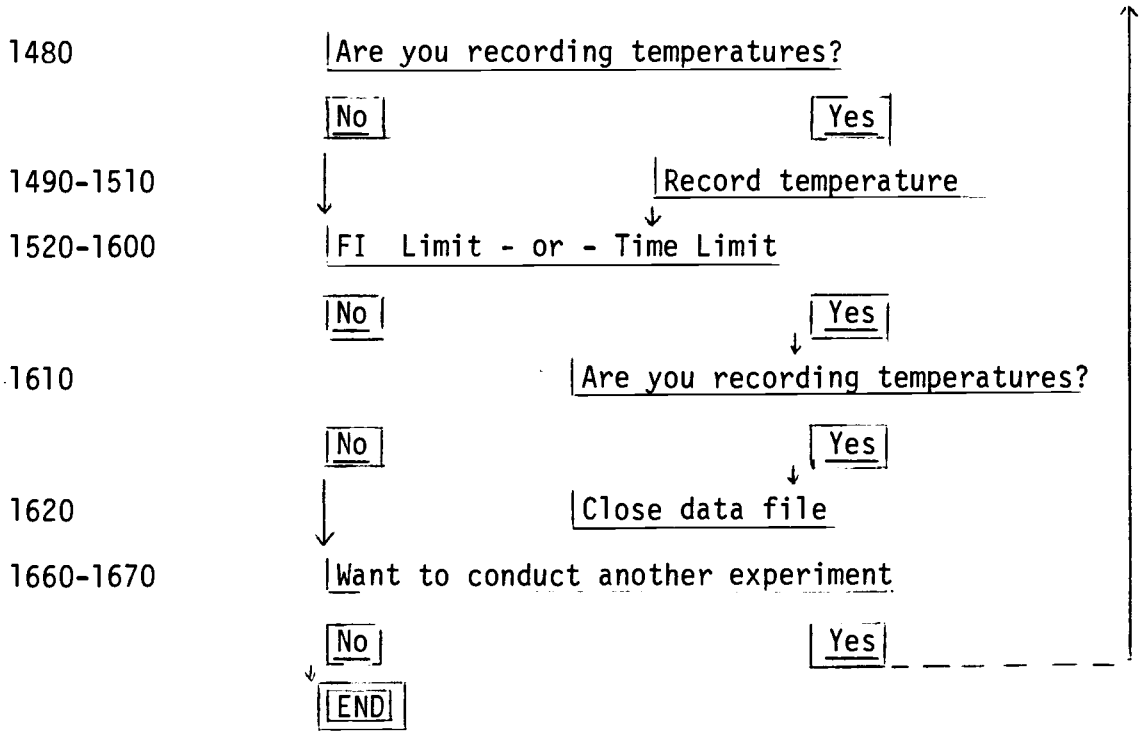
1480
Are you recording temperatures?
No
Yes
1490-1510
Record temperature
1520-1600
FI Limit - or - Time Limit
No
Yes
1610
Are you recording temperatures?
No
Yes
1620
Close data file
1660-1670
Want to conduct another experiment
No
Yes
END

Program "LOAD": Flowchart

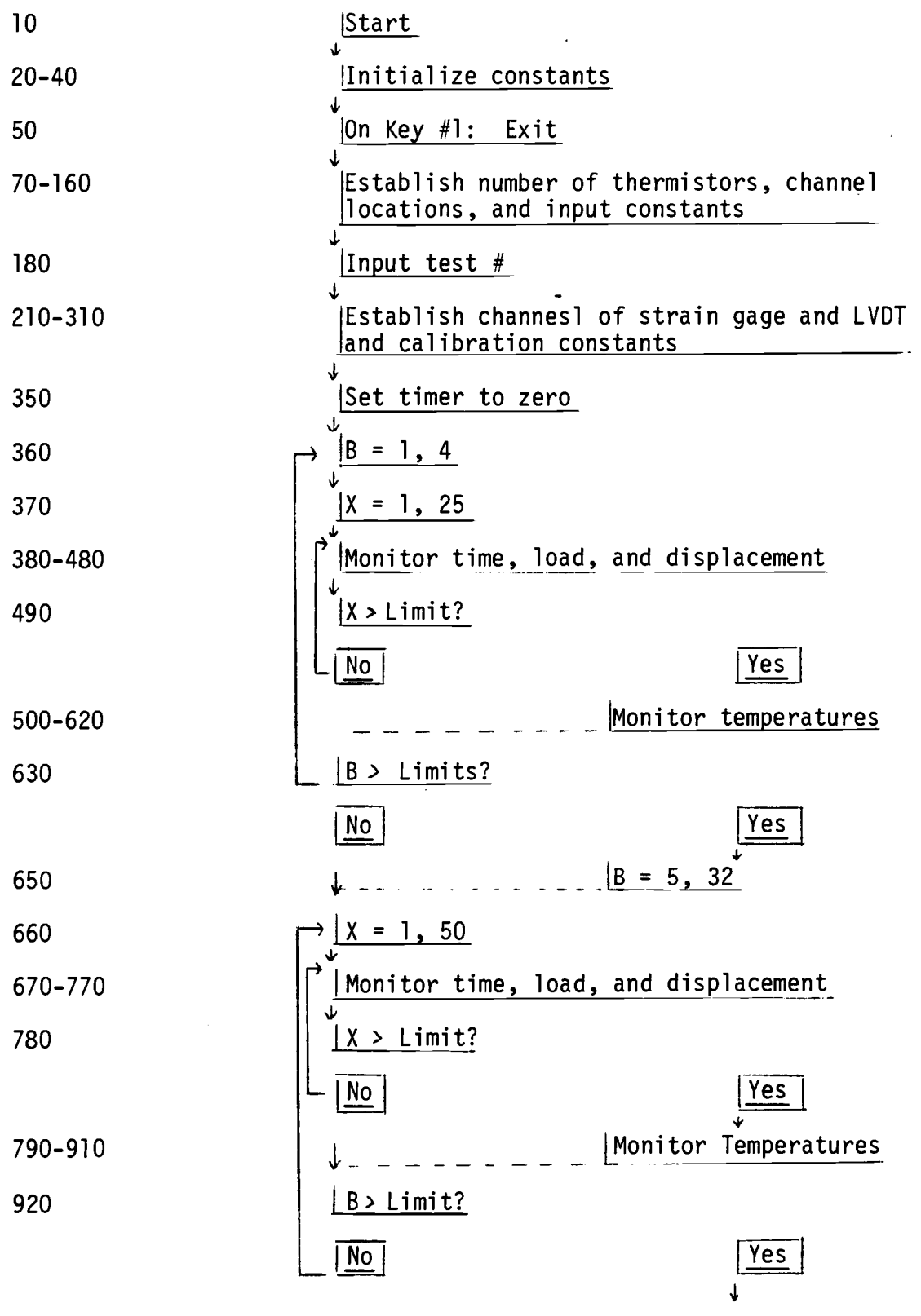

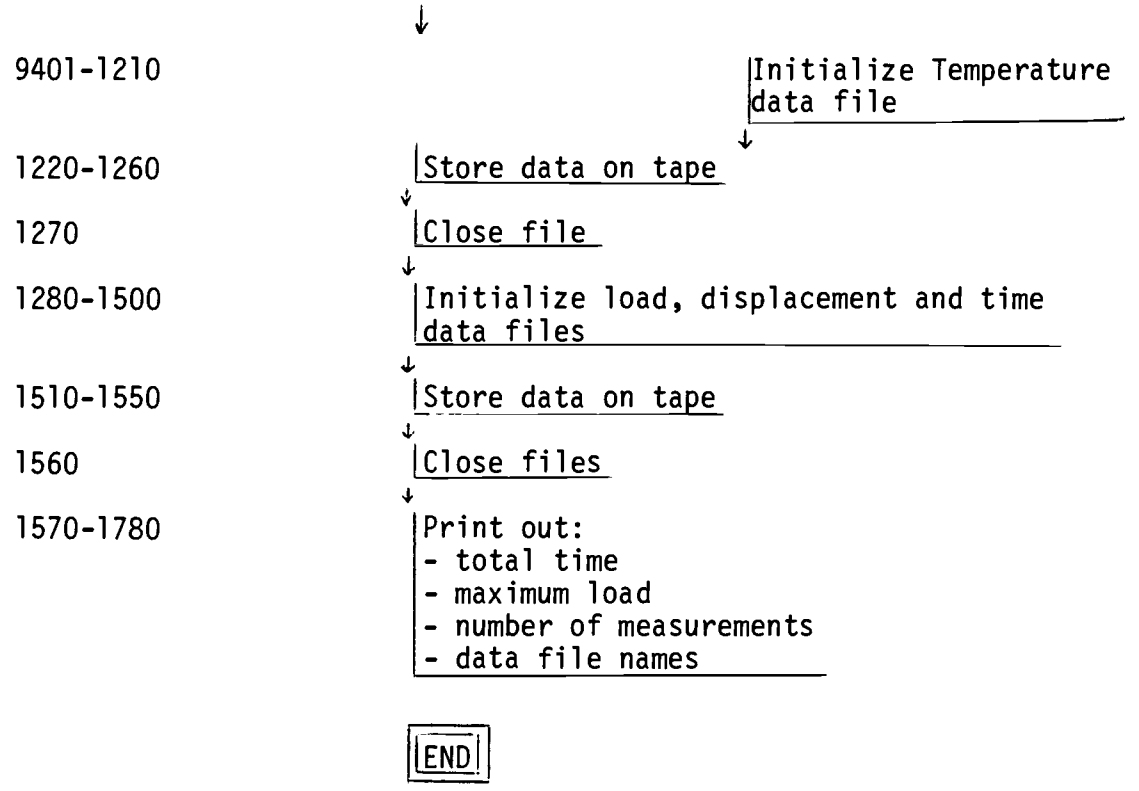
9401-1210
Initialize Temperature data file
1220-1260
Store data on tape
1270
Close file
1280-1500
Initialize load, displacement and time data files
1510-1550
Store data on tape
1560
Close files
1570-1780
Print out:
- total time
- maximum load
- number of measurements
- data file names
END

APPENDIX

Program "FI"

```
10 OPTION BASE 1
20 DIM P(30),T(2,10),X(2,30),G(
   10),F(30),E(70),E1(30),C(30)
30 01= 001486338 @ 02=.00023624
   2 @ 03=1.096145E-7
40 J=1
50 ON KEY# 1,"TEMPS" GOSUB 1700
60 ON KEY# 2,"RECOV" GOTO 240
70 BEEP
80 DISP "Input number of thermi
   stors in  air, water, and ic
   e, separated  by commas(<=10
    ea)."
90 INPUT A,W,I
100 BEEP
110 DISP "Input initial channel
   number of thermistors."
120 INPUT A1
130 BEEP
140 DISP "Input therm corr fact
   by increasing channel number
   , separated    by END LINE."
150 FOR W=1 TO A+W+I
160 INPUT C(W)
170 NEXT W
180 FOR Y=1 TO 10
190 F(Y)=0
200 NEXT Y
210 BEEP
220 DISP "If you want to see tem
   ps, press K1, otherwise pres
   s K2."
230 GOTO 230
240 BEEP
250 DISP "Does freeze index(FI)
   or time(T) control the lenet
   h of freezing?  Type FI or T
   "
260 INPUT A$
270 IF A$="FI" THEN 330
280 BEEP
290 DISP "Input freezing process
    time      limit in minutes."
300 INPUT L
310 L=L*60
320 GOTO 360
330 BEEP
340 DISP "Input freeze index lim
   it in      SQRT(deg-min)."
350 INPUT L1
360 BEEP
370 DISP "Input time interval to
   r FI      printout in seconds
   "
380 INPUT L2
390 BEEP
400 DISP "Input test #, 1 throug
   h 10."
410 INPUT N
420 BEEP
430 DISP "Do you want to record
   temps,    type yes or no."
440 INPUT B$
450 IF B$="NO" THEN 680
460 IF A$="FI" THEN 490
470 K1=INT((A+W+I)*L/L2/32+1)
480 GOTO 500
490 K1=INT((A+W+I)*7200/L2/32+1
500 BEEP
510 DISP "Insert data tape and p
   ress CONT."
520 PAUSE
530 BEEP
540 DISP "Input number of data r
   ecords    already in use on
   data tape."
550 INPUT R
560 IF K1+R/850 THEN DISP "Excee
   ds tape capacity: insert  ne
   w tape and press CONT." ELSE
    GOTO 580
570 PAUSE
580 IF N=1 THEN CREATE "TEMP 1",
   K1
590 IF N=2 THEN CREATE "TEMP 2",
   K1
600 IF N=3 THEN CREATE "TEMP 3",
   K1
610 IF N=4 THEN CREATE "TEMP 4",
   K1
620 IF N=5 THEN CREATE "TEMP 5",
   K1
630 IF N=6 THEN CREATE "TEMP 6",
   K1
640 IF N=7 THEN CREATE "TEMP 7",
   K1
650 IF N=8 THEN CREATE "TEMP 8",
   K1
660 IF N=9 THEN CREATE "TEMP 9",
   K1
670 IF N=10 THEN CREATE "TEMP10"
   ,K1
680 PRINT USING 690 : N,A,W
690 IMAGE 12X,"Test #",DD,3/,5X,
   "Thermistors in:",//,15X,"ai
   r",5X,DD,/,15X,"water",3X,DD
700 PRINT USING 710 : I
710 IMAGE 15X,"ice",5X,DD,/
720 IF B$="NO" THEN 750
730 PRINT USING 740 : N
740 IMAGE "Temps stored under",/
   ,10X,"file name TEMP",DD
750 PRINT USING 760
760 IMAGE //,"TIME (sec)",10X,"F
   ave",/,16X,"(SQR(deg-min))"
   /
770 D=1
780 IF B$="NO" THEN 890
790 IF N=1 THEN ASSIGN# 1 TO "TE
   MP 1"
```

```
800 IF N=2 THEN ASSIGN# 1 TO "TE
    MP 2"
810 IF N=3 THEN ASSIGN# 1 TO "TE
    MP 3"
820 IF N=4 THEN ASSIGN# 1 TO "TE
    MP 4"
830 IF N=5 THEN ASSIGN# 1 TO "TE
    MP 5"
840 IF N=6 THEN ASSIGN# 1 TO "TE
    MP 6"
850 IF N=7 THEN ASSIGN# 1 TO "TE
    MP 7"
860 IF N=8 THEN ASSIGN# 1 TO "TE
    MP 8"
870 IF N=9 THEN ASSIGN# 1 TO "TE
    MP 9"
880 IF N=10 THEN ASSIGN# 1 TO "T
    EMP10"
890 BEEP
900 DISP "When liquid nitrogen i
    s on,      Press CONT."
910 PAUSE
920 SETTIME 0,10
930 BEEP
940 DISP "CONTROL TEMPERATURE"
950 FOR Z6=1 TO A+W+I
960 T(1,Z6)=0
970 X(1,Z6)=0
980 NEXT Z6
990 FOR K=1 TO 100000
1000 FOR K3=1 TO 30
1010 E(K3)=0 @ E1(K3)=0
1020 NEXT K3
1030 A2=A
1040 J=1
1050 FOR M=A1 TO A1+A+W+I-1
1060 OUTPUT 709 ;"AC";M
1070 OUTPUT 709 ;"VC0VR5VN1VA1VF
    1VD5VS0VW0VT3"
1080 OUTPUT 709 ;"VC2"
1090 OUTPUT 709 ;"VT3"
1100 ENTER 709 ; P(J)
1110 IF P(J)<20 THEN 1160
1120 E(J)=M
1130 PRINT USING 1140 ; E(J)
1140 IMAGE 4/,"Open circuit on c
    hannel ",DD.3/
1150 IF E(J)<=A1+A-1 THEN E1(J)=
    E(J)
1160 IF M>A1+A-1 THEN 1180
1170 T(2,J)=TIME
1180 J=J+1
1190 NEXT M
1200 S=0
1210 FOR M1=1 TO A+W+I
1220 IF E(M1)=0 THEN 1260
1230 X(2,M1)=0
1240 IF M1<=A THEN A2=A2-1
1250 GOTO 1290
1260 Q8=P(M1)*10000+C(M1)
1270 Q4=LOG(Q8)
1280 X(2,M1)=1/(Q1+Q4*(Q2+Q4*Q4*
    Q3))-273.15
1290 IF M1>A THEN 1310
1300 S=S+X(2,M1)
1310 NEXT M1
1320 T1=S/A2
1330 BEEP
1340 DISP USING 1350 ; T1
1350 IMAGE 7X,MD.D
1360 S1=0
1370 FOR X1=1 TO A
1380 IF E1(X1)=0 THEN 1400
1390 GOTO 1420
1400 F(X1)=F(X1)+(T(1,X1)-T(2,X1
    ))*.5*(X(1,X1)+X(2,X1))
1410 S1=S1+F(X1)
1420 NEXT X1
1430 F=SQR(S1/A2/60)
1440 IF TIME<D*L2 THEN 1520
1450 D=D+1
1460 PRINT USING 1470 ; T(2,1),F
1470 IMAGE DDDD.DD,10X,MD.DDE
1480 IF B$="NO" THEN 1520
1490 FOR Y6=1 TO A+W+I
1500 PRINT# 1 ; X(2,Y6)
1510 NEXT Y6
1520 IF A$="FI" THEN 1550
1530 IF TIME>=L THEN 1610
1540 GOTO 1560
1550 IF F>=L1 THEN 1610
1560 FOR X2=1 TO A+W+I
1570 IF X2>A THEN 1590
1580 T(1,X2)=T(2,X2) @ X(1,X2)=X
    (2,X2)
1590 NEXT X2
1600 NEXT K
1610 IF B$="NO" THEN 1630
1620 ASSIGN# 1 TO *
1630 PRINT USING 1640 ; N
1640 IMAGE 4/,7X,"End Experiment
     ",DD,10/
1650 BEEP
1660 DISP "Do you want to run an
    other       experiment?  Typ
    e yes or no."
1670 INPUT C$
1680 IF C$="NO" THEN 1930
1690 GOTO 180
1700 PRINT USING 1710
1710 IMAGE 4/,10X,"Temperatures"
    ,/,14X,"Deg C",2/,3X,"Therm
    istor",9X,"Temp",/
1720 J1=1
1730 FOR M=A1 TO A1+A+W+I-1
1740 OUTPUT 709 ;"AC";M
1750 OUTPUT 709 ;"VC0VR5VN1VA1VF
    1VD5VS0VW0VT3"
1760 OUTPUT 709 ;"VC2"
1770 OUTPUT 709 ;"VT3"
```

```
1780 ENTER 709 ; P(J1)
1790 J1=J1+1
1800 NEXT M
1810 FOR M1=1 TO A+W+I
1820 IF P(M1)<20 THEN 1860
1830 PRINT USING 1840 ; M1
1840 IMAGE 7X,DD,5X,"Open circui
     t"
1850 GOTO 1910
1860 Q8=P(M1)#10000+C(M1)
1870 Q4=LOG(Q8)
1880 Z=1/(Q1+Q4*(Q2+Q4*Q4*Q3))-2
     73.15
1890 PRINT USING 1900 ; M1,Z
1900 IMAGE 7X,DD,12X,MDD.D
1910 NEXT M1
1920 RETURN
1930 END
```

Program "LOAD"

```
10 OPTION BASE 1
20 SHORT T(1500),T1(32,30),C(30
   ),L(1500),D(1500)
30 01=.001486338 @ 02=.00023624
   2 @ 03=1.096145E-7
40 J=1
50 ON KEY# 1,"EXIT" GOTO 930
60 BEEP
70 DISP "Input number of thermi
   stors in  air, water, and ic
   e; separated  by commas(<=10
    ea)."
80 INPUT A,W,I
90 BEEP
100 DISP "Input initial channal
   number of thermistors."
110 INPUT A1
120 BEEP
130 DISP "Input therm corr fact
   by increasing channel number
   , separated    by END LINE."
140 FOR V=1 TO A+W+I
150 INPUT C(V)
160 NEXT V
170 BEEP
180 DISP "Input test #, 1-5."
190 INPUT Y
200 BEEP
210 DISP "Input channel numbers
   of strain gage and LVDT, sep
   arated by a comma."
220 INPUT L2,D2
230 BEEP
240 DISP "Input calibration cons
   tants for strain gage and LV
   DT, separated by a comma."
250 INPUT C1,C2
260 N=1
270 OUTPUT 709 ;"AC";L2
280 OUTPUT 709 ;"VC0VR5VN1VA1VF1
   VD5VS0VW0"
290 OUTPUT 709 ;"VT3"
300 ENTER 709 ; L7
310 C3=L7*C1
320 BEEP
330 DISP "When motor turned on,
   press CONT."
340 PAUSE
350 SETTIME 0,10
360 FOR B=1 TO 4
370 FOR X=N TO N+24
380 OUTPUT 709 ;"AC";L2
390 OUTPUT 709 ;"VC0VR5VN1VA1VF1
   VD5VS0VW0"
400 OUTPUT 709 ;"VT3"
410 ENTER 709 ; L(X)
420 L(X)=C1*L(X)-C3
430 T(X)=TIME
440 OUTPUT 709 ;"AC";D2
450 OUTPUT 709 ;"VC0VR5VN1VA1VF1
   VD5VS0VW0"
460 OUTPUT 709 ;"VT3"
470 ENTER 709 ; D(X)
480 D(X)=C2*D(X)
490 NEXT X
500 J1=1
510 FOR M=A1 TO A1+A+W+I-1
520 OUTPUT 709 ;"AC",M
530 OUTPUT 709 ;"VC0VR5VN1VA1VF1
   VD5VS0VW0VT3"
540 OUTPUT 709 ;"VC2"
550 OUTPUT 709 ;"VT3"
560 ENTER 709 ; T1(B,J1)
570 08=T1(B,J1)*10000+C(J1)
580 04=LOG(08)
590 T1(B,J1)=1/(01+04*(02+04*04*
   03))-273.15
600 J1=J1+1
610 NEXT M
620 N=N+25
630 NEXT B
640 N=101
650 FOR B=5 TO 32
660 FOR X=N TO N+49
670 OUTPUT 709 ;"AC";L2
680 OUTPUT 709 ;"VC0VR5VN1VA1VF1
   VD5VS0VW0"
690 OUTPUT 709 ;"VT3"
700 ENTER 709 ; L(X)
710 L(X)=C1*L(X)-C3
720 T(X)=TIME
730 OUTPUT 709 ;"AC";D2
740 OUTPUT 709 ;"VC0VR5VN1VA1VF1
   VD5VS0VW0"
750 OUTPUT 709 ;"VT3"
760 ENTER 709 ; D(X)
770 D(X)=C2*D(X)
780 NEXT X
790 J1=1
800 FOR M=A1 TO A1+A+W+I-1
810 OUTPUT 709 ;"AC";M
820 OUTPUT 709 ;"VC0VR5VN1VA1VF1
   VD5VS0VW0VT3"
830 OUTPUT 709 ;"VC2"
840 OUTPUT 709 ;"VT3"
850 ENTER 709 ; T1(B,J1)
860 08=T1(B,J1)*10000+C(J1)
870 04=LOG(08)
880 T1(B,J1)=1/(01+04*(02+04*04*
   03))-273.15
890 J1=J1+1
900 NEXT M
910 N=N+50
920 NEXT B
930 BEEP
940 DISP "Insert data tape and p
   ress CONT."
950 PAUSE
960 BEEP
970 DISP "Input # of data record
   s already in use on tape."
```

```
980 INPUT K2
990 K1=INT(B*(A+W+I)/32+1)
1000 IF K1+K2<850 THEN 1040
1010 BEEP
1020 DISP "Exceeds tape capacity
     , insert new tape and Press
      CONT."
1030 PAUSE
1040 IF Y>1 THEN 1080
1050 CREATE "TEMP A",K1
1060 ASSIGN# 1 TO "TEMP A"
1070 GOTO 1220
1080 IF Y>2 THEN 1120
1090 CREATE "TEMP B",K1
1100 ASSIGN# 1 TO "TEMP B"
1110 GOTO 1220
1120 IF Y>3 THEN 1160
1130 CREATE "TEMP C",K1
1140 ASSIGN# 1 TO "TEMP C"
1150 GOTO 1220
1160 IF Y>4 THEN 1200
1170 CREATE "TEMP D",K1
1180 ASSIGN# 1 TO "TEMP D"
1190 GOTO 1220
1200 CREATE "TEMP E",K1
1210 ASSIGN# 1 TO "TEMP E"
1220 FOR P=1 TO B-1
1230 FOR P1=1 TO A+W+I
1240 PRINT# 1 ; T1(P,P1)
1250 NEXT P1
1260 NEXT P
1270 ASSIGN# 1 TO *
1280 K6=INT(X/32+1)
1290 IF K1+K2+96<850 THEN 1330
1300 BEEP
1310 DISP "Exceeds tape capacity
     , insert new tape and Press
      CONT."
1320 PAUSE
1330 IF Y>1 THEN 1370
1340 CREATE "LOAD A",K6 @ CREATE
      "DISP A",K6 @ CREATE "TIME
      A",K6
1350 ASSIGN# 1 TO "LOAD A" @ ASS
     IGN# 2 TO "DISP A" @ ASSIGN
     # 3 TO "TIME A"
1360 GOTO 1510
1370 IF Y>2 THEN 1410
1380 CREATE "LOAD B",K6 @ CREATE
      "DISP B",K6 @ CREATE "TIME
      B",K6
1390 ASSIGN# 1 TO "LOAD B" @ ASS
     IGN# 2 TO "DISP B" @ ASSIGN
     # 3 TO "TIME B"
1400 GOTO 1510
1410 IF Y>3 THEN 1450
1420 CREATE "LOAD C",K6 @ CREATE
      "DISP C",K6 @ CREATE "TIME
      C",K6
1430 ASSIGN# 1 TO "LOAD C" @ ASS
     IGN# 2 TO "DISP C" @ ASSIGN
     # 3 TO "TIME C"
1440 GOTO 1510
1450 IF Y>4 THEN 1490
1460 CREATE "LOAD D",K6 @ CREATE
      "DISP D",K6 @ CREATE "TIME
      D",K6
1470 ASSIGN# 1 TO "LOAD D" @ ASS
     IGN# 2 TO "DISP D" @ ASSIGN
     # 3 TO "TIME D"
1480 GOTO 1510
1490 CREATE "LOAD E",K6 @ CREATE
      "DISP E",K6 @ CREATE "TIME
      E",K6
1500 ASSIGN# 1 TO "LOAD E" @ ASS
     IGN# 2 TO "DISP E" @ ASSIGN
     # 3 TO "TIME E"
1510 FOR R=1 TO X-1
1520 PRINT# 1 ; L(R)
1530 PRINT# 2 ; D(R)
1540 PRINT# 3 ; T(R)
1550 NEXT R
1560 ASSIGN# 1 TO * @ ASSIGN# 2
     TO * @ ASSIGN# 3 TO *
1570 Z=0
1580 FOR G=1 TO X-1
1590 IF Z<L(G) THEN Z=L(G)
1600 NEXT G
1610 PRINT USING 1620 ; Y,T(X-1)
1620 IMAGE 3/,12X,"TEST # ",D,/
     ,"TOTAL TIME",10X,DDD.D,X,"
     sec",/
1630 PRINT USING 1640 ; Z
1640 IMAGE 2X,"MAX LOAD",10X,DDD
     .D,X,"lbs"
1650 Z3=(B-1)*(A+W+I)
1660 PRINT USING 1670 ; X,Z3
1670 IMAGE 3/,"# LOAD MEASMTS",7
     X,DDDD,/,"# TEMP MEASMTS",8
     X,DDD,3/
1680 IF Y=1 THEN Y$="A"
1690 IF Y=2 THEN Y$="B"
1700 IF Y=3 THEN Y$="C"
1710 IF Y=4 THEN Y$="D"
1720 IF Y=5 THEN Y$="E"
1730 PRINT USING 1740 ; Y$,Y$
1740 IMAGE "Data stored under:"
     /,5X,"Temps",10X,"TEMP ",A
     ,/,5X,"Loads",10X,"LOAD ",A
1750 PRINT USING 1760 ; Y$,Y$
1760 IMAGE 5X,"Disps",10X,"DISP
     ",A,/,5X,"Time ",10X,"TIME
     ",A
1770 PRINT USING 1780 ; /
1780 IMAGE 4/,8X,"END EXPERIMENT
      ",D,10/
1790 END
```